Technische Universität München
Fakultät für Medizin
Institut für Molekulare Immunologie & Experimentelle Onkologie

Restoration of HBV-specific CD8$^+$ T cell immunity in chronic HBV infection via a dual mode of action induced by Interferon-signaling

Annika Schneider

Vollständiger Abdruck der von der Fakultät für Medizin der Technischen Universität München zur Erlangung des akademischen Grades eines Doktors der Naturwissenschaften (Dr. rer. nat.) genehmigten Dissertation.

Vorsitzender: Prof. Dr. Marc Schmidt-Supprian

Prüfer der Dissertation:
1. Prof. Dr. Percy A. Knolle
2. Prof. Dr. Bernhard Küster
3. Prof. Dr. Ulrich Kalinke

Die Dissertation wurde am 07.09.2020 bei der Technischen Universität München eingereicht und durch die Fakultät für Medizin am 13.04.2021 angenommen.

ABSTRACT

Chronic hepatitis B virus (HBV) infection represents a significant health problem with currently about 257 million chronically infected people and more than 850.000 deaths per year due to HBV-related diseases. Therapy with pegylated interferon-alpha (PEG-IFNα), which is currently the most effective curative therapy for chronic hepatitis B infection (CHB), accomplishes off-treatment control of HBV in 10 to 12% of patients. Because HBV-specific $CD8^+$ T cell responses are essential to achieve HBV cure, it is assumed that PEG-IFNα restores HBV-specific $CD8^+$ T cell immunity in patients responding to therapy. However, restoration of impaired HBV-specific $CD8^+$ T cell immunity in CHB patients treated with PEG-IFNα could not be demonstrated so far. Hence, the molecular and cellular mechanism of how HBV cure is achieved in some patients under PEG-IFNα-therapy remains completely unknown.

Here, the potential of type I IFNs (IFNα/β) to restore impaired HBV-specific $CD8^+$ T cell immunity was explored. An adenoviral vector delivering an HBV1.3 genome coupled to a luciferase sequence (Ad-HBV-Luc) was used to either mimic persistent or acute, self-limiting HBV infections in immunocompetent mice. In established persistent Ad-HBV-Luc infection, continuous hepatocyte-specific IFNβ expression restored phenotype and functionality of HBV-specific $CD8^+$ T cells in the liver. Due to severe side effects evoked by prolonged hepatocyte-specific IFNβ expression, clearance of persistent Ad-HBV-Luc infection was not achieved.

In contrast, sequential injections of the TLR3-ligand polyI:C were well tolerated and demonstrated also to restore HBV-specific $CD8^+$ T cell immunity and further sustain the antiviral response until complete eradication of persistent Ad-HBV-Luc infection had occurred.

After proving that IFN-based therapies have the potential to restore exhausted HBV-specific $CD8^+$ T cell immunity apparent in CHB, cell type specific IFNAR1 knockout mice were utilized to shed light on the mechanisms of action. The data revealed that IFNAR signaling in hepatocytes, which is in particular important for the reduction of viral antigen load, and IFNAR signaling in HBV-specific $CD8^+$ T cells, is crucial for the restoration of exhausted HBV-specific $CD8^+$ T cells. Further, adoptive transfer experiments provide evidence that type I IFN targets a subpopulation of exhausted precursor HBV-specific $CD8^+$ T cells that, in response to IFN signaling, repopulate the niche of terminal exhausted, dysfunctional HBV-specific $CD8^+$ T cells with functional HBV-specific effector $CD8^+$ T cells.

In summary, the presented work highlights that two mechanisms induced by type I IFNs, i.e., the reduction of HBV antigen burden and provision of stimulatory signals for HBV-specific $CD8^+$ T cells, are required for the restoration of exhausted HBV-specific $CD8^+$ T cell immunity. Thus, this thesis extends the understanding of prerequisites for the induction of efficient anti-HBV immunity in CHB, which may pave the way for the development of new therapeutic

approaches that more specifically and reproducible reduce HBV antigen load into a certain range and simultaneously provide a specific stimulus that pushes exhausted T cells.

ZUSAMMENFASSUNG

Die Infektion mit dem chronischen Hepatitis B Virus (HBV) stellt mit derzeit etwa 257 Millionen chronisch infizierten Menschen und jährlich mehr als 850.000 Todesfällen aufgrund von HBV-assoziierten Folgeerkrankungen ein globales Gesundheitsproblem dar. Die Therapie mit pegyliertem Interferon-alpha (PEG-IFNα), die derzeit die wirksamste Therapie zur Behandlung einer chronischen Hepatitis B (CHB) ist, führt nur bei 10 bis 12% der Patienten zur Kontrolle von HBV. Eine funktionale HBV-spezifische $CD8^+$ T-Zell-Antwort ist essentiell zur Kontrolle von HBV. Daher geht man davon aus, dass Typ I IFN bei Patienten, die auf die Therapie ansprechen, die beeinträchtigte HBV-spezifische $CD8^+$ T-Zell-Immunität wiederherstellt. Eine Reaktivierung der gestörten HBV-spezifischen $CD8^+$ T-Zell-Immunität bei CHB-Patienten konnte bisher jedoch nicht bewiesen werden. Daher ist der Wirkmechanismus, der zur Reaktivierung der beeinträchtigen HBV-spezifischen T-Zell Immunität in chronisch infizierten Patienten unter PEG-IFNα-Behandlung führt, unbekannt.

In dieser Arbeit wurde der Mechanismus von Typ I IFN zur Wiederherstellung der beeinträchtigten HBV-spezifischen $CD8^+$ T-Zell-Immunität erforscht. Ein adenoviraler Vektor, welcher HBV Überlängengenome mit einer Luziferase-Sequenz in murine Hepatozyten einbringt (Ad-HBV-Luc), wurde zur Etablierung persistenter oder akuter, selbstlimitierter HBV-Infektionen in immunkompetenten Mäusen verwendet. Bei Mäusen mit persistierender Ad-HBV-Luc-Infektion stellte eine kontinuierliche Hepatozyten-spezifische IFNβ-Expression den Phänotyp und die Funktionalität der HBV-spezifischen $CD8^+$T-Zellen in der Leber wieder her, ähnlich wie bei Mäusen mit akuter, selbstlimitierter Infektion. Langanhaltende, kontinuierliche Hepatozyten-spezifische IFNβ-Expression rief schwere Nebenwirkungen hervor, sodass eine vollständige Eliminierung des Virus nicht erreicht wurde.

Es zeigte sich, das tägliche, wiederholte Injektionen des TLR3-Liganden PolyI:C besser verträglich waren und IFN-abhängig eine effiziente, langanhaltende HBV-spezifische Immunantwort induzierten, die zur vollständigen Eliminierung des Virus führte.

Nachdem gezeigt worden war, dass Typ I IFN-basierte Therapien das Potenzial haben, eine dysfunktionale HBV-spezifische $CD8^+$ T-Zell-Immunität in chronischer Ad-HBV-Luc Infektion wiederherzustellen, wurden zelltyp-spezifische Typ-I-Interferon-Rezeptor-Knockout-Mäuse (IFNAR1 KO) verwendet, um die dabei operierenden Wirkmechanismen zu identifizieren. Die Daten zeigten, dass zwei der multiplen durch Typ I IFN-induzierten Effekte, die Reduktion der viralen Antigenlast und die Stimulation der $CD8^+$ T-Zellen durch IFNAR1-Stimulation, entscheidend für die Wiederherstellung erschöpfter HBV-spezifischer $CD8^+$ T-Zellen sind.

Zusammenfassend zeigen die Ergebnisse dieser Arbeit, dass zwei der durch Typ I Interferone induzierten Effekte, die Reduzierung der HBV-Antigenlast und die Bereitstellung stimulierender Signale für T-Zellen, für die Wiederherstellung der dysfunktionalen HBV-

spezifischen $CD8^+$ T-Zell-Immunität erforderlich sind. Damit erweitert diese Arbeit das Wissen über die Voraussetzungen zur Wiederherstellung einer HBV-spezifischen Immunantwort und kann den Weg für die Entwicklung neuer therapeutischer Ansätze ebnen, die die HBV-Antigenlast spezifischer reduzieren und gleichzeitig eine spezifische Immunstimulation für erschöpfte HBV-spezifische $CD8^+$ T-Zellen bietet

TABLE OF CONTENTS

1. INTRODUCTION

1.1 Hepatitis B Virus

Hepatitis B Virus (HBV), first described by Dane et. al[1], is a small, enveloped, partially double-stranded DNA virus belonging to the family of the Hepadnaviridae. It replicates through reverse transcription of an RNA-intermediate, the pregenomic RNA (pgRNA), and therefore belongs to the para-retroviruses[2]. Based on nucleotide sequence variations, HBV is classified into ten genotypes A-J, which differ in more than 8% of the genome[3, 4]. Each genotype exhibits a distinct geographic distribution[5, 6]. Characteristic for HBV is its high tropism for hepatocytes and its narrow host specificity, with humans and chimpanzees being the only natural hosts[7].

Infectious HBV virions, so-called Dane particles, exhibit a spherical, double-shelled structure of 42-44 nM in diameter. Each virion consists of an outer lipoprotein envelope composed of Hepatitis B envelope proteins and an inner nucleocapsid[1, 8]. The inner nucleocapsid is composed of 180-240 proteins of the HBV core protein (HBc) and contains the viral genome as a partially double-stranded, circular but not covalently closed DNA of 3.2 kb, named relaxed circular DNA (rcDNA)[8]. With each nucleotide exhibiting coding function, the HBV genome encodes for seven proteins via four partially overlapping open reading frames (ORFs): presurface-surface (preS-S), pre-core-core (preC-C), P and X[9].

HBV infects hepatocytes through unspecific and reversible binding to heparan sulfate proteoglycans followed by specific binding to its cellular receptor, Sodium taurocholate cotransporting polypeptide (NTCP)[10]. After binding to NTCP, HBV enters the cell via endocytosis. Subsequently, the nucleocapsid is transported to the nucleus, where it releases the rcDNA, which is then converted into a plasmid-like covalently closed circular DNA (cccDNA). The cccDNA, which resides in the nucleus of infected hepatocytes as an episomal, plasmid-like molecule, is often referred to as the virological key to HBV persistence[9].

From the cccDNA, several genomic and subgenomic RNAs are transcribed. From those genomic and subgenomic RNAs, all viral proteins are translated[11]. Next to the three forms of surface proteins (HBs) and the core protein (HBc), the nonstructural HBV X protein (HBx), and the secreted Hepatitis E antigen (HBe) are translated. From all transcribed RNAs, the pgRNA is, after binding to the viral polymerase, selectively packed into progeny capsids. Within the capsid, the pgRNA is reverse transcribed into rcDNA, and subsequently, the matured capsid can take two different routes: It can either be re-transported to the nucleus and thereby intracellular cccDNA is amplified, or it can be enveloped and released from the cell as mature progeny virion. Besides the infectious HBV virions, non-infectious subviral particles (SVPs) are released from infected cells and can be detected in patients' blood[8]. SVPs, either filaments or

spheres, are exclusively composed of HBsAg and host-derived lipids and differ in structure, size, and HBV surface-protein composition[12].

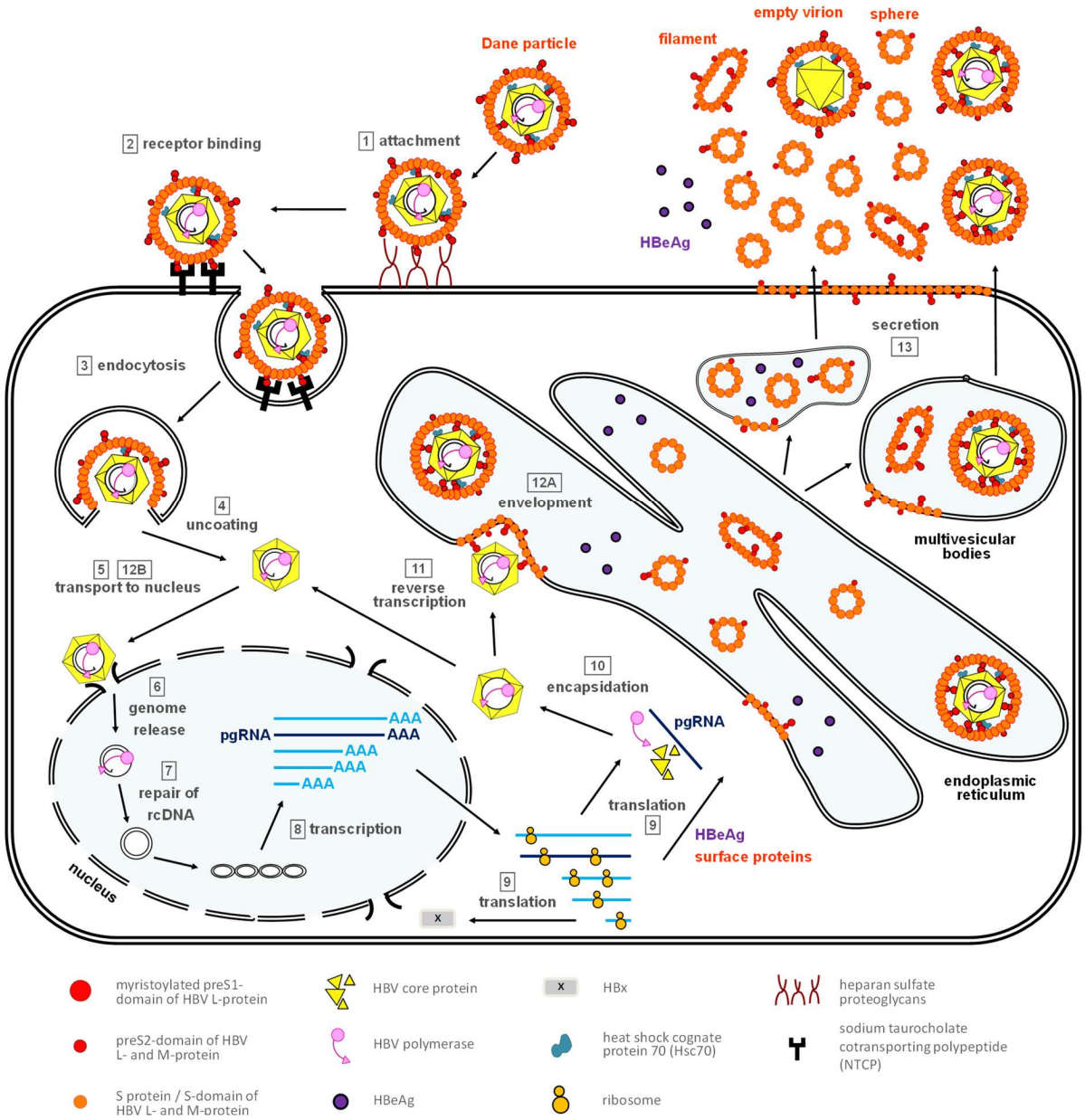

Figure 1.1| Hepatitis B virus life cycle
(1) HBV infects hepatocytes through unspecific and reversible binding to heparan sulfate proteoglycans followed by (2) specific binding to its cellular receptor NTCP and (3) endocytosis. After (4) uncoating and (5) transport to the nucleus, (6) rcDNA is released. (7) Host proteins repair rcDNA to cccDNA, (8) from which several genomic and subgenomic RNAs are transcribed. (9) Then viral proteins are translated, and (10) pgRNA is encapsidated and (11) reverse transcribed into rcDNA. Subsequently, the capsid is either (12A) enveloped by the envelope proteins S, M, and L or (12B) recycled and re-transported to the nucleus. The enveloped capsid is transported through the endoplasmatic reticulum, and multivesicular bodies and finally (13) secreted from the cell. Additionally, Empty virions, filaments, spheres, and HBeAg are released from the cell. The scheme was derived from[13]

1.1.1 Pathogenesis of HBV infection

HBV is transmitted via blood, blood products, unprotected sexual contact, or by vertical transmission from mother to the neonate and infection can be either eliminated in an acute, self-limiting course or become chronic. Chronic Hepatitis B (CHB) is defined by the presence

of circulating hepatitis B virus surface antigen (HBsAg) in the blood for more than six months. The risk to develop CHB is directly related to the age at which a person is first exposed to HBV. While the exposure of adults mostly (in approximately 95% of occurring infections) induces a self-limiting acute infection, about 90% of infants infected within the first six months of life develop chronic infections[14]. Besides the age of first exposure, immunosuppression is considered a risk factor to develop CHB[15]. The world health organization (WHO) estimated that in 2015 approximately 257 million people were living with CHB and that more than 850.000 died from HBV-associated diseases (WHO, 2019).

In acute, self-limiting HBV infections, symptoms range from asymptomatic infection to self-limited hepatitis and, in rare cases, fulminant hepatitis. HBV itself has been demonstrated to be non-cytopathic. The observed liver pathology, which is characteristic of acute, self-limiting HBV infection, is induced by a strong and polyclonal T cell response[16]. In contrast, HBV-specific T cells are scarce or dysfunctional in chronically infected HBV carriers[17]. However, HBV-specific immune response is not inert in chronically infected carriers. A weak but permanently ongoing immune response in the liver is associated with liver fibrosis, cirrhosis, and hepatocellular carcinoma (HCC)[16, 18]. Epidemiological and molecular studies demonstrated that HBV infection represents the main risk factor for HCC development[19, 20]

CHB is a dynamic process with interactions between the host immune system and viral replication and spread. Therefore, the spectrum of disease is diverse, and individuals with CHB usually progress through distinct clinical phases (Fig 1.2). There are four clinical phases of CHB defined by HBeAg status, HBV DNA, and Alanine Aminotransferase (ALT) levels[21]. Although most patients progress from one phase to the next, not all patients go through each phase, and reversions to earlier phases can occur. Patients who acquired HBV-infection perinatal or in early-childhood, have an initial immune tolerance phase of CHB. Characteristics for the immune tolerance phase are high serum HBV DNA levels (typically > 1 million IU/mL), presence of HBeAg, and normal ALT levels. In the immune active phase of CHB, which usually follows the immune tolerance phase, ALT levels are intermittently or persistently elevated, serum HBV DNA levels are lower (depending on HBeAg status), and liver biopsy or non-invasive tests reveal hepatitis with moderate or severe necroinflammation. Patients are subdivided in HBeAg positive (with > 20.000 IU/mL serum HBV DNA) or HBeAg negative (with 2.000-20.000 IU/mL serum HBV DNA). Immune active CHB can eventually progress into inactive CHB. Patients with inactive CHB have serum HBV-DNA levels < 2.000 IU/mL, are HBeAg negative and anti-HBe positive, and have normal ALT values with no signs of necroinflammation in the liver[22].

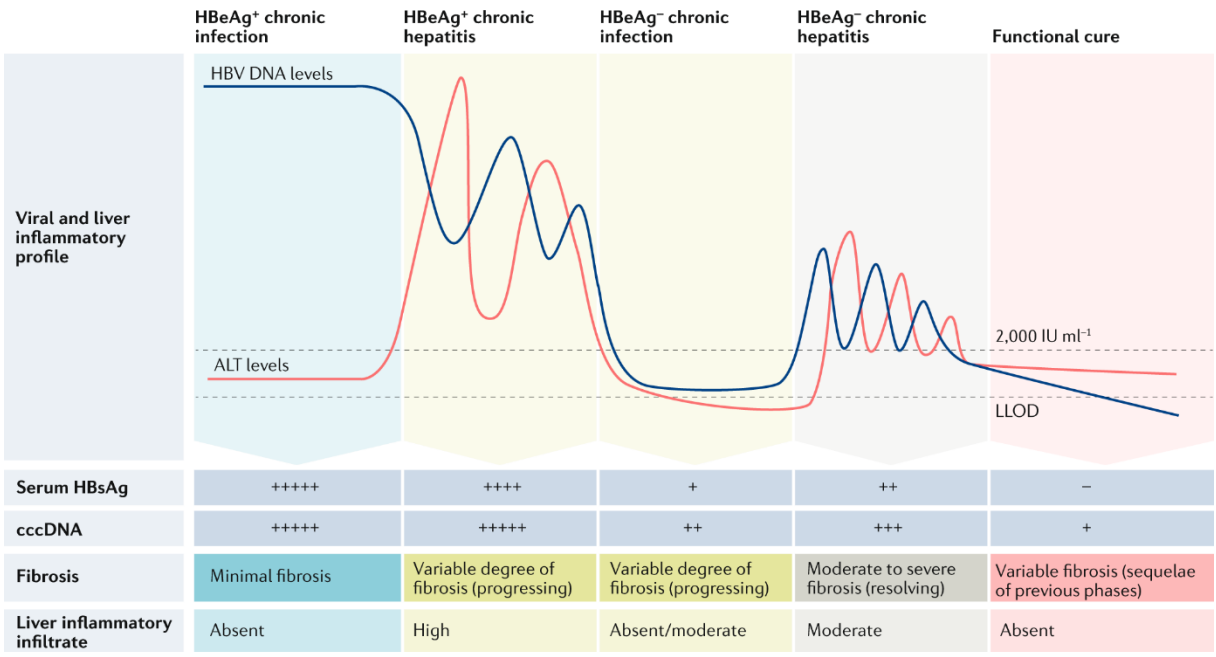

Figure 1.2| Clinical phases of chronic HBV infection
The four clinical or virological phases of chronic HBV infection are depicted according to the European Association for the Study of the Liver 2018 Guidelines. Patients can develop, depending on the balance of viral replication and immune control, from one phase to another and do not necessarily stick to a sequential order. Serum ALT levels are elevated in the immune active phase (hepatitis phases) and normal in the immune tolerant phase (chronic phases), independent of the HBeAg status. Serum HBsAg levels and HBV DNA levels do decline over time. Levels of cccDNA decline over time, but cccDNA is never completely eliminated. Clinical phases of CHB may develop in a functional cure, defined as HBsAg loss. Modified from: [23]

1.1.2 Innate immunity in HBV infection

Immediately after infection, most viruses induce activation of the innate immune system, measured by induction of type I Interferons (IFNs). The role of early innate immune activation during natural HBV infection in humans is difficult to study as HBV infection is mainly diagnosed several weeks after onset of infection when viremia is high and the virus may already have escaped early innate immune responses[24]. Studies in experimentally infected chimpanzees demonstrated the absence of type I IFN response after infection with HBV[25]. Based on this study, it was proposed that HBV bypasses recognition by sensors of the innate immune system and behaves like a stealth virus[26]. Induction of innate immune response could not be measured in liver biopsies from patients with CHB, but IFN-production in liver tissue of these patients was measured following experimental activation of Toll like receptor 3 (TLR3)[27]. As an innate immune response could be induced by unrelated stimuli, this study supports the hypothesis that HBV is invisible to innate sensors instead of actively suppressing innate activation. However, several studies challenge the idea of HBV acting as a stealth virus in humans. It was shown that HBV induces type I IFNs, although at lower levels compared to HIV or HCV, suggesting an innate recognition of HBV[28]. As the low levels of innate immune cytokines were detected systemically, one cannot exclude that HBV induces local production of cytokines in the liver. Using primary human liver cell cultures, non-parenchymal cells (NPCs)

were demonstrated to produce IL-6 and other pro-inflammatory cytokines within five hours after contact with HBV[29]. IL-6 was demonstrated to regulate early HBV gene expression and replication in hepatocytes at the level of transcription. Dunn *et al.* demonstrated that Interleukin-10 (IL-10) production is induced early after HBV infection, proposing that HBV infection is sensed by the immune system, but actively inhibits the induction of type I IFNs[30]. Another human study, in which two patients were monitored early after infection in the incubation phase of HBV, revealed that HBV was sensed by the human innate immune system and elicited an NK and NK T cell response[31].

In HBV transgenic mice deficient for type I interferon receptor (IFNAR), HBV replicates at higher levels than in control littermates implying that baseline levels of type I IFNs control HBV replication[32]. As follow up, the authors showed that HBV replication is also significantly increased in HBV-transgenic mice deficient of protein kinase R (PRK) or interferon regulatory factor 1 (IRF1)[33]. These studies suggest that HBV is sensitive to type I IFNs and that innate immunity is essential in the natural control of HBV replication. Several in vitro studies provide evidence that various HBV proteins can counteract the IFN signaling pathway[34, 35, 36]. Besides this inhibition downstream of the IFN signaling pathway, there is evidence that HBV also interferes with the host recognition system by regulating the expression of TLRs[37, 38, 39], or by inhibiting TLR signaling cascades[40]. In biopsies of CHB patients, various genes of innate immunity were downregulated compared to healthy controls providing further evidence for an active counteraction of HBV against innate immunity[41].

In summary, the available data suggest three possibilities. (1) Either HBV is invisible to innate immunity or (2) HBV induces an innate immune response but rapidly inhibits it or (3) HBV elicits an innate immune response to a lower, hardly detectable extent.

1.1.3 Adaptive immunity in HBV infection

During HBV infection, the adaptive immune response is responsible for viral clearance but also for disease pathogenesis[42, 43]. As experimental deletion of $CD8^+$ T cells in chimpanzees delays viral clearance of acute, self-limiting HBV infection[44], $CD8^+$ T cells are recognized as the main effector cells. Compared to other virus infections like SIV, HIV[45], or CMV[46], in which virus-specific T cells are usually detected within two weeks after infection, HBV-specific $CD8^+$ T cells in patients are detected not earlier than two months after infection regardless of the outcome of infection[31, 47]. A possible explanation for this long incubation phase may be the lack of innate immune activation, which is required for proper $CD8^+$ T cell priming. In addition, the first 4 to 7 weeks after HBV infection, patients are negative or only weakly positive for HBV-DNA[48, 49], and therefore priming and activation may occur delayed. However, these early events occurring in the incubation phase of HBV are not well studied as HBV infection in patients is usually detected after the appearance of clinical symptoms, which is after the incubation phase. Another characteristic of primary HBV infection is low frequencies of HBV-specific $CD8^+$ T

cells, which also in the acute phase of acute, self-limiting HBV infections do not exceed 1% of circulating $CD8^+$ T cells[16]. Cytotoxicity of effector T cells is mediated either cytolytic via granule exocytosis or Fas-mediated programmed cell death or non-cytolytic via secreted cytokines. Several studies indicate that cytolytic as well as non-cytolytic activities of $CD8^+$ T cells contribute to control of HBV infection[50, 51, 52, 53]. Next to the direct induction of apoptosis of HBV-infected hepatocytes, cytotoxic $CD8^+$ T cells release Interferon-gamma (IFNy) upon antigen encounter. IFNy inhibits HBV gene expression and replication by preventing the assembly of HBV-RNA containing capsids in the cytoplasm[54, 55, 56], and by destabilizing viral RNA in the nucleus[57]. There is evidence that even cccDNA can be partially eliminated from hepatocytes by a non-cytolytic mechanism[58].

$CD4^+$ T cells seem to not directly participate in viral clearance and liver pathology in patients with acute self-limiting HBV infection[44]. In the case of sufficient inflammatory stimuli, the formation of a functional primary immune response in the context of acutely resolved infections is $CD4^+$ T cell help independent. In the case of HBV, $CD4^+$ T cells were shown to be required for the resolution of acute infections in mice[59]. $CD4^+$ T-cells are recognized to be crucial for priming of HBV-specific $CD8^+$ T cells and are thereby thought to contribute indirectly to the control of HBV infection[60].

The cellular-arm of the adaptive immune response executed by $CD4^+$ helper and $CD8^+$ effector T cells was shown to be strong and multi-specific during acute, self-limiting HBV infections[16, 61]. In contrast, low frequencies of HBV-specific $CD8^+$ T cells that exhibit a dysfunctional phenotype, are detected in chronically infected carriers[62].

1.1.4 Treatment of chronic hepatitis B

Although the infection can be prevented by a vaccine, there is still no curative treatment available for those living with CHB. Current available antiviral therapy aims to reduce viremia and prevent progression to liver cirrhosis or, if cirrhosis is already present, to avoid or delay progression to end-stage complications of liver disease or HCC[63]. The ultimate goal of HBV therapy is a “functional cure”, which is defined as off-treatment loss of HBsAg, seroconversion to anti-HBs, and undetectable HBV DNA in the serum. Standard therapy is either IFNα, nucleos(t)ide analogues (NAs) or a combination of both[22]. There are two different therapeutic approaches depending on the stage of the disease and physical condition of patients, both aiming to suppress disease activity: (1) achieving elimination of all measured viral parameters with a time-limited course of antiviral treatment capable of achieving sustained off-treatment control of HBV replication or (2) suppressing viral replication permanently by continuous antiviral therapy. IFNα-based therapy is the standard therapy of the former strategy. IFNα was the first drug approved for the treatment of CHB and was in 2002 replaced by its pegylated form (PEG-IFNα) due to its more convenient subcutaneous administration once per week[64]. IFNα-based therapies achieve a functional cure in a limited number of patients. Following 48

weeks of treatment, HBeAg seroconversion was achieved by 32-36% of patients[65, 66], and a functional cure was achieved by 10% to 12% of patients at five years post treatment[67, 68].
While during IFNα/Peg-IFNα treatment, adverse effects are common and can occasionally cause significant morbidity or mortality, NAs are well tolerated. Despite efficient viral suppression induced by treatment with NAs, the rate of HBsAg or HBeAg seroconversion is very low, and sustained off-treatment responses are rare[69]. The persistence of cccDNA after long-term treatment with NAs is likely due to the replenishment of the intrahepatic cccDNA pool by the recycling of cccDNA within infected hepatocytes[70]. Long-term, eventually lifelong treatment with NAs is preferred for patients with advanced or decompensated cirrhosis or after the failure of IFNα-based therapy[71].

1.1.5 Animal models to study HBV infection

Due to poor accessibility of robust *in vitro* infection systems and the narrow host range of HBV, the study of HBV biology is limited. The chimpanzee model represents the only immunocompetent animal model that is fully susceptible to HBV infection and can develop an acute and chronic HBV infection. The chimpanzee model contributed substantially to the understanding of HBV-host interaction and immune response. However, their use has always been highly restricted and expensive and is now completely banned in most countries[7]. Besides chimpanzees, Tupaias (Asian threw shrews) have been shown susceptible to HBV infection. However, although the establishment of chronic HBV infection could be shown for neonatal shrews, in vivo infection rates for HBV are generally low[72, 73].
Essential data on HBV replication and pathogenesis of infection were obtained from the duck or woodchuck model, which are naturally infectable with viruses similar to HBV, the duck hepatitis virus (DHBV), and woodchuck hepatitis virus (WHV). However, both viruses are similar to HBV but not identical, and analysis of the immune response and liver disease is hampered by the lack of appropriate reagents[74].
Therefore, various mouse models have been generated, aiming to mimic the human infection setting. HBV transgenic mice express the complete HBV genome and produce infectious virions[75]. Since the HBV genome is integrated into the mouse genome and additionally a high level of immunotolerance is operative in HBV transgenic mice, an immune-mediated elimination of the virus is not possible. Although these mice enabled the study of antiviral agents in vivo and substantially contributed to the understanding of HBV pathogenesis, this model is not suitable to assess viral entry, spread, and immune-mediated clearance.
Alternatively, HBV genomes are transferred to murine hepatocytes via hydrodynamic injection, via an adenoviral vector (AdV) or adenovirus associated vector (AAV) transfer. The transfer via hydrodynamic injection is associated with hepatocyte damage and HBV replication is transient in these mice. As hydrodynamic injection of HBV DNA solves the problem of central tolerance occurring in HBV transgenic mice but does not effectively induce persistent HBV

infection, this model is preferably used to study acute, self-limiting infection and evaluation of its clearance[74, 76].

In contrast, the AdV- or AAV-mediated transfer approaches establish persistent HBV replication for months[77, 78]. Although HBV genome transfer approaches enable the study of an HBV transcription template elimination in immunocompetent mice, there is no actual HBV infection, and therefore the authentic transcription template, the HBV cccDNA, is not generated. Recently, a hydrodynamic injection (HI) model that supports cccDNA-dependent transcription was established. In this model, HBV-minicircle DNA, which is a close mimic to cccDNA, is injected into mice and can persist over months. The disadvantages of this model are hepatocyte damage induced by HI and incomplete reconstruction of the HBV life cycle[79].In contrast to immunocompetent mouse models, immunodeficient chimeric mice that contain human hepatocytes (referred to as “humanized” mice) are suitable to study viral infection, spread, and the nature of cccDNA[80]. However, immunodeficiency makes this model unsuitable for studying an immune response mounted against HBV.

1.2 Type I Interferons

The type I IFN family consists of 13 (in humans) or 14 (in mice) IFNα subtypes, one single IFNβ and several poorly defined IFNs[81]. Type I IFNs are produced by almost any cell type in response to the stimulation of pattern recognition receptors (PRRs) by virus-associated nucleic acids. Almost all nucleated cells produce IFNβ, while IFNα production is limited to specific cell types such as macrophages and dendric cells (DCs)[82]. During viral infections, type I IFNs induce a cell-intrinsic antiviral state in infected and neighboring cells and they initiate and modulate innate and adaptive antiviral immune responses.

1.2.1 Induction of type I IFNs

Pathogen-associated molecules like DNA, RNA, or double-stranded RNA (dsRNA) can be recognized by various PRRs located in either the cytosol, on the cell surface, or in endosomal compartments. Two complementary receptor systems account for most viral infection-induced induction of type I IFNs. The first receptor class, Toll like receptors (TLRs), are transmembrane proteins located in plasma membranes or endosomal membranes of specialized cell types like dendritic cells and macrophages. There are several different TLRs, which recognize different types of nucleic acids: Double-stranded RNA (dsRNA), which is a common feature of RNA and DNA viruses, is recognized by TLR3, single-stranded RNA (ssRNA) is detected by TLR7 and TLR8 and unmethylated CpG motifs in DNA, which is common in DNA viruses, is detected by TLR9. Unlike other TLRs, TLR3, 7, and 9, which signal from an acidified endosomal compartment, sample material entering cells from the outside and thus do not detect the

presence of viral infection from within. Further, this mode of detection does not require that the IFN-producing cells are infected themselves[83].

The second class of receptors, exemplified by RIG-I and MDA-5, are ubiquitously expressed and are located in the cytosol, where they detect intracellular viral nucleic acids. Thus, almost all nucleated cells produce type I IFNs in response to viral infections.

Cytosolic dsRNA is detected by RIG-I or MDA-5, which upon activation act with the adaptor mitochondrial antiviral signaling protein (MAVS) followed by phosphorylation of IRF3 and IRF7 resulting in the induction of IFNα and IFNβ. In addition to the recognition of intracellular dsRNA, foreign intracellular DNA is sensed by cyclic-GMP-AMP-synthase (cGAS)[84]. Interestingly, the signaling pathway downstream of cGAS is distinct from the pathways downstream of MDA-5 or RIG-I, suggesting the induction of distinct IFN response to DNA and RNA viruses[85, 86].

1.2.2 Type I IFN signaling

All IFNα subtypes and IFNβ signal through a heterodimeric transmembrane receptor termed IFNα receptor (IFNAR), which is composed of two subunits, IFNAR1 and IFNAR2. Engagement of the INFAR receptor activates the receptor-associated tyrosine kinases Janus kinase 1 (JAK1) and tyrosine kinase 2 (TYK2), which phosphorylate the cytosolic signal transducer and activator of transcription 1 (STAT1) and 2 (STAT2)[87]. During canonical type I IFN signaling tyrosine-phosphorylated STAT1 and two dimerize, translocate to the nucleus and assemble with IRF9 to form a complex named IFN-stimulated gene factor 3 (ISGF3). ISGF3 binds to IFN-stimulated response elements (ISREs) and induces transcription of several hundred IFN-stimulated genes (ISGs). This combination of genes is uniquely induced by canonical IFN signaling as most other cytokines or non-canonical type I IFN signaling induce STAT homodimers, which bind to a gamma activated factor (GAF) and thereby induce another distinct set of ISGs via binding of gamma activated sequences (GAS) upstream of ISGs. The components of the canonical type I IFN pathway are able to exert non-canonical activities, including tyrosine kinase-independent actions of JAKs, induction of transcriptional complexes other than ISGF3 or GAF and several actions of unphosphorylated STATs (U-STATs)[88]. Thus, ligation of INFAR can induce various different responses that are cell-type and context dependent[89]. The differing responses to IFNAR ligation are regulated on several levels. Magnitude and pattern of IFNAR signaling are modulated via expression levels of IFNAR and the posttranscriptional modifications of IFNAR or JAK-STAT signaling components. Further downstream, the induction of distinct ISGs is specified by the induction of transcription factors that cooperate with STATs and modulate chromatin states at target gene loci. Additionally, the magnitude of ISG protein expression is regulated depending on cellular factors that modify translation. And finally, there are several signals augmenting or suppressing type I IFN signaling and thereby fine-tune the response induced by IFNAR ligation[89].

1.2.3 Direct antiviral properties

Type I IFNs, produced by infected cells or non-infected DCs or macrophages that sensed extracellular viral nucleic acids, act in an autocrine and paracrine manner in order to activate the expression of hundreds of ISGs that together establish the so-called “antiviral state”. Even though the function of many ISGs is not resolved yet, several of those genes act to cripple every state of the viral life cycle. Several well-studied ISGs, exemplified by OAS-1 and PKR, act together to inhibit viral replication by inducing degradation of viral and host RNA transcripts (OAS-1) or by blocking translation of cellular and viral mRNAs (PKR) and thereby strongly reduce viral load and spread[90, 91]. Some ISGs, like PKR and OAS-1, were found to act non-specifically on various viruses, while other ISGs act only on particular viruses. Further, it was shown that type I IFN signaling sensitizes cells towards cell-intrinsic apoptosis upon subsequent viral infection[92,90].

1.2.4 Regulation of innate and adaptive immunity

Apart from their direct antiviral actions, type I IFNs are critical regulators of innate and adaptive immune responses. It was shown that during viral infections type I IFN signaling promotes expansion[93] and activation of NK cells and thereby enhances cytotoxic activity[94, 95]. Additionally, type I IFNs were reported to enhance activation and maturation of DCs, leading to increased cross-presentation of viral antigen, upregulation of co-stimulatory molecules, and increased migration to lymph nodes[96, 97, 98, 99]. Further, antigen presentation is enhanced by type I IFN mediated promotion of MHC class II synthesis and antigen processing[100]. Together, these IFN-mediated effects on DCs increase their ability to prime $CD8^+$ T cells. A study in the LCMV model revealed that $CD8^+$ T cells that lack IFNAR expression were strongly impaired in their ability to expand and differentiate into effector $CD8^+$ T cells. This result implies that type I IFNs directly act on $CD8^+$ T cells to promote their expansion and differentiation into effector cells[101]. An *in vitro* study conducted by Marrack *et al.* shows that type I IFN acts as a survival factor for activated T cells[102].

1.2.5 Context-dependent actions of type I IFNs

Type I IFNs have long been considered as the key to effective antiviral responses by inducing an antiviral state in infected cells and neighboring cells and by the potentiation of innate and adaptive immune responses. However, most observations were made in the context of acute, self-limiting infections. There is an increasing number of studies reporting deleterious immunomodulatory effects of type I IFNs, depending on the context of IFN signaling. Two independent studies revealed that prolonged type I IFN signaling during chronic LCMV infection promotes viral persistence[103, 104]. In these studies, DCs were shown to exhibit an immunoregulatory phenotype characterized by PDL1 expression and IL10 production. Further, an IFN-mediated negative regulation of virus-specific $CD4^+$ T cells was reported[105]. These

studies suggest deleterious immunomodulatory effects of type I IFNs evoked by prolonged IFN stimulation.

The outcome of type I IFN signaling seems to depend on the presence of other cues like, for example, co-stimulatory signals or the presence of viral antigen[83]. This context-dependent outcome of type I IFN signaling was extensively studied for direct actions of type I IFNs on $CD8^+$ T cells. It was shown that type I IFNs act as potent signal three cytokines during T cell activation when TCR stimulation coincides or shortly precedes IFNAR stimulation. In contrast, when IFNAR signaling precedes TCR engagement, $CD8^+$ T cells are negatively regulated by IFN-mediated induction of anti-proliferative or pro-apoptotic signals in T cells[106, 107]. The differing direct effects of type I IFNs on $CD8^+$ T cells depending on the relative timing to TCR engagement can be explained by the intracellular composition of the different STATs at the time of IFNAR engagement. Signaling via STAT1 is known to be pro-inflammatory, pro-apoptotic, and anti-proliferative while signaling through STAT3,4 and 5 is pro-survival, pro-proliferative and pro-differentiation[87, 108, 109, 110]. Type I IFNs have the unique ability to activate all 7 STATs, and thereby many different homodimer and heterodimer complexes can be formed in response to INFAR engagement depending on the intracellular composition of different STATs.

1.3 T cell exhaustion in chronic viral infection

T cell exhaustion is a term that describes the hyporesponsive state of effector T cells during chronic antigen stimulation in the setting of chronic viral infections or cancer and appears to result from the accumulation of multiple signals or pathways that negatively regulates T cell responses. In order to persist, viruses need to evade sterilizing immunity, defined as the complete elimination of a virus, and survival of the host needs to be assured. Therefore, the host's immune system needs to balance the continuous antigen-driven inflammatory response in order to control viral replication to an acceptable level without causing too strong immunopathology. Viruses employ different strategies to establish chronic infections, namely continuous replication and latency. Latency, a strategy used by Epstein-Barr virus (EBV), human immunodeficiency virus (HIV), or herpesviruses, for instance, is a unique transcriptional and translational state of a virus, in which the viral replication cycle is silent but can reinitiate. Such latent virus-infected cells are not recognized by the immune system and cannot be cleared unless the virus is reactivated[111].

A different strategy is a continuous replication despite ongoing antiviral immunity, employed by HBV, HCV, and HIV in humans, SIV in nonhuman primates, and LCMV in mice. These viruses express high amounts of potential antigenic viral proteins resulting in continuous antigenic stimulation of the host's immune system[111]. Since $CD8^+$ T cells control viral infection by killing infected cells or producing pro-inflammatory cytokines capable of causing excessive

immunopathology, negative regulation of $CD8^+$ T cells is particularly crucial in infections with high numbers of infected cells in order to prevent fatal immunopathology.

Exhausted T cells (Tex) are by now referred to as a unique immune cell type, which functionally differs from effector T cells (Teff) and memory T cells (Tmem). Tex are defined by loss or partial loss of effector functions and proliferative potential, expression of multiple inhibitory receptors, skewed metabolism, and an altered epigenetic and transcriptional program. During exhaustion, loss of function occurs in a hierarchical manner: First, T cells lose their ability to produce IL-2, to proliferate or to exert killing ex vivo. More severely exhausted T cells further lose their ability to produce TNF and IFNy and to degranulate. And the final state of T cell exhaustion is their physical deletion[112].

There are three categories of negative regulatory pathways playing a central role in T cell exhaustion: Cell surface inhibitory receptors, immunoregulatory cytokines, and immunoregulatory cell types. Although the expression of inhibitory receptors is a crucial feature of exhausted T cells, their expression is not unique to exhausted T cells. While inhibitory receptors are transiently upregulated during $CD8^+$ T cell responses in acute, self-limiting viral infections, prolonged high-level expression of inhibitory receptors is a hallmark of exhausted T cells[111]. One important and the most prominent inhibitory receptor is PD1. Blocking PD1 signaling during chronic LCMV infection reinvigorated exhausted $CD8^+$ T cells and resulted in a lower viral load[113]. In addition to PD1, many other inhibitory receptors like Lag3, TIGIT, Tim3, CD244 (2B4), CTLA4, and CD160, regulate or co-regulate T cell exhaustion[114, 115]. Further, immunoregulatory cytokines like IL-10[116, 117, 118] or TGFβ[119] and immunoregulatory cells like Tregs[120] influence T cell exhaustion.

Although Tex cells are referred to as dysfunctional, several findings indicate that they retain residual functions. Their effector functions seem suboptimal, but crucial in limiting ongoing pathogen replication or tumor progression. The depletion of $CD8^+$ T cells during chronic SIV infection led to increased viremia and enhanced progression to AIDS[121, 122]. In addition, $CD8^+$ T cells from patients with chronic HCV infection were demonstrated to contribute to liver damage during the course of infection[123, 124]. It is proposed that T cell exhaustion is an important mechanism, which protects the host against tissue damage[125]. The rationale for T cell exhaustion may be to establish a host-pathogen stalemate. However, some pathogens exploit this mechanism for enhanced replication and spreading.

1.3.1 Development of T cell exhaustion

Antigen-specific T cells in ongoing chronic infections are continuously exposed to antigen and gradually progress from early Tex cells to terminal Tex cells[126]. Terminal differentiation is defined as loss of multipotency, proliferative capacity, and telomerase activity. Therefore, it is assumed that terminal Tex lost their potential to differentiate to fully functional effector T cells or memory T cells and are thereby irrevocably fixed to their hypofunctional state until cell

death[127, 128]. Although our understanding of the complex molecular mechanisms underlying T cell exhaustion is progressing, the pathways involved in the initial development of T cell exhaustion remain poorly understood. There is evidence that persistent infections begin with massive expansion and acquisition of T cell effector functions, suggesting the existence of a transient acute phase in chronic infections[129, 130, 131]. The failure to eradicate the virus leads to a prolonged phase of antigen exposure and inflammation, resulting in the development of Tex. Early Tex or Tex precursor arise from the pool of KLRG-1^{lo} CD127^{hi} memory precursor effector cell pool (MPEC), the same pool, which also gives rise to Tmem following acute infections[128]. During persistent antigen stimulation and inflammation, MPECs develop into early Tex/ Tex precursor instead of Tmem or resident memory T cells Trm and progressively lose their memory potential ending up in terminal Tex (Fig 1.3)[128].

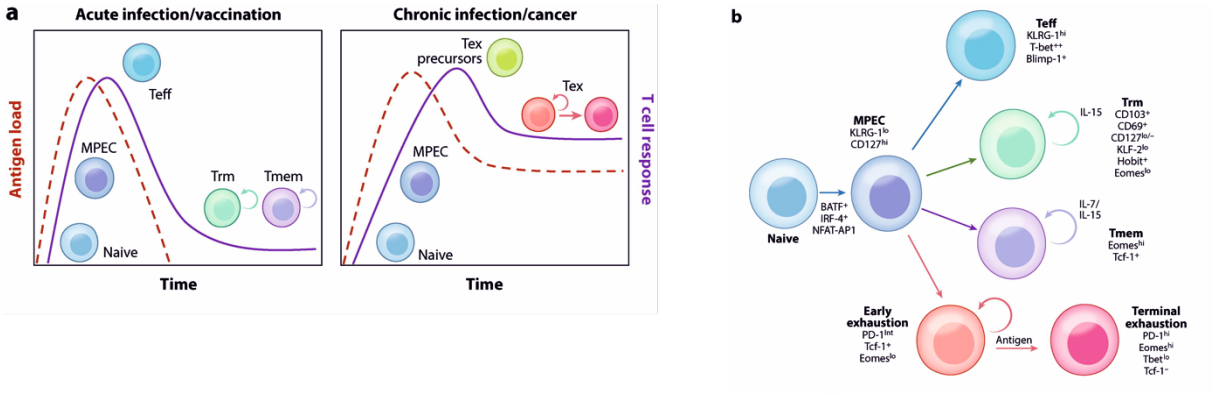

Figure 1.3| Development of exhausted CD8⁺ T cells (Tex)
(A) After priming of naïve CD8⁺ T cells, a pool of KLRG1^{lo}CD127^{hi}memory precursor effector cells (MPECs) arises. During acute infections/vaccination MPECs develop into terminal effector cells (Teff). After the elimination of viral antigen, remaining MPEC differentiate into memory T cells (Tmem) or tissue-resident memory T cells (Trm). In chronic viral infections or cancer, Tex precursor fail to entirely clear antigen and further differentiate into early Tex that retain some proliferative potential. In the context of persistent antigen, cells of the early Tex pool differentiate further into terminal exhausted T cells (terminal Tex). (B) After initial antigen-driven activation of naïve T cells, a pool of memory precursor effector cells (MPECs) arise, which can follow multiple paths of differentiation. In acute infections, MPECs differentiate into fully functional Teff or after antigen clearance into Tmem or Trm. Early Tex form during chronic infections in a setting of persistent antigen. Those early Teff are PD1^{int}, Eomes^{hi}, TCF1^{+}. Those early Tex give rise to terminal Tex, which are characterized by high levels of PD1 and Eomes and loss of TCF1 and thereby their potential to proliferate upon additional antigen stimulation. Modified from: [126]

A negative correlation between level and duration of antigen exposure and CD8⁺ T cell function has been shown for several chronic infections in humans and mice[132, 133, 134, 135, 136, 137, 138, 139], suggesting that high antigen load and prolonged antigen exposure lead to T cell exhaustion[112, 134, 138, 140]. Furthermore, exhausted CD8⁺ T cells are mainly detected in persistent infections with high antigen load like LCMV, HCV, HIV, and untreated, viremic HBV[62, 141, 142]. A study by Richter *et al.* demonstrates that alterations of antigen levels can substantially influence CD8⁺ T cell function. This study suggests a scenario in which not the cell type presenting the antigen, but the overall amount of antigen dictates the functionality of CD8⁺ T cells[137]. However, apart

from this single study in mice using the LCMV infection model, little is known about the timing and context of antigen sensing that influences $CD8^+$ T cell function.

Adoptive transfer approaches in the LCMV infection model revealed that $CD8^+$ T cells primed in a chronic setting could recover and differentiate into fully functional memory $CD8^+$ T cells when transferred into uninfected mice between weeks 1 and 3 after infection. In contrast, exposure longer than three weeks to antigen in chronically infected animals prevents restoration of normal $CD8^+$ T cell function after transfer into uninfected mice[127, 128]. These results suggest that T cell exhaustion is not irreversibly imprinted during priming but develops and progresses over time.

Although continuous high antigen stimulation seems to be the main factor of T cell exhaustion, other factors like the absence of $CD4^+$ T cell help, immunoregulatory cells, soluble factors, or inhibitory receptor signals clearly contribute to development and progression of exhaustion. While memory precursor T cells or Tmem were shown to develop preferentially in a less pro-inflammatory environment[143], Tex are suggested to preferentially develop in a pro-inflammatory environment typically present in chronic infections or cancer. High levels of pro-inflammatory cytokines in chronic infections or cancer were shown to induce the release of negative regulatory cytokines. However, it was shown that a pro-inflammatory milieu alone is not sufficient to drive T cell exhaustion[144]. Nevertheless, IL-10 and TGFβ were shown to promote T cell exhaustion, as blocking of both resulted in enhanced viral control[116, 119, 145, 146].

1.3.2 Tex subpopulations

Tex were shown to represent a heterogeneous cell population with a differing degree of functionality and proliferation potential. PD1 and CD44 have been the first marker to distinguish the functionality of Tex. It was shown that the $PD1^{hi}CD44^{int}$ Tex subset was more exhausted than the $PD1^{int}CD44^{hi}$ subset[114]. Further studies revealed that the more functional $PD1^{int}CD44^{hi}$ subset additionally express low levels of the transcription factor Eomes and high levels of the transcription factor T-bet. Adoptive transfer experiments then demonstrated that the $PD1^{int}CD44^{hi}Eomes^{lo}Tbet^{hi}$ subset has a high proliferative potential and give rise to $PD1^{high}CD44^{int}Eomes^{hi}Tbet^{lo}$ progeny with impaired proliferative potential[147]. Utzschneider *et al.*[148] demonstrated the existence of virus-specific $CD8^+$ T cells expressing the transcription factor TCF1 with a stem-cell-like activity that sustained the ongoing immune response during chronic LCMV infection. The authors further showed that the $TCF1^+$ subpopulation of LCMV specific $CD8^+$ T cells generated during a chronic LCMV infection re-expanded and controlled a viral infection upon adoptive transfer into naïve mice[149]. In summary, the $TCF1^+$ Tex subpopulation lacks the characteristic signature of effector T cells, share multiple molecular and functional properties with central memory cells, display an exhausted phenotype, and produce more differentiated progeny.

Recently, it was shown by Chen *et al*..[150] that the transcription factor TCF1 is critical for the initial development of Tex precursor cells instead of KLRG1^{hi} Teff. Furthermore, they demonstrated that PD1 supports the development of Tex precursor cells early during chronic infection.

1.3.3 Restoration of antiviral T cell response

The concept of functional restoration of the host's antiviral immune response has been confirmed already in a study published 1962, where the authors proved that the adoptive transfer of functional virus-specific T cells controlled an established persistent LCMV infection[151].

Immune checkpoint inhibition (ICI) via blockade of the PD1-PDL1 interaction was demonstrated to restore antiviral CD8$^+$ T cell responses in chronic LCMV infection[113], in SIV-infected macaques[152] and during HCV infection in patients[153, 154]. Further investigations revealed that responsiveness to PD1 blockade was influenced by the severity of exhaustion and the abundance of antiviral T cells as T cells with the highest levels of PD1 were shown to be unresponsive to PD1-blockade[155, 156] probably explaining the variable success of ICI therapy.

In cancer settings, different Immune checkpoint inhibitors were shown to reinvigorate anti-tumor immune responses and promote CD8$^+$ T cell mediated elimination of tumor cells and are today successfully used to treat multiple cancers. However, low response rates and immune-mediated adverse effects in some patients obstruct mainstream ICI therapy[157].

Cytokines can also be therapeutically targeted to restore antiviral T cell responses. The application of recombinant IL-2[158] or IL-7[159] enhanced antiviral T cell response in a model of chronic LCMV infection. Similarly, blocking the immunosuppressive IL-10 receptor reduced the extent of CD8$^+$ T cell exhaustion and improved viral control during chronic LCMV infection[160, 161].

Importantly, all these preclinical and clinical studies demonstrated the recovery of exhausted T cell responses, indicating that T cell responses are downregulated rather than being terminated during chronic infections. As effector T cell responses are sustained over long periods of time during chronic infections, it is likely that there is either recruitment of naïve T cell clones from the thymus or a pool of memory T cells that replenish the pool of terminal differentiated Tex. While the recruitment of T cells from the thymus during chronic infection has been described[162], the development of memory T cells during chronic viral infection is controversial. There is evidence that virus-specific CD8$^+$ T cells during chronic LCMV infection fail to develop virus-specific memory T cells with the ability of antigen-independent long-term persistence[163, 164]. Recently, a TCF1$^+$ population within the total population of virus-specific CD8$^+$ T cells with a strong re-expansion potential, and the ability of antigen-independent

retention that is maintained during chronic LCMV infection was described[149]. Further, this TCF^+ population was shown to be the target for therapeutic interventions[165].

1.4 Immunotherapeutic strategies for the treatment of chronic HBV

Immunotherapies aim to reinvigorate exhausted, dysfunctional innate and adaptive immune responses to cure chronic diseases like cancer or chronic infections. It was observed that in CHB patients, which received a bone marrow transplant from donors that resolved HBV infection, a functional cure could be achieved[166, 167]. This observation revealed that immune-mediated control of HBV is generally possible in CHB patients. The association of a potent HBV-specific $CD8^+$ T cell response in patients with the clearance of HBV[16] renders HBV infection a suitable target for immunotherapy.

1.4.1 Immunotherapeutic strategies targeting innate immunity

The innate immune system is poorly activated during natural acute or chronic HBV infection due to mechanisms discussed in section 1.1.2. However, HBV is efficiently suppressed by innate effector molecules. It was, for instance, reported that activation of RIG-1 or ABOBEC3A/B deaminase efficiently suppresses HBV replication[168, 169]. Additionally, studies of hepatic co-infections with viruses like HCV or HDV, which efficiently trigger innate immunity, demonstrated that innate immunity could efficiently suppress HBV replication or even eradicate HBV from infected hepatocytes[170, 171].

To boost innate immunity, RIG-I or TLR agonists have been developed to trigger the release of antiviral cytokines from hepatocytes (RIG-I agonists) or neighboring immune cells (TLR agonists)[172]. GS-9620, a TLR7 agonist that was shown to induce IFNα from plasmacytoid dendritic cells (pDCs), showed induction of anti-HBV activity when administered to HBV-infected chimpanzees or WHV-infected woodchucks[173, 174]. In a phase I/II clinical trial, administration of GS-9620 was without side effects but also without robust induction of antiviral immunity[175]. TLR8 agonists were shown to more potently induce secretion of IL-12 and IL-18 via activation of PRRs in the liver and thereby evoke an enhanced IFNy response[176]. Il-12 has been shown to promote recovery of exhausted HBV-specific T cells suggesting that TLR agonists may instead of only trigger the release of antiviral cytokines also stimulate antiviral HBV-specific T cell response[177]. Currently, several oral TLR7/8 agonists are in clinical trials phase I or II.

1.4.2 IFNα-based Immunotherapy

IFNα/ PEG-IFNα provides a dual mode of action, antiviral via inhibition of viral replication and immunomodulation via stimulation of innate and adaptive immunity. Several direct antiviral actions of IFNα like inhibition of HBV transcription[178] or inhibition of HBV replication via

prevention of HBV RNA containing capsid formation or accelerated decay of replication-competent nucleocapsids[56, 178, 179, 180, 181] have been demonstrated *in vitro* or in HBV transgenic mice. However, the slow kinetics of HBV DNA inhibition after the start of IFN-based therapy revealed a limited antiviral potency in patients[182]. The success of IFN-based therapy in CHB is more likely associated with its immunomodulatory effects[183, 184]. However, very little information is available about a possible IFNα-mediated restoration of innate and adaptive immunity in CHB. A study in the woodchuck model demonstrated the induction of a T/NK cell signature in the liver after IFNα therapy, that correlates with treatment outcome[185]. In HBeAg-negative CHB patients with long-term response to IFNα and HBsAg clearance, the *in vitro* reactivity of T cells appeared to be restored[186]. Furthermore, patients showing higher $CD8^+$ T cell function and higher IFNα at baseline were more likely to show complete viral inhibition early during treatment, suggesting a significant role of adaptive immunity in the overall response to IFNα-based therapy[186].Studies evaluating peripheral HBV-specific $CD8^+$ T cells in IFNα/ PEG-IFNα-treated patients, during treatment or in the first six months after discontinuation of treatment, could not show any restoration of effector functions[183, 187].

As PEG-IFNα has limited response rates and severe side effects in some patients, an accurate prediction of treatment response would optimize and increase its clinical use. Several host and HBV biomarkers, such as HBV genotype, HBeAg status, serum HBsAg levels, HBV DNA level, and ALT level, have been identified to be associated with treatment response to PEG-IFNα[21, 188, 189, 190]. Nevertheless, the use of baseline predictors (HBeAg status, HBsAg level, HBV DNA level) is limited due to the low precision of prediction.

1.4.3 TLR3-stimulation based Immunotherapy

Polyinosic:polycytidylic acid (PolyI:C) is a synthetic analog of virus-derived double-stranded RNA (dsRNA) and is used as a potent inducer of type I IFNs. PolyI:C was reported to be sensed by TLR3[191, 192], RIG-I, MDA-5, and PKR[193, 194, 195, 196]. Though the recruitment of different adaptor molecules, engagement of TLR3, MDA-5, and RIG-1 activate partially the same transcription factors downstream, including IRF3, IRF7, and NFκb. Besides a strong induction of type I IFNs, several pro- and anti-inflammatory cytokines and co-stimulatory molecules are induced upon polyI:C stimulation[197].

Using the Ovalbumine-OT-1 system, PolyI:C has been shown to enhance both primary and memory $CD8^+$ T cell responses[198]. TLR-signaling induces pro-inflammatory cytokines and chemokines and the maturation of dendritic cells[199, 200, 201] together, promoting the activation of cytotoxic $CD8^+$ T cells and NK cells[201, 202, 203]. However, it was also shown that $CD8^+$ T cells could directly respond to polyI:C[204] suggesting a direct effect of polyI:C on adaptive immune responses.

Concerning the effects of polyI:C on HBV, it was demonstrated that injection of polyI:C inhibited HBV replication in HBV transgenic mice in a type I IFN dependent manner[205]. TLR3 stimulation was shown to potently induce IFNβ production by parenchymal (hepatocytes) and non-parenchymal (Kupffer cells, LSECs) cells of the liver. Further, the polyI:C mediated effect on HBV replication was shown to be exclusively mediated through IFNβ[206]. A study conducted by Wu *et al.* revealed that hydrodynamic injection of polyI:C in immunocompetent mice with an established chronic HBV infection leads to HBV clearance in an IFN type I, IFN type II and CXCR3 dependent manner. The dependence on IFN type II and CXCR3 and an increase in T cell marker in the liver indicate that HI of polyI:C enhances HBV-specific $CD8^+$ T cell immunity in chronically HBV infected mice[207].

1.4.4 Immunotherapeutic strategies targeting adaptive immunity

$CD8^+$ T cells were identified to play a crucial role during antiviral immune response in patients with acute self-limiting HBV infection and are therefore targeted by various immunotherapeutic strategies. Most approaches, like immune checkpoint blockade or therapeutic vaccinations, are designed to restore defective, dysfunctional HBV-specific $CD8^+$ T cells present in chronically infected patients. In contrast, adoptive T cell transfer approaches aim to engineer new HBV-specific $CD8^+$ T cells that can be adoptively transferred into chronic HBV carriers.

1.4.4.1 Immune Checkpoint Inhibitors

The high expression of inhibitory receptors on $CD8^+$ T cells in chronically HBV infected patients suggests a possible role for checkpoint inhibitors in CHB. A study conducted by Boni *et al*. demonstrated that HBV-specific $CD8^+$ T cells are more likely to be detected in patients with low viremia. The function of those cells was partly restored using checkpoint inhibitors (anti PD1, anti CTLA4) *in vitro*[62, 208, 209]. These results suggested that treatment with checkpoint inhibitors should be preceded by a reduction of antigen load via NA administration. However, results from clinical trials phase I/II were disappointing. An open-label, noncomparative, phase 1/2 dose escalation and expansion trial of nivolumab in patients with advanced HCC (CheckMate 040) could not achieve functional cure in any patient[210]. Another phase I clinical trial has been performed injecting one dose Nivolumab (anti-PD1) in HBeAg negative chronic HBV carrier under NA treatment with or without injection of therapeutic vaccine. Although there were no severe adverse effects reported, a reduction of HBsAg was only observed in a limited proportion of patients, and only one patient achieved a complete and persistent loss of HBsAg[211]. Overall, despite great success in multiple cancer settings and some encouraging *in vitro* results for HBV, the eradication of HBV with checkpoint inhibitors still appears unrealistic.

1.4.4.2 Therapeutic vaccination

The aim of therapeutic vaccination in chronic viral infections is to boost the patient's dysfunctional immune response towards virus-infected cells. *In vitro*, therapeutic vaccination strategies were shown to partially restore anti-HBV immunity[212]. However, all results from clinical trials in patients with various different formulations demonstrated only minor antiviral effects. DNA-based vaccines[213, 214], existing prophylactic vaccines[215], therapeutic vaccines combined with antivirals[216, 217], and new vaccine formulations[218] have not been effective in patients. Also, therapeutic vaccine approaches that demonstrated an excellent antiviral response in chimpanzees[219] displayed disappointing results in patients[220]. A new heterologous prime-boost strategy demonstrated promising results in HBV transgenic mice[221]. Here, a protein prime using recombinant HBsAg, HBcAg and an adjuvant induces antibodies that capture viral antigens and primes $CD4^+$ and $CD8^+$ T cells. The subsequent vector-boost vaccination using a modified vaccinia virus Ankara (MVA) expressing HBV envelope and core proteins then amplifies HBV-specific T cell responses. This specific combination of protein-prime and vector-boost was able to overcome HBV-specific tolerance in HBV transgenic mice with low and medium antigen levels, but not with high antigenemia. Recently, Michler and Kosinska et al.[222] demonstrated efficient control of CHB in high-antigenemic carrier mice combining knockdown of HBV antigen expression using shRNA or siRNAs against the common 3'-end of all HBV transcripts in combination with the vaccination strategy described by Backes *et al.*[221].

1.4.4.3 Adoptive T cell transfer

The idea of adoptive T cell transfer is to redirect the patient's own T cells towards a particular target. Therefore, patients' peripheral blood mononuclear cells (PBMC) are extracted by apheresis, then T cells are expanded or manipulated ex vivo and subsequently re-infused into the patient. Adoptive transfer of T cells armed with a TCR with the desired specificity is achieved by either selecting for T cells with desired specificities (e.g., tumor-infiltrating lymphocytes, TILs) or by modifying patients T cells. T cells are modified to express either a natural TCR with desired specificity or a chimeric antigen receptor (CAR). This strategy is supported by clinical evidence that patients with chronic HBV infection receiving a bone marrow transplant from a donor with an HBV-specific T cell response, control HBV infection after transplantation[166, 167]. Although attempts of adoptive T cell transfer in HBV transgenic mice[223] and in patients with relapse of HBV-related HCC[224] demonstrated encouraging results, clinical management in the setting of chronic HBV infection is technically challenging and difficult to apply for a large number of patients.

1.5 Aim of the study

Restoration of HBV-specific $CD8^+$ T cell immunity is assumed to be essential to achieve sustained off-treatment control of HBV infection. However, studies concerning HBV-specific $CD8^+$ T cell responses are hampered by bad accessibility of intrahepatic HBV-specific $CD8^+$ T cells in patients, low quantities of peripheral HBV-specific $CD8^+$ T cells in patients, and the lack of appropriate immunocompetent animal models. As a result, the restoration of HBV-specific $CD8^+$ T cell immunity could not be shown in patients yet, and the mechanism underlying reinvigoration of exhausted HBV-specific $CD8^+$ T cells remains unclear. Because IFNα-based therapies achieve sustained off-treatment control in a limited number of CHB patients and are therefore assumed to restore adaptive HBV-specific immunity, type I IFNs appear to be an interesting tool. Type I IFNs provide a dual mode of action, combining antigen reduction via direct antiviral actions and immunomodulation. In order to distinguish between both modes of action, I used a new adenoviral vector-based model of HBV infection in immunocompetent mice, which allows sensitive and non-invasive assessment of intracellular HBV antigen load. Using the Ad-HBV-Luc vector to establish persistent HBV infection in immunocompetent mice and two different strategies to induce type I IFNs in the liver, I aim to demonstrate the potential of type I IFNs to restore HBV-specific $CD8^+$ T cell immunity during chronic HBV infection. Further, I addressed the question whether both actions of type I IFNs, antigen reduction and immunostimulation, are required for the restoration of HBV-specific $CD8^+$ T cell immunity during chronic HBV infection

2. RESULTS

2.1 Implementation of a new *in vivo* model to study the impact of antigen load on anti-HBV immunity

To tackle the connection between HBV antigen load and functionality of HBV-specific $CD8^+$ T cells in the liver, it is crucial to reduce variability and unknown variables. Therefore, demands on the infection model are (1) establishment of infections with highly reproducible antigen loads, (2) resolution of intracellular vs. secreted vs. presented antigen load, (3) sensitive tracking of viral antigen load in real-time and (3) accessibility of liver resident HBV-specific $CD8^+$ T cells.

In order to overcome the limitations inherent in patient material or large animal models like chimpanzees, HBV genomes were delivered via adenoviral vector transfer into immunocompetent mice. To this end, a new adenoviral vector named Ad-HBV-Luc was generated via modification of the established adenoviral vector Ad-HBV1.3[225].

2.1.1 Validation of Ad-HBV-Luc i*n vivo*

The Ad-HBV-Luc vector (Fig 2.1 A) was used to deliver the HBV1.3 over-length genome combined with the reporter gene luciferase controlled by the HBV core-promoter into murine hepatocytes. As the sequence of the click beetle green (CBG) luciferase is coupled via a T2A sequence behind the second incomplete HBcore protein sequence, an equimolar expression of CBG luciferase and HBV core protein is assumed. The luciferase reporter protein allows non-invasive and frequent detection of Ad-HBV-Luc infection via bioluminescence imaging of the liver (Fig 2.1 B). Detection of pgRNA (3.2 kb), preS/S RNA (2.4/2.1 kb), and HBV DNA in liver tissue (Fig 2.1 C, E) and detection of HBeAg and HBsAg (Fig 2.1 D) in the serum of Ad-HBV-Luc infected mice demonstrated that the HBV1.3 genome remained intact. Further, detection of HBV DNA in the serum of Ad-HBV-Luc infected mice (Fig 2.1 E) revealed that HBV1.3 remained replicative, even though at lower levels compared to Ad-HBV1.3.

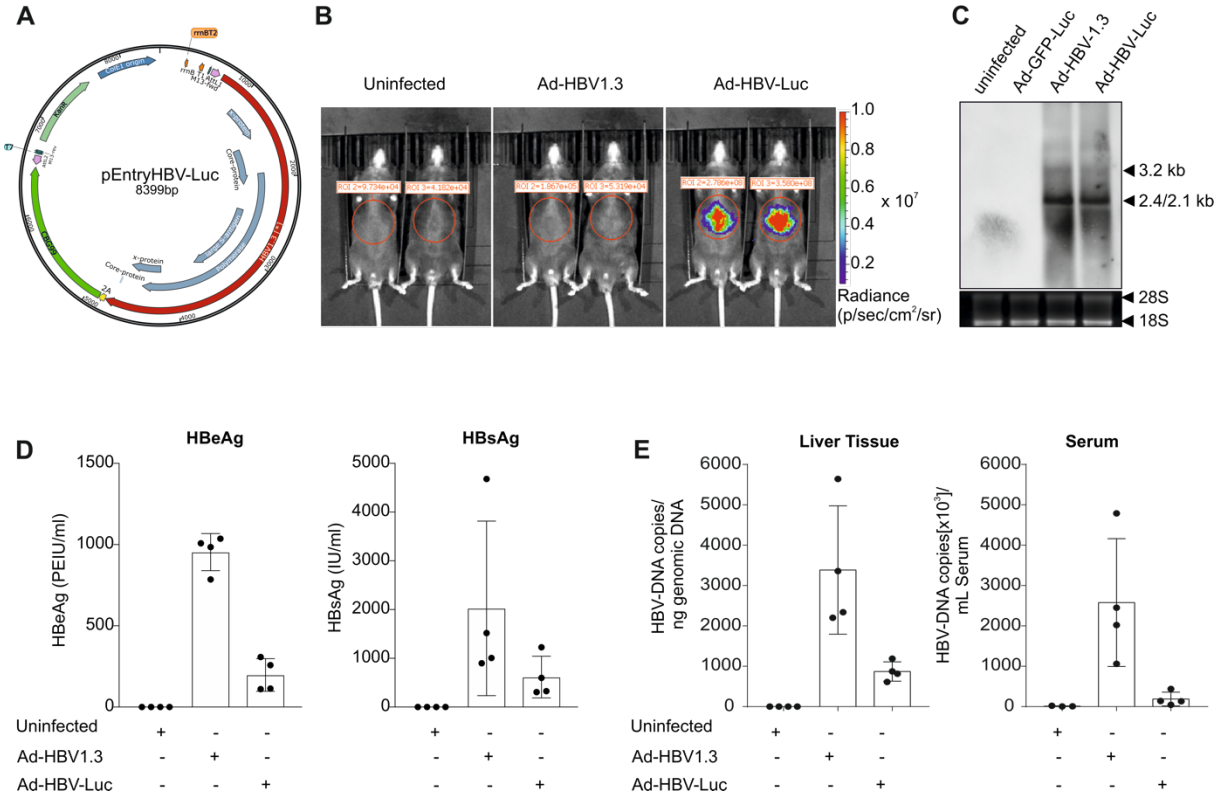

Figure 2.1| Validation of Ad-HBV-Luc *in vivo*
A) Plasmid map of the pEntry-HBV-Luc: In the pEntryHBV-Luc, the click beetle green (CBG) Luciferase sequence is coupled via T2A sequence to the second incomplete sequence of the HBcore protein in the HBV1.3 overlength construct. (B) Bioluminescence imaging of uninfected mice, mice, infected with Ad-HBV1.3 (5x 10^8 pfu), or Ad-HBV-Luc (5x 10^8 pfu) at day 8 p.i.. (C) Northern Blot analysis of total liver RNA from mice infected with 5x 10^8 pfu Ad-GFP-Luc, Ad-HBV or Ad-HBV-Luc for eight days. 28S and 18S ribosomal RNAs served as a loading control and were detected by exposition to ultraviolet light for 0.6 s. HBV-specific fragments with 3.2 kB (pgRNA) and 2.4/2.1 kb (preS/S RNA) length were detected using an HBV-specific probe. Chemiluminescence signal was recorded for 3 min. (D) Quantification of HBeAg and HBsAg in the serum of mice treated as in (B). (E) Quantification of HBV DNA copies in liver tissue or in the serum of mice treated as in (B). Mean and SD are shown (n=4).

The injected infectious dose correlated with bioluminescence signals measured in the liver (Fig 2.2 A) and with HBeAg levels measured in the blood (Fig 2.2 B). Importantly, the nearly perfect correlation between HBeAg levels measured in the blood and bioluminescence signals in the liver of mice (Fig 2.2 C) indicates that bioluminescence measurement accurately reflects serologically assessed HBV parameters.

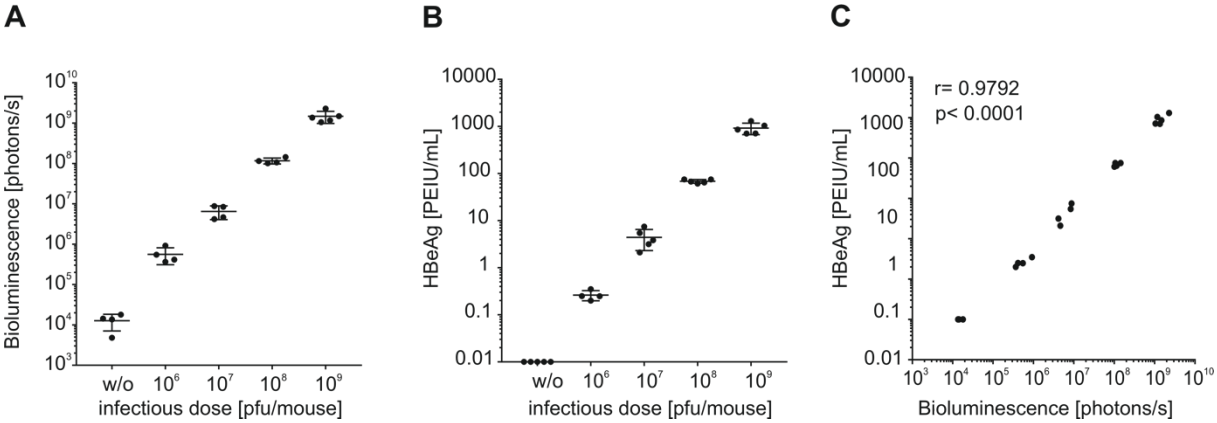

Figure 2.2| Dose-dependency of Ad-HBV-Luc *in vivo*
A) Quantification of bioluminescence signal in mice at day 7 p.i. with the indicated dose of Ad-HBV-Luc. B) HBeAg measured in the serum at day 7 of mice from (A). (C) Correlation between HBeAg from (B) and bioluminescence levels from (A). Mean and SD are shown (n=4-5).

Following the transfer of Ad-HBV-Luc into mice, several parameters of HBV infection were detected in liver tissue or serum of mice, and HBV1.3 remained replicative. Further, in vivo bioluminescence signals accurately reflect serologically assessed HBV parameters. Taken together, these results suggest that the Ad-HBV-Luc vector is well-suited to investigate the impact of intrahepatic antigen during HBV infection in immunocompetent mice.

2.1.2 Infectious dose-dependent outcome of infection

Dose-titration revealed the elimination of Ad-HBV-Luc at an infectious dose of 1 x 10^7 pfu and persistence at doses higher than 1 x 10^8 pfu. To this end, immunocompetent C57Bl/6J mice were intravenously (i.v.) infected with 1 x 10^7 or 1 x 10^8 pfu Ad-HBV-Luc. Bioluminescence signal in the liver (Fig 2.3 A, B), serum alanine aminotransferase (sALT) levels (Fig 2.3 C), and serum HBeAg levels (Fig 2.3 D) were monitored over 30 days to determine the course of infection.

In the high dose infection setting (10^8 pfu), stable bioluminescence signals and stable HBeAg levels were observed from day two p.i. onwards (Fig 2.3 B, D). Serum ALT levels were slightly elevated during the complete course of high dose infection (Figure 2.3 C). Relative expression levels of pregenomic RNA (pgRNA) remained unchanged from day 10 to day 30 p.i. (Fig 2.3 E). In the lower dose infection setting (10^7 pfu), serum HBeAg was undetectable from day 20 p.i. onwards (Fig 2.3 D) and bioluminescence signal in the liver was down to detection limit from day 27 p.i. onwards (Fig 2.3 B). A transient, substantial increase of sALT levels around day 15 p.i. (Fig 2.3 C) preceded the loss of serum HBeAg and bioluminescence signal in the liver. Additionally, in liver tissue of mice infected with the low dose Ad-HBV-Luc, pgRNA was not detectable any longer in liver tissue at day 30 post infection (Fig 2.3 E). As pgRNA is considered as a marker for active HBV replication, we propose that there is no ongoing HBV replication at day 30 p.I in mice infected with the low dose of Ad-HBV-Luc.

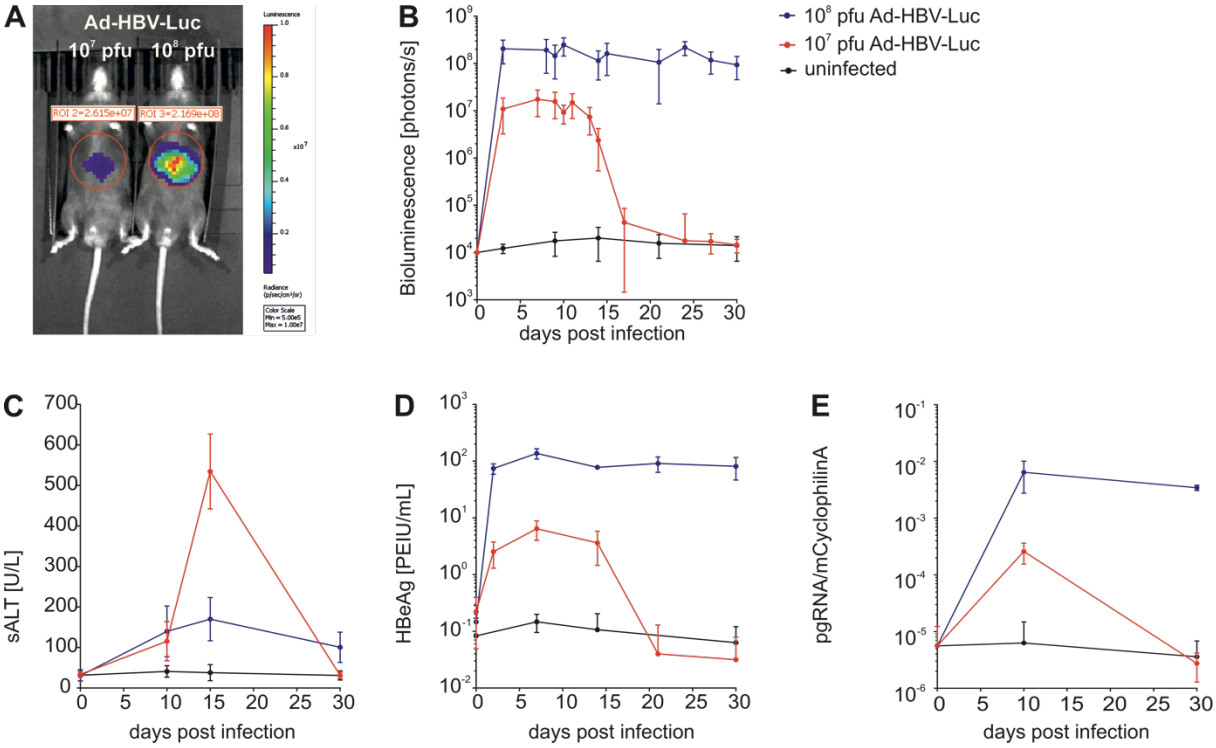

Figure 2.3| Infectious dose-dependent outcome of Ad-HBV-Luc infection in immunocompetent mice
(A) Quantification of bioluminescence signal in the liver of mice after infection with the acute, self-limiting (10^7 pfu) or chronic infectious dose (10^8 pfu) of Ad-HBV-Luc. (B) Kinetics of HBeAg levels in the blood after infection with the acute, self-limiting (10^7 pfu) or chronic infectious dose (10^8 pfu) of Ad-HBV-Luc. (C) Kinetics of serum ALT levels in the blood after infection with the acute, self-limiting (10^7 pfu) or chronic infectious dose (10^8 pfu) of Ad-HBV-Luc. (D) Levels of HBeAg in the serum of mice after infection with the acute, self-limiting (10^7 pfu) or chronic infectious dose (10^8 pfu) of Ad-HBV-Luc (E)Levels of pgRNA in liver tissue of mice after infection with the acute, self-limiting (10^7 pfu) or chronic infectious dose (10^8 pfu) of Ad-HBV-Luc relative to Cyclophilin determined by qPCR. Mean and SD are shown (n=5).

These results indicate that the low dose of Ad-HBV-Luc (10^7 pfu) is eliminated in an acute, self-limiting course and that infection with a higher dose (10^8 pfu) establishes persistent infections. In order to unravel the role of the immune system during low-dose elimination of Ad-HBV-Luc infection, $CD8^+$ T cells were depleted in mice infected with the acute, self-limiting dose of Ad-HBV-Luc (Fig 2.4 A). The depletion of $CD8^+$ T cells led to a stable bioluminescence signal in mice (Fig 2.4 B). These data demonstrate that $CD8^+$ T cells were required for the control of Ad-HBV-Luc infection, which was already demonstrated before for wildtype HBV infection in chimpanzees [44].

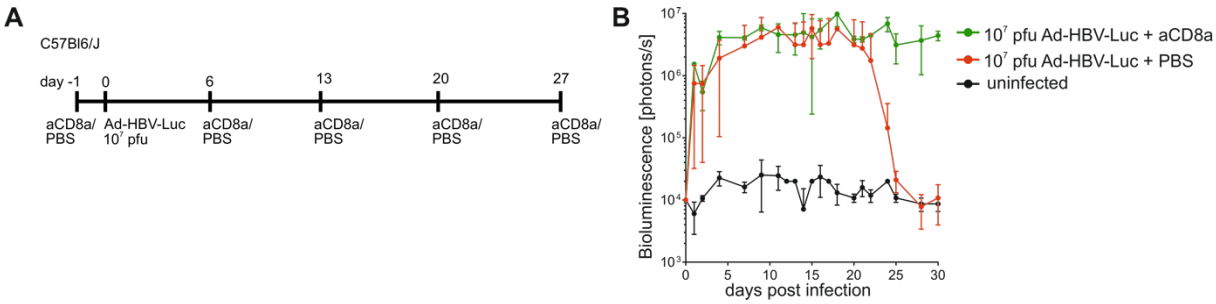

Figure 2.4| Importance of $CD8^+$ T cells during the elimination of an acute, self-limiting Ad-HBV-Luc infection
(A) Schematic overview: C57Bl/6J mice were i.v. injected with 10^7 pfu Ad-HBV-Luc on day 0. Every 7 days, starting at day -1, a depleting antiCD8a antibody was injected in the $CD8^+$ T cell depleted group while in the $CD8^+$ T cell

sufficient group PBS was injected. (B) Quantification of bioluminescence signal in mice after infection with 10^7 pfu Ad-HBV-Luc with or without depletion of $CD8^+$ T cells. SD and mean are shown (n=3).

In summary, adenoviral-vector mediated transfer of HBV1.3 over-length genome combined with the reporter gene luciferase can result in either acute, self-limiting, or persistent HBV infection in immunocompetent C57Bl/6J mice depending on the infectious dose. A high infectious dose of Ad-HBV-Luc (10^8 pfu/mouse) establishes a persistent HBV infection. Application of a 1 log lower dose (10^7 pfu/mouse) of Ad-HBV-Luc led to $CD8^+$ T cell mediated control of HBV within 30 days.

2.1.3 Quantitative and phenotypic differences of HBV-specific $CD8^+$ T cells in acute, self-limiting and persistent Ad-HBV-Luc infection

Ineffective $CD8^+$ T cell responses are caused by either functional exhaustion or physical deletion of antigen-specific $CD8^+$ T cells or by a combination of both[112]. In order to differentiate between a functional $CD8^+$ T cell response in acute, self-limiting Ad-HBV-Luc infection and an ineffective $CD8^+$ T cell response in persistent Ad-HBV-Luc infection, quantity and phenotype of HBV-specific $CD8^+$ T cells were assessed at different time points during the course of infection: On day 10 p.i., which is shortly before the onset of $CD8^+$ T cell mediated elimination of Ad-HBV-Luc, on day 15 p.i., which is at the peak of serum ALT elevation, and on day 35 p.i., which is after control of infection in the low dose infection.

To quantify HBV-specific $CD8^+$ T cells, we identified intrahepatic $CD8^+$ T cells specific for the peptide 93-100 (MGLKFRQL) from the HBc protein, C93-specific $CD8^+$ T cells, via pentamer staining and determined absolute cell counts by flow cytometry (Fig 2.5 A). At day 10 p.i., less than 1000 C93-specific $CD8^+$ T cells were detected in the liver of mice infected with the low dose, while numbers were significantly higher (6000-15000 C93-specific $CD8^+$ T cells) in livers of mice infected with the high dose (Fig 2.5 B). At the peak of the immune response in the acute, self-limiting infection (day 15 p.i.), C93-specific $CD8^+$ T cells expanded on average 15-fold. In mice infected with the persisting dose, numbers declined to a mean of 5000 C93-specific $CD8^+$ T cells per liver. After control of infection (day 35 p.i.), less than 500 C93-specific $CD8^+$ T cells were detected in livers of mice infected with the acute, self-limiting dose, while numbers of C93-specific $CD8^+$ T cells in livers of mice infected with the persisting dose remained unaffected (Fig 2.5 B). Different quantities of intrahepatic C93-specific $CD8^+$ T cells between the acute-resolving and persistent group suggest a different kinetic of expansion and contraction of HBV-specific $CD8^+$ T cells depending on the initial level of viral infection.

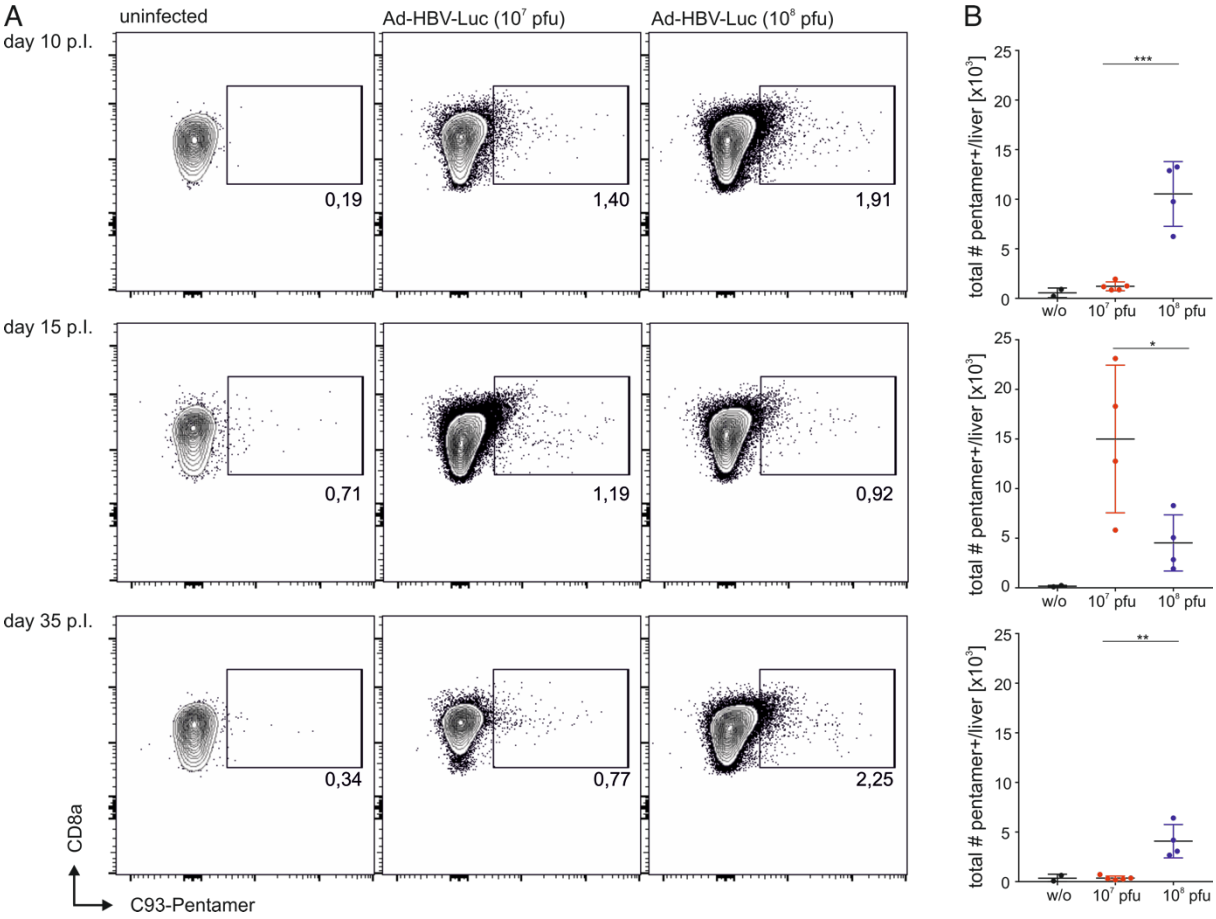

Figure 2.5| Kinetic of intrahepatic HBV-specific CD8⁺ T cells in acute, self-limiting and persistent Ad-HBV-Luc infection
(A) Flow cytometric analysis of C93-pentamer positive cells gated on living CD8⁺CD44⁺ liver associated lymphocytes isolated from mice infected with 10^7 or 10^8 pfu of Ad-HBV-Luc on day 10,15 and 35 p.i.. (B) Quantification of intrahepatic C93-specific CD8⁺ T cells from (A). SD and mean are shown (n=4-5).

The phenotype of C93-specific CD8⁺ T cells was determined by expression levels of the inhibitory surface receptors PD1 and TIGIT, the HMG-box transcription factor TOX, the cytotoxicity marker KLRG1, and the effector molecule granzyme B. The sustained increased expression of multiple inhibitory receptors is a hallmark of exhausted CD8⁺ T cells [126]. Almost all intrahepatic C93-specific CD8⁺ T cells in mice from the persistent group expressed high levels of the inhibitory surface receptors PD1 (~ 95%) and TIGIT (~80%) already at day 10 p.i., which remained high during the observed time of infection (Fig 2.6 A-F). In mice infected with the acute dose of Ad-HBV-Luc, a smaller proportion of intrahepatic C93-specific CD8⁺ T cells was positive for PD1 (~50%) and TIGIT (~ 30%) at day 10 p.i. and expression levels were also lower than in mice infected with the persisting dose (Fig 2.6 A-F). During the peak of the immune response (day 15 p.i.) in mice infected with the acute, self-limiting dose, the proportion of PD1⁺ and TIGIT⁺ C93-specific CD8⁺ T cells and also the level of surface expression increased transiently but returned to lower levels at day 35 p.i. (Fig 2.6 A-F). The HMG-box transcription factor TOX was identified as a critical factor for the formation of exhausted CD8⁺ T cells in mice [226]. We verified a high expression of TOX in approx. 90% of C93-specific CD8⁺

T cells in mice infected with the persisting dose of Ad-HBV-Luc. In C93-specific CD8$^+$ T cells from mice infected with the acute dose, we observed low expression levels of TOX in a small proportion of cells at day 10 and 35 and a transient high expression at day 15 p.i., comparable to the kinetics of PD1 and TIGIT expression (Fig 2.6 G-I).

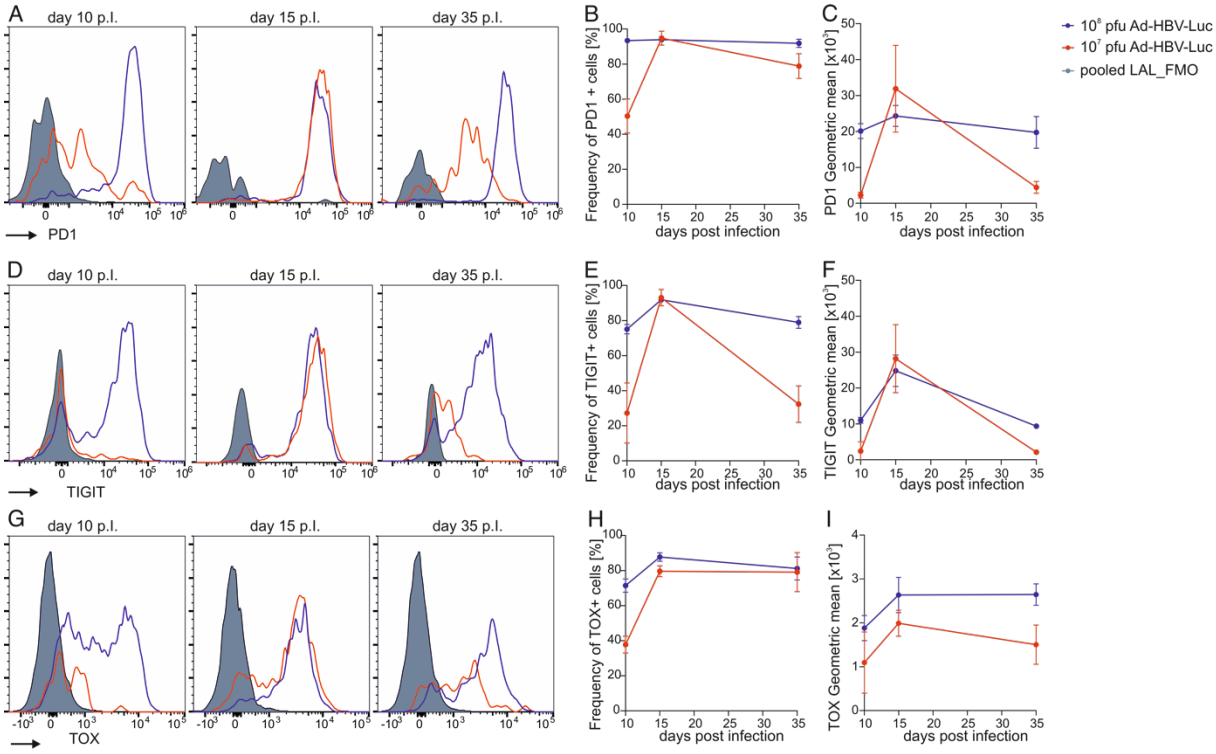

Figure 2.6| Exhaustion marker expression by HBV-specific CD8$^+$ T cells in acute, self-limiting and persistent Ad-HBV-Luc infection
Flow cytometric analysis and quantification of C93-specific CD8$^+$ T cells isolated from livers of mice infected with 10^7 (red) or 10^8 pfu (blue) of Ad-HBV-Luc on day 10,15 and 35 p.i. The fluorescence minus one control is depicted in grey. (A) Representative histogram plots of PD1 expression levels. (B) Frequencies of PD1 positive C93-specific CD8$^+$ T cells. (C) PD1 expression levels (geometric mean of fluorescence intensity) (D) Representative histogram plots of TIGIT expression levels. (E) Frequencies of TIGIT positive C93-specific CD8$^+$ T cells (F) TIGIT expression levels (geometric mean of fluorescence intensity) of C93-specific CD8$^+$ T cells (G) Representative histogram plots of TOX expression levels (H) Frequencies of TOX positive C93-specific CD8$^+$ T cells (I) TOX expression levels (geometric mean of fluorescence intensity) of C93-specific CD8$^+$ T cells (B), (C), (E), (F), (H), (I) Mean and SD are shown (n=4-5).

In addition to the activation/exhaustion marker PD1, TIGIT and TOX, CD8$^+$ T cells were stained for KLRG1, which is expressed on highly cytotoxic effector CD8$^+$ T cells [227, 228]. In the acute infection setting, the proportion of KLRG1$^+$ C93-specific CD8$^+$ T cells increased from day 10 (~20%) to day 15 (~30%) and declined until day 35 to a very basal level (~5%). In the chronic infection setting, the proportion of KLRG1$^+$ C93-specific CD8$^+$ T cells was overall lower and declined from day 10 to a low basal expression level at day 15 and day 35 (Fig 2.7 A-C). Similar results were obtained for granzyme B, a cytotoxic effector molecule that is upregulated in CD8$^+$ T cells with effector potential. In the persistent infection setting, granzyme B$^+$ C93-specific CD8$^+$ T cells were detected only early at day 10 p.i., whereas in low dose infection, granzyme B$^+$ C93-specific CD8$^+$ T cells were detected over the whole course of infection (Fig 2.7 D-F). As the total number of C93-specific CD8$^+$ T cells in the acute setting increased 10-

fold at the peak of the effector phase (day 15 p.i.), the slightly decreased frequency actually reflects increased total CD8$^+$ T cell numbers (Fig 2.7 E). Further, lower expression levels of granzyme B (Fig 2.7 F) at day 15 may be due to the release of cytotoxic granules at the peak of the effector phase (peak of sALT elevation).

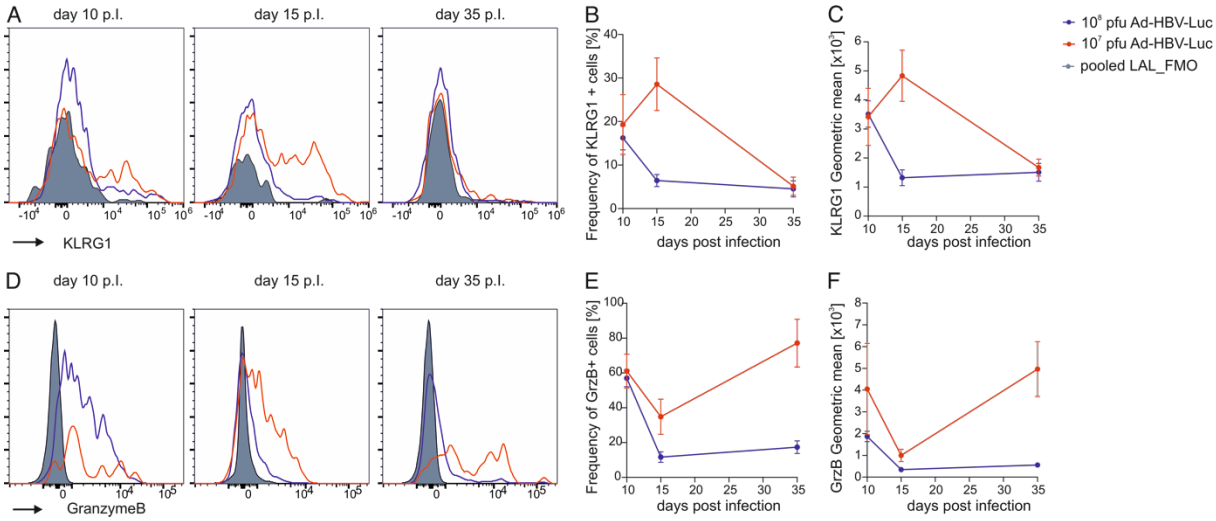

Figure 2.7| Cytotoxicity marker expression by HBV-specific CD8$^+$ T cells in acute, self-limiting and persistent Ad-HBV-Luc infection
Flow cytometric analysis and quantification of C93-specific CD8$^+$ T cells isolated from livers of mice infected with 10^7 (red) or 10^8 pfu (blue) of Ad-HBV-Luc on day 10,15 and 35 p.i. The fluorescence minus one control is depicted in grey (filled). (A) Representative histogram plots of KLRG1 surface expression. (B) Frequencies of KLRG1 positive C93-specific CD8$^+$ T cells. (C) Quantification of KLRG1 surface expression (geometric mean of fluorescence intensity) on C93-specific CD8$^+$ T cells. (D) Representative histogram plots of intracellular granzyme B. (E) Frequencies of granzyme B positive C93-specific CD8$^+$ T cells. (F) Quantification of intracellular granzyme B expression (geometric mean of fluorescence intensity) in C93-specific CD8$^+$ T cells. (B), (C), (E), (F) Mean and SD are shown (n=4-5).

Effector cytokine production was examined after *ex vivo* stimulation of intrahepatic lymphocytes isolated at the same time points from mice after infection with the acute, self-limiting or persistent dose. Intrahepatic lymphocytes were stimulated with C93-peptide or unspecific SIINFEKL-peptide as a negative control. Significant induction of IFNγ$^+$ CD8$^+$ T cells upon C93-stimulation compared to SIINFEKL-stimulation was only detected in mice infected with the acute, self-limiting dose on day 35 p.i. when infection was already eliminated from these mice (Fig 2.8 A, B).

High numbers of IFNγ$^+$ or TNF$^+$ CD8$^+$ T cells upon *ex vivo* C93-peptide as well as SIINFEKL-peptide stimulation indicate ongoing effector functions *in vivo*. Highly increased numbers of IFNγ+ - and TNF+ CD8$^+$ T cells were detected at day 15 p.i. in mice infected with the acute, self-limiting dose compared to mice infected with the persistent dose upon C93-peptide and SIINFEKL-peptide stimulation indicating ongoing effector functions in those mice (Fig 2.8 A-C). However, there was no further induction of cytokine production by restimulation with C93-peptide over SIINFEKL-peptide at day 15 p.i. (Fig 2.8 A-C).

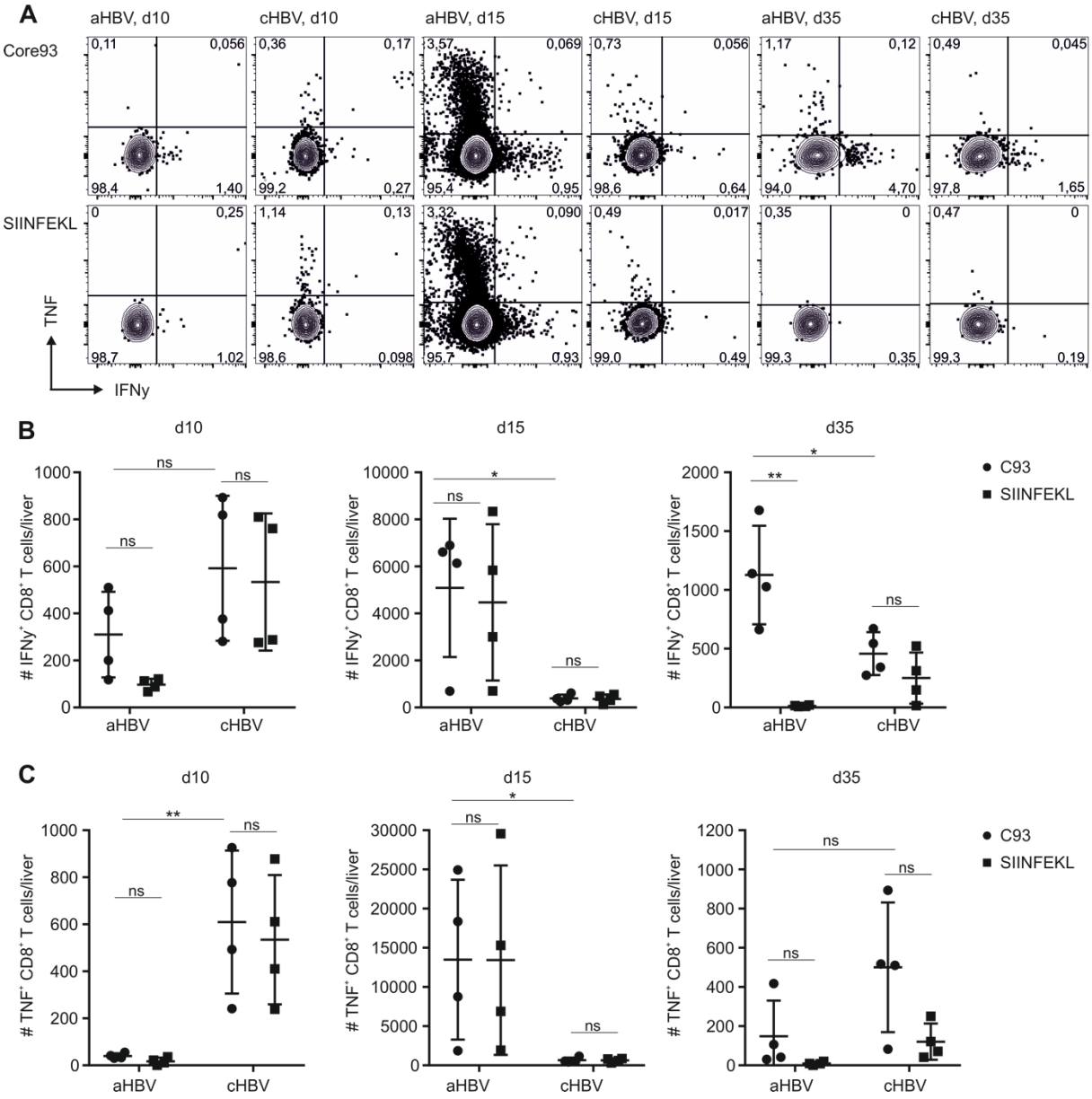

Figure 2.8| *Ex vivo* peptide stimulation of CD8⁺ T cells from mice infected with the acute, self-limiting or persistent dose of Ad-HBV-Luc
Flow cytometric analysis and quantification of C93-specific CD8⁺ T cells isolated from livers of mice infected with 10^7 (aHBV) or 10^8 pfu (cHBV) of Ad-HBV-Luc at day 10,15 and 35 p.i.. Liver associated lymphocytes were stimulated *ex vivo* with C93-peptide (1µM) or SIINFEKL-peptide (1µM) for 6h. (A) Representative dot plots of intracellular IFNγ and TNF staining. Gated on living CD44⁺ CD8⁺ lymphocytes. (B) Quantification of total intrahepatic IFNγ⁺ CD8⁺ T cells. (C) Quantification of total intrahepatic TNF⁺ CD8⁺ T cells.

In summary, we observed a different kinetic of expansion and activation of HBV-specific CD8⁺ T cells during persistent and acute, self-limiting Ad-HBV-Luc infection. In the persistent infection setting, HBV-specific CD8⁺ T cells expanded and displayed an activated phenotype early after infection (day 10 p.i.). However, without the exertion of notable effector functions measured by means of ALT elevation and reduction of HBV-positive hepatocytes, numbers of HBV-specific CD8⁺ T cells contracted slightly. Further, activation and cytotoxicity markers decreased from day 10 p.i. onwards, while high levels of inhibitory receptors were maintained.

In the acute infection setting, HBV-specific $CD8^+$ T cells expanded and displayed an activated effector T cell phenotype later (day 15 p.i.), and contraction occurred after the exertion of effector function along with the elimination of the virus.

2.2 Generation and functional characterization of AAVs expressing murine IFNβ in the liver

In order to analyze the effects of type I IFN on HBV and HBV immunity, we generated an AAV (Adeno-associated virus) serotype 2 pseudotyped with an AAV serotype 8 capsid encoding for murine IFNβ controlled by the hepatocyte-specific transthyretin (TTR) promoter, named AAV-IFN hereafter. In contrast to systemic administration of recombinant IFNs/PEG-IFNs, we aimed at achieving high and continuous levels of type I IFNs locally in the liver, thereby reducing adverse effects.

2.2.1 Long-term expression of IFNβ in the liver

First, to control for infection efficiency and stability of transgene expression, we generated a construct with an equimolar expression of murine IFNβ and Renilla luciferase driven by the strong ubiquitous cytomegalovirus (CMV) promoter, called AAV-CMV-IFNRL hereafter (Fig 2.9 A). In a control vector, IFNβ was replaced by eGFP (AAV-CMV-GRL) (Fig 2.9 A). Immunocompetent C57Bl/6J mice were transduced with 1×10^{11} genome copies (gc) of AAV-CMV-IFNRL or AAV-CMV-GRL and bioluminescence signal, sALT level, and body weight was monitored for 60 days. Bioluminescence levels in livers of AAV-CMV-IFNRL transduced mice were 1 log lower compared to bioluminescence level in livers of mice transduced with the same dose of AAV-CMV-GRL, but both remained stable for 60 days (Fig 2.9 C). There was no significant induction of sALT in mice transduced with AAV-CMV-IFNRL or AAV-CMV-GRL compared to treatment naïve mice (Fig 2.2.7 D). However, AAV-CMV-IFNRL transduced mice showed reduced weight increase after transduction (Fig 2.9 E). Within 60 days, weight difference accumulated to 10 to 15% reduced body weight compared to AAV-CMV-GRL or untreated mice (Fig 2.9 E). Type I IFN signaling induces the expression of various genes, referred to as interferon stimulated genes (ISGs). To confirm ongoing interferon signaling in livers of AAV-CMV-IFNRL transduced mice, we measured RNA levels of two ISGs, 2'-5'-oligoadenylate synthetase 1 (OAS-1) and interferon-induced GTP binding protein MX-1. As expected, RNA levels of MX-1 (Fig 2.9 F) and OAS-1 (Fig 2.9 G) were highly upregulated in livers of AAV-CMV-IFNRL transduced mice over AAV-CMV-GRL or untreated mice. While OAS-1 upregulation was stable from day 14 on until day 60 (Fig 2.9 F), MX-1 upregulation was highest very early upon transduction (d2) and then declined until day 60 (Fig 2.9 G).

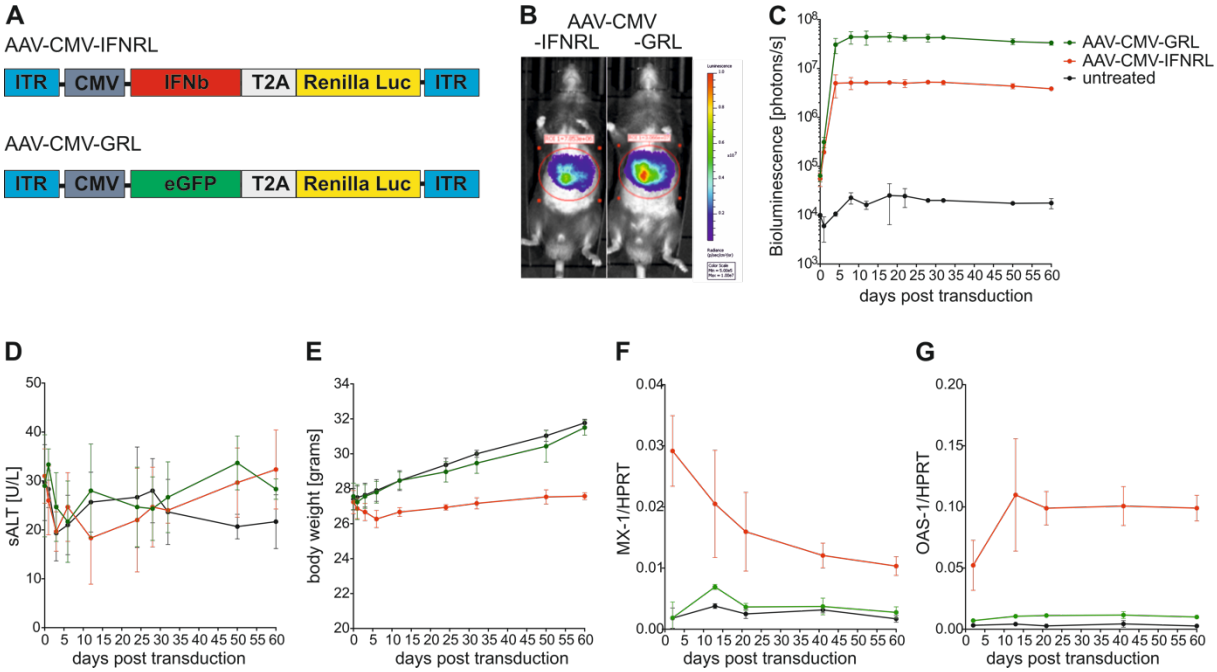

Figure 2.9| Adenoviral-associated virus vector-mediated long-term expression of IFNβ in the liver
(A) schematic illustration of 1st generation AAV constructs: IFNβ and Renilla luciferase (or eGFP and Renilla luciferase) gene coupled via T2A element are flanked by AAV2 ITRs and expressed under the control of the ubiquitous CMV promoter. The T2A element allows for an equimolar expression of either IFNβ and Renilla luciferase or eGFP and Renilla luciferase. (B) Bioluminescence imaging of mice transduced with either AAV-CMV-IFNRL (10^{11} gc) or AAV-CMV-GRL (10^{11} gc) at day 4 post transduction. (C) Quantification of bioluminescence in the liver of mice transduced with either AAV-CMV-IFNRL (10^{11} gc) or AAV-CMV-GRL (10^{11} gc) or untreated. (D) Time kinetics of serum ALT levels of mice from (C). (E) Bodyweight of mice from (C). (F) MX-1 RNA expression levels or (G) OAS-1 expression levels in liver tissue of mice transduced with either AAV-CMV-IFNRL (10^{11} gc) or AAV-CMV-GRL (10^{11} gc) or untreated relative to HPRT determined by qPCR. Mean and SD are shown (n=3-4).

Thus, the expression of IFNβ in the liver via AAV-mediated gene expression led to a high induction of ISGs over 60 days.

2.2.2 Efficiency of AAV transduction

Estimation of AAV transduction efficiency was accomplished via transduction of immunocompetent C57Bl/6J mice with increasing doses of AAV-CMV-GRL. The injection of 10^9 gc per mouse resulted in a mean percentage of 0,9 (+/- 0,3) % GFP^+ hepatocytes, the injection of 10^{10} gc per mouse in a mean percentage of 4,6 (+/- 0,8) % GFP^+ hepatocytes and the injection of the highest dose of 10^{11} gc per mouse in a mean percentage of 25,5 (+/- 5,4) % GFP^+ hepatocytes (Fig 2.10 A, B)

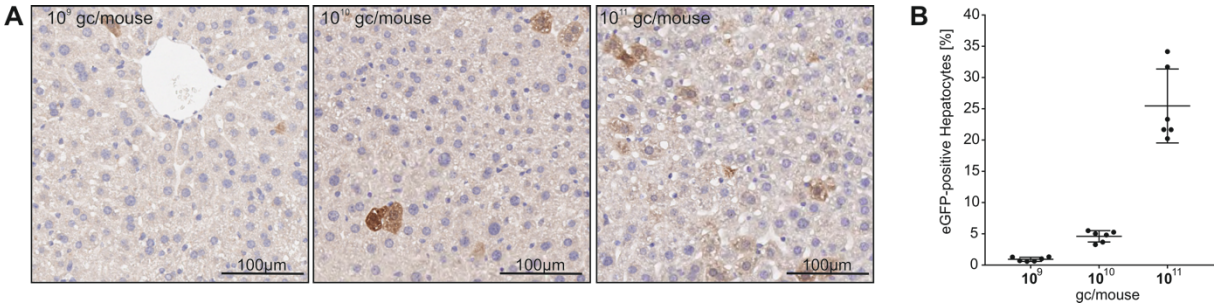

Figure 2.10| Transduction efficiency of AAV-vectors
(A) Representative immunohistochemical GFP staining of liver sections at day 2 post AAV-CMV-GRL transduction. (B) Quantification of GFP+ hepatocytes: 3 ROIs per liver section were counted, and the mean percentage of GFP+ hepatocytes was calculated, dividing GFP+ hepatocytes/total number of hepatocytes.

2.2.3 Hepatocyte-specific IFNβ expression

Despite the natural hepatotropism of AAV serotype 8, we replaced the strong ubiquitous CMV promoter with the hepatocyte-specific TTR promoter to restrict the primary source of IFNβ expression to hepatocytes (Fig 2.11 A). Furthermore, we removed reporter proteins to avoid any immune response elicited by exogenous proteins. To this end, second generation AAV vectors, named AAV-IFN and AAV-Empty, were constructed and produced. ALT levels in the serum were not increased in AAV-IFN compared to AAV-Empty transduced animals, except for a slight increase of ALT levels in the serum at day one after transduction (Fig 2.11 B). Similar to transduction with the 1st generation vector expressing IFNβ reduced body weight increase was measured in animals transduced with AAV-IFN (Fig 2.11 C). Liver weight was not affected after AAV-IFN transduction (Fig 2.11 D), but spleens were significantly enlarged by factor 1.5 in animals transduced with AAV-IFN compared to AAV-Empty (Fig 2.11 E). The ISGs ISG15 and OAS1 were significantly upregulated on RNA level in livers of mice transduced with AAV-IFN on day 3 post transduction. At day 10 post transduction, RNA levels of ISG15 and OAS1 were lower than on day 3, but ISG15 was further significantly increased in AAV-IFN over AAV-Empty transduced livers (Fig 2.11 F, G).

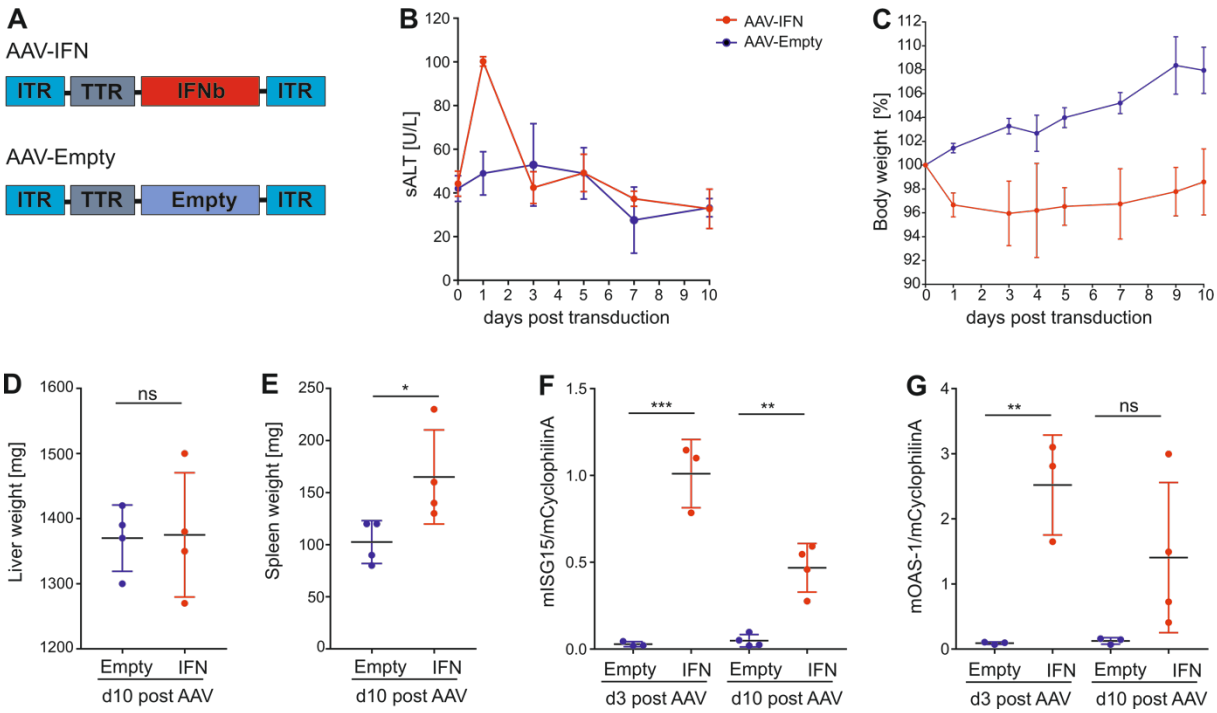

Figure 2.11| Establishment of second generation AAV vectors: AAV-IFN vs. AAV-Empty
A) Schematic illustration of 2nd generation AAV constructs: murine IFNβ gene (or a non-coding sequence) expressed under the control of the hepatocyte-specific TTR promoter flanked by AAV2 ITRs. (B) Serum ALT levels of mice after transduction with either AAV-IFN (10^{11} gc) or AAV-Empty (10^{11} gc). (C) Normalized bodyweight of mice transduced with AAV-IFN (10^{11} gc) or AAV-Empty (10^{11} gc). (D) Weight of livers or (E) spleens from mice transduced with AAV-Empty or AAV-IFN at day 10 post transduction. (F) ISG15 mRNA expression levels and (G) OAS-1 mRNA expression levels in liver tissue of mice transduced with either AAV-IFN (10^{11} gc) or AAV-Empty (10^{11} gc) relative to CyclophilinA determined by qPCR. Mean and SD are shown (n=3-4).

2.2.4 Modulation of intracellular and presented viral antigen by hepatocyte-specific IFNβ-expression

Several of the described ISGs are involved in the regulation of intracellular antigen load and presentation of viral antigen. Protein kinase R (PKR), 2'5 OAS, and RNase L inhibit cellular protein synthesis, thereby reducing intracellular viral antigen load. Type I IFNs are also known to upregulate MHC class I expression leading to enhanced antigen presentation on infected cells. The overall/combined effect of reduced intracellular viral antigen load and increased MHC class I expression on antigen presentation in the context of MHC-I needs to be elucidated. Since antibodies recognizing HBV-specific peptides in the context of MHC-I molecules in the murine system are not available, we addressed this question in the Ovalbumin infection model[229]. In this model, the antibody 25-D1.16, recognizing the ovalbumin-derived peptide SIINFEKL bound to the murine MHC-I molecule H2-K^b was used. To this end, mice were infected with 2 x 10^8 pfu of Ad-CMV-GOL, expressing ovalbumin and the reporter proteins GFP and luciferase followed by transduction with AAV-IFN or AAV-Empty 2 days after Ad-CMV-GOL. Primary hepatocytes were isolated and analyzed on day 4 after infection (Fig 2.12 A). Quantification of hepatic bioluminescence *in vivo*, measuring intracellular levels of the reporter protein luciferase, depicted a mean 8-fold decrease in mice transduced with AAV-IFN

compared to mice transduced with AAV-Empty (Fig. 2.12 B). Although AAV-IFN treatment increased surface expression of the MHC-I molecule H2-K^b by factor 2 (Fig 2.12 C), surface expression of SIINFEKL bound to H2-K^b was 3-fold lower in these mice (Fig 2.12 D). In line with the decreased intracellular levels of luciferase, the intensity of GFP expression was 4-fold lower in mice treated with AAV-IFN (Fig 2.12 E).

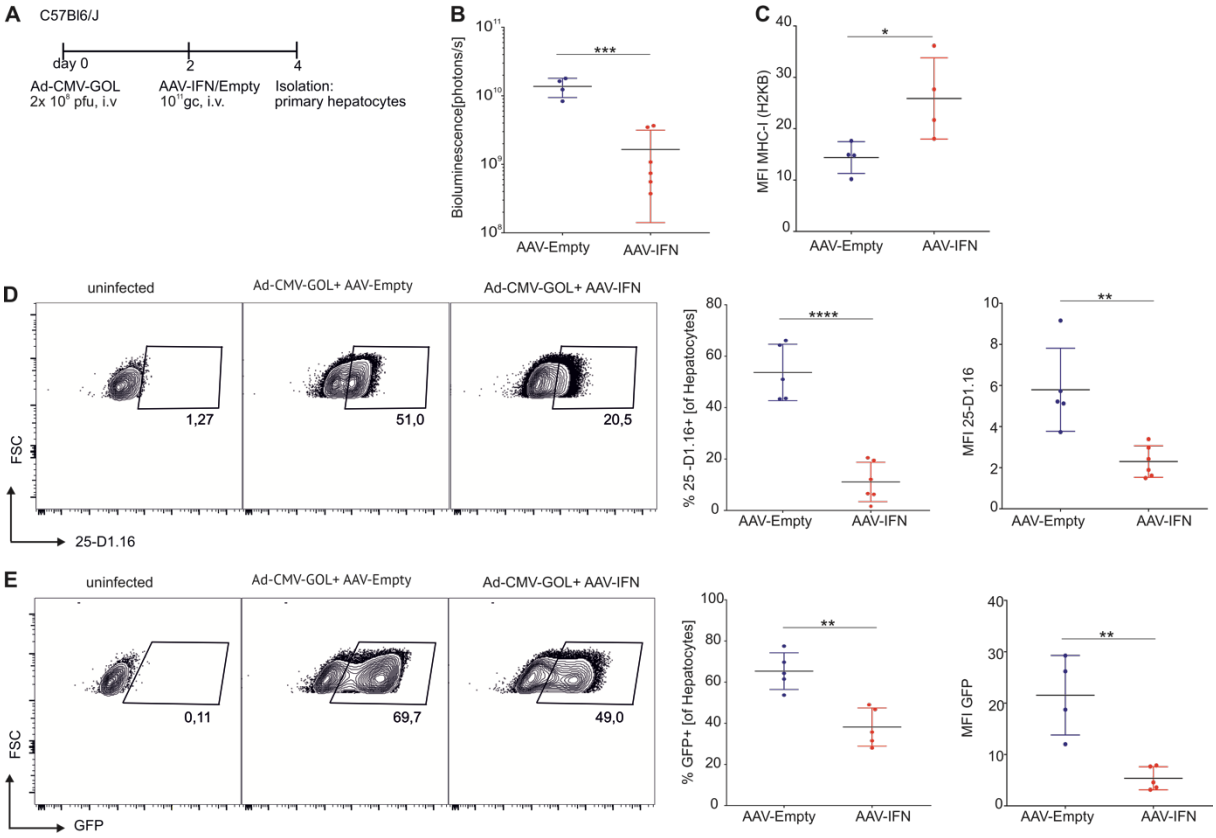

Figure 2.12| Analysis of intracellular viral antigen load and reduction of antigen presentation in the context of MHC-I after AAV-IFN treatment
Flow cytometric analysis of hepatocytes isolated from livers of mice infected with 2x10^8 pfu of Ad-CMV-GOL and transduced with either AAV-Empty (blue) or AAV-IFN (red). (A) schematic overview: wildtype C57Bl/6J mice were i.v. injected with 2 x 10^8 pfu Ad-CMV-GOL. 2 days p.i. mice were transduced with 1 x 10^{11} gc AAV-Empty or AAV-IFN. At day 4 p.i./ at day 2 post AAV-transduction primary murine hepatocytes were isolated and analyzed. (B) Quantification of bioluminescence in mice at day 4 p.i.. (C) Quantification of MHC-I (H2KB) surface expression levels on isolated hepatocytes. (D) SIINFEKL bound to H2K^b (25-D1.16) surface expression on hepatocytes: Representative contour plots and quantification of percentages of 25-D1.16+ and MFI. (E) Intracellular GFP expression in hepatocytes: Representative contour plots and quantification of percentages of GFP+ and MFI. Mean and SD are shown (n=4-5).

In summary, hepatocyte-specific expression of IFNβ reduces intracellular viral antigen load leading, even though MHC-I surface expression was increased, to a significantly lower presentation of viral antigen in the context of MHC-I on infected hepatocytes.

2.3 Targeting viral antigen load in chronic Ad-HBV-Luc infection via hepatocyte-specific IFNβ expression

Interferons own the unique ability to reduce intracellular viral antigen load and, at the same time, exert direct immunostimulatory functions on various cells of the immune system. The reduction of intracellular viral antigen implies reduced antigen presentation in the context of MHC-I on infected hepatocytes (section 2.2.2) and reduced levels of secretory viral antigen in the circulation. The following experiments aim at investigating the impact of IFN-mediated antigen reduction on the restoration of anti-HBV immunity in a setting of chronic Ad-HBV-Luc infection.

2.3.1 Induction of anti-HBV immunity in mice with an established chronic Ad-HBV-Luc infection by hepatocyte-specific IFNβ expression

To evaluate the potential of hepatocyte-specific IFNβ expression to restore antiviral immunity in chronic HBV infection, we used the established Ad-HBV-Luc model of chronic HBV infection (section 2.1). To this end, C57Bl/6J mice were i.v. injected with 10^8 pfu Ad-HBV-Luc. 34 days after infection, when chronic infection was established, mice were i.v. injected with either AAV-Empty or AAV-IFN. To dissect the antigen-reducing effect of IFNβ from antiviral immunity, NK cells and $CD8^+$ T cells were depleted by injection of depleting antibodies in additional groups 1 day before and 6 days after AAV-treatment (Fig 2.13 A). *In vivo* bioluminescence imaging was used as a direct and sensitive measurement for viral antigen levels in the liver. On day 2 after AAV-transduction, we measured equally reduced bioluminescence signal in the liver in all groups injected with AAV-IFN, indicating that this early decline of viral antigen level is not caused by cytotoxic $CD8^+$ T cells or NK cells (Fig 2.13 B). In mice depleted of $CD8^+$ T cells, the ongoing decline was abrogated at day 3 after AAV treatment, and the signal was stable thereafter, while in fully immunocompetent and NK cell deficient mice a further decline to 10^5 photons/s at day 9 after AAV treatment was observed. The decline in bioluminescence signal between day 3 (day 37 p.i.) and day 9 (day 43 p.i.) after AAV-IFN treatment in immunocompetent and NK cell deficient mice was accompanied by increased sALT levels suggesting ongoing hepatocyte cell death. There was no increase in sALT levels observed in mice treated with AAV-Empty or in $CD8^+$ T cell deficient mice treated with AAV-IFN (Fig 2.13 C). However, from day 9 after AAV-transduction until the end of the experiment, we observed a slight rebound of bioluminescence signal in all AAV-IFN transduced groups (Fig 2.13 B).
Serum HBeAg levels were controlled in immunocompetent and NK cell deficient animals treated with AAV-IFN, but still low levels of HBeAg (<10 PEIU/mL) were detected at the end of the experiment (12 days after AAV-IFN treatment). In the AAV-Empty treated group, serum HBeAg levels stayed stable at around 90 PEIU/mL over the treatment period, while levels were

reduced 2-3-fold (30-45 PEIU/mL) in the AAV-IFN treated $CD8^+$ T cell depleted group (Fig 2.13D).

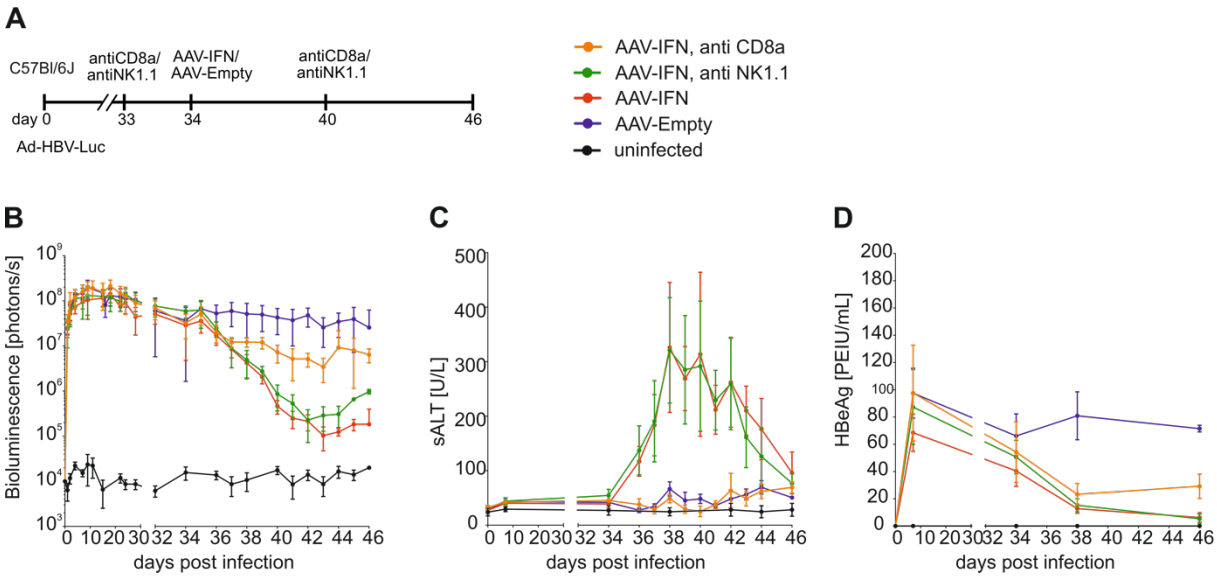

Figure 2.13| Hepatocyte-specific expression of IFNβ induces $CD8^+$ T cell mediated antiviral immunity in chronically Ad-HBV-Luc infected mice
(A) Schematic overview: C57Bl/6J mice were i.v. injected with 10^8 pfu Ad-HBV-Luc. 34 days p.i., mice were i.v. injected with 10^{11} gc AAV-Empty or AAV-IFN. At day 33 and 40 p.i. mice were i.v. injected with antiNK1.1/antiCD8a depleting antibody or NaCl. (B) Quantification of bioluminescence signal in mice treated as in (A). (C) Serum ALT levels of mice treated as in (A). (D) HBeAg levels of mice treated as in (A). Mean and SD are shown (n=5).

In summary, hepatocyte-specific IFNβ expression in chronically Ad-HBV-Luc infected animals led to a 2-3-log fold reduction of viral antigen load in the liver, measured via bioluminescence imaging and a 10-fold reduction of serum HBeAg levels. The early (2-3 days post treatment) 1 log reduction of viral antigen load in the liver was mediated via inhibition of protein synthesis. The further 2-log reduction, which was measured from day 3 to day 12 after AAV transduction, was due to $CD8^+$ T cell mediated elimination of virus-infected hepatocytes.

Immunohistochemical HBcAg staining of liver tissue at different time points after AAV-IFN treatment visualized the reduction of viral antigen (Fig 2.14 A). On day 7 after AAV-IFN treatment, the reduction of HBc^+ nuclei per mm^2 liver tissue (23-fold), and the reduction of pgRNA levels in liver tissue was most pronounced (Fig. 2.14 B). Consistent with the bioluminescence signal, a slight rebound of HBc^+ nuclei per mm^2 liver tissue and pgRNA levels was observed at day 10 post AAV-IFN treatment.

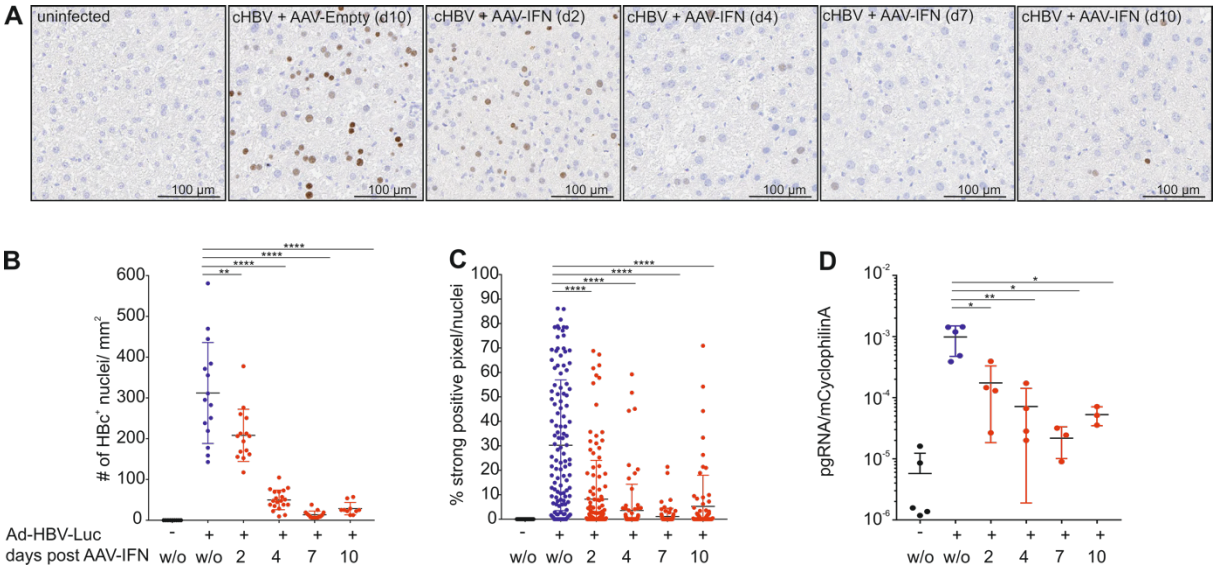

Figure 2.14| Quantification of HBcAg and pgRNA expression levels in liver tissue of chronically Ad-HBV-Luc infected animals treated with AAV-IFN
(A) Representative Immunohistochemical HBcAg staining of liver sections 43 days post Ad-HBV-Luc infection treated with AAV-Empty or AAV-IFN at indicated time points. Scale bars indicate 100 µm. (B) Quantification of HBc^+ nuclei per mm^2. 5 ROIs per liver section were counted. (C) Quantification of strong positive pixel per nuclei. 10 Nuclei per liver section were analyzed. (D) pgRNA expression in liver tissue of mice treated as in (A) at indicated time points relative to CyclophilinA. Mean and SD are shown (n=3-4).

The increase in numbers of HBc+ nuclei, the pgRNA expression, and the intensity of HBcAg staining per nuclei (Fig 2.14 C) suggest reduced levels of IFN signaling and thereby inhibition of protein synthesis. To investigate whether the observed rebound of viral antigen was provoked by reduced IFN signaling, IFN signaling was quantified by measuring phosphorylated STAT1 in liver tissue sections and mRNA levels of ISG15 and OAS-1 in liver tissue. Quantification of pSTAT1 expression revealed a maximum of pSTAT1-expression (a 19-fold increase over AAV-Empty transduced) at day 4 after AAV-IFN transduction.

From day 4 post transduction on, pSTAT1 expression declined until day 10 (a 3-fold increase over AAV-Empty transduced) (Fig 2.15 B). Relative expression of ISG15 and OAS-1 mRNA was only significantly increased at day 2 post AAV-IFN transduction (Fig 2.15 C, D). High within-group variance impedes a claim over a significant reduction of ISG15 and OAS-1 on mRNA level at day 4, 7, and 10 over day 2 after AAV-IFN transduction. However, there is a trend towards reduced ISG induction from day 4 after transduction onwards

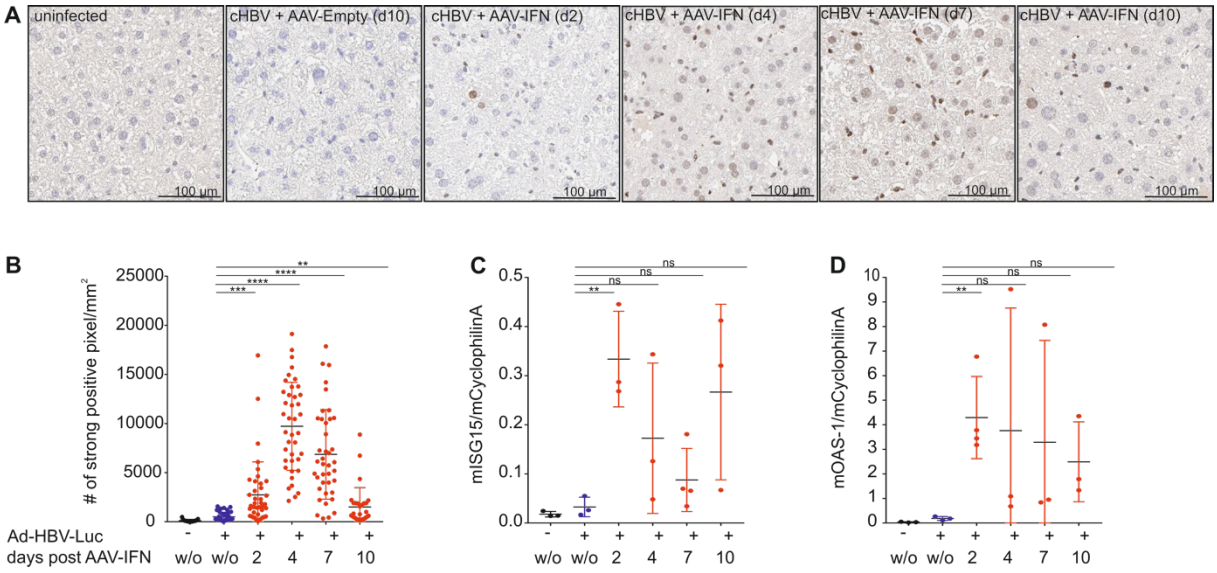

Figure 2.15| Analysis of pSTAT1 in liver tissue of chronically Ad-HBV-Luc infected animals treated with either AAV-Empty or AAV-IFN
(A) Representative Immunohistochemical pSTAT1 staining of liver sections 43 days post Ad-HBV-Luc infection treated with AAV-Empty (w/o) or AAV-IFN at indicated time points. Scale bars indicate 100 µm. (B) Quantification of strong positive pixel per mm^2. 10 ROIs per liver section were analyzed. (C) ISG15 expression in liver tissue of mice treated as in (A) at indicated time points relative to CyclophilinA. (D) OAS-1 expression in liver tissue of mice treated as in (A) at indicated time points relative to CyclophilinA. Mean and SD are shown (n=3-4).

The chronological sequence of hepatocyte cell death, determined by ALT elevation (day 3 to 6 post transduction), followed by reduced IFN-signalling afterward (day 7 post transduction), followed by a rebound of viral antigen (day 10 post transduction), indicate a link between those events. Hence, the most probable explanation for the observed rebound of viral antigen is that the HBV-specific immune-response lead to reduced numbers of AAV-IFN transduced hepatocytes and thereby less efficient inhibition of viral protein synthesis.
Nevertheless, these results demonstrate that hepatocyte-specific expression of IFNβ has the potential to re-activate anti-HBV immunity in chronically Ad-HBV-Luc infected mice and that this reactivation occurs in a temporal connection to the reduction of viral antigen load.

2.3.2 Hepatocyte-specific IFNβ expression restores exhausted HBV-specific $CD8^+$ T cell immunity in mice with an established chronic Ad-HBV-Luc infection

Hepatocyte-specific IFNβ expression in mice with established chronic Ad-HBV-Luc infection induced a profound reduction of Ad-HBV-Luc infected hepatocytes (section 2.2.3). The elimination of virus-infected hepatocytes was mediated by $CD8^+$ T cells suggesting a restoration of exhausted HBV-specific $CD8^+$ T cells. In order to prove the restoration of exhausted HBV-specific CD8+ T cells, we analyzed intrahepatic HBV-specific $CD8^+$ T cells after AAV-IFN treatment directly *ex vivo*. Numbers of bulk $CD8^+$ T cells in the liver were slightly increased at day 2 after AAV-transduction, but not significantly affected at any time after AAV-transduction (Fig 2.16 D). The frequency of C93-specific $CD8^+$ T cells of total intrahepatic $CD8^+$

T cells was increased 2,4,7 and 10 days after AAV-IFN transduction (Fig 2.16 B, C). Total numbers of C93-specific CD8$^+$ T cells were significantly increased at day 2 and 7 after AAV-IFN treatment (Fig 2.16 B, C).

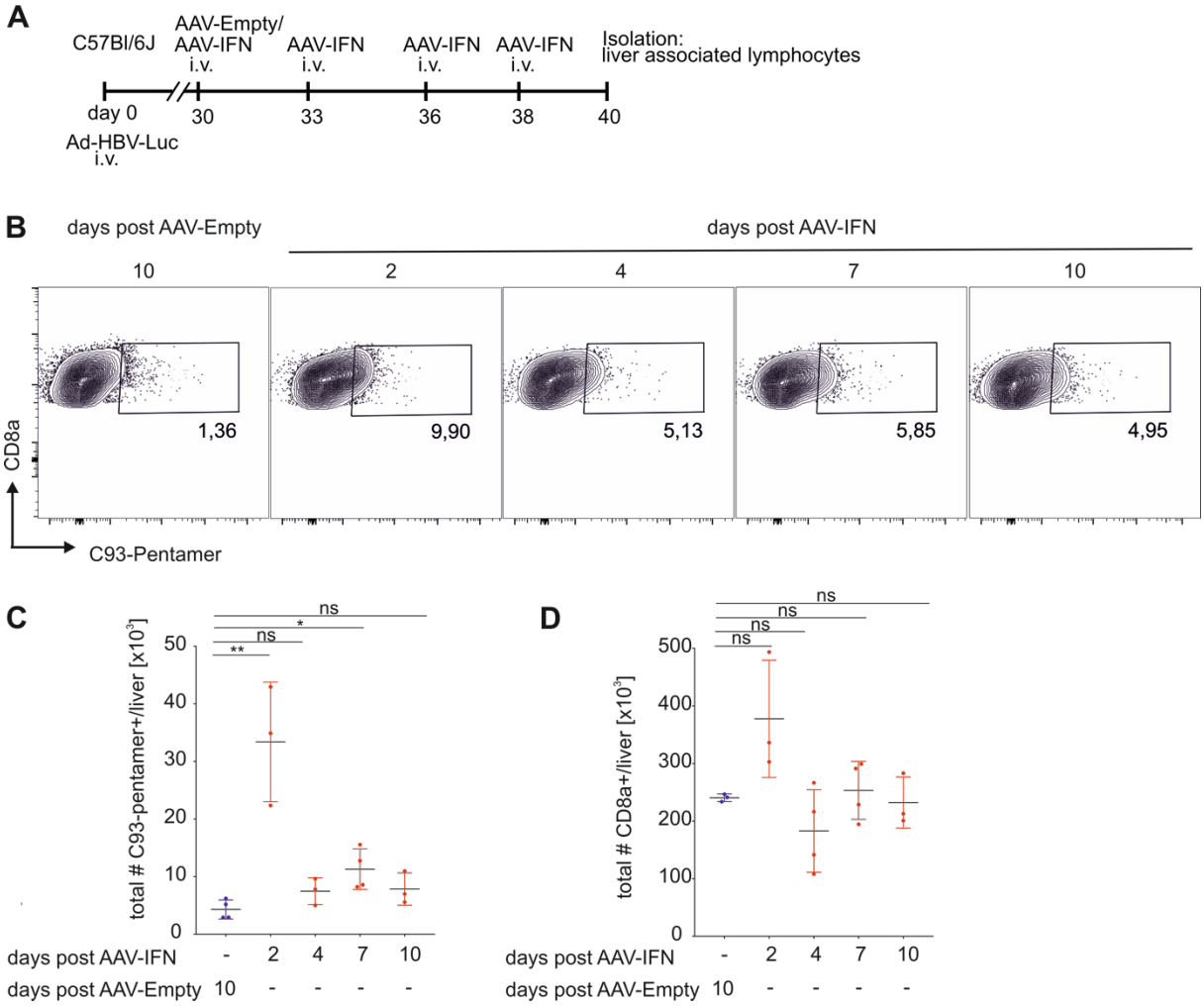

Figure 2.16| Quantity of HBV-specific CD8$^+$ T cells in the liver of chronically Ad-HBV-Luc infected mice after AAV-IFN treatment
(A) Schematic overview: C57Bl/6J mice were i.v. injected with 10^8 pfu Ad-HBV-Luc. 30 days p.i.. Different groups of mice were i.v. injected with 10^{11} gc AAV-Empty or AAV-IFN at indicated times. 40 days p.i., which was day 2, 4, 7, and 10 after AAV-IFN and day 10 after AAV-Empty treatment, liver associated lymphocytes were isolated and analyzed. The group depicted as w/o AAV-IFN was injected with AAV-Empty at day 30 p.i.. (B) Flow cytometric *ex vivo* analysis of C93-specific intrahepatic CD8$^+$ T cells (gated on living CD44+ CD8$^+$ cells) (C) Quantification of C93$^+$CD8$^+$ T cells from (B). (D) Quantification of total CD8$^+$ T cells (gated on living CD8$^+$ cells) from (B). Mean and SD are shown (n=3-4).

In addition, we analyzed the phenotype of intrahepatic HBV-specific CD8$^+$ T cells 2,4,7 and 10 days after AAV-IFN treatment and compared it to AAV-Empty treatment.

High expression of the exhaustion/activation marker PD1 and the exhaustion marker TIGIT was observed on intrahepatic HBV-specific CD8$^+$ T cells in chronically infected mice treated with the control vector AAV-Empty (Fig 2.17 A-C). Surface expression levels of PD1 were already slightly lower at day 2 after AAV-IFN treatment and significantly further reduced at day

4,7 and 10 after treatment (Fig 2.17 B). Surface expression levels of TIGIT were already significantly reduced at day 2 after AAV-IFN and gradually decreased further until day 10 after treatment (Fig 2.17 C). After AAV-IFN treatment, a large proportion of HBV-specific CD8$^+$ T cells was stained negative for TIGIT (Fig 2.17 A).

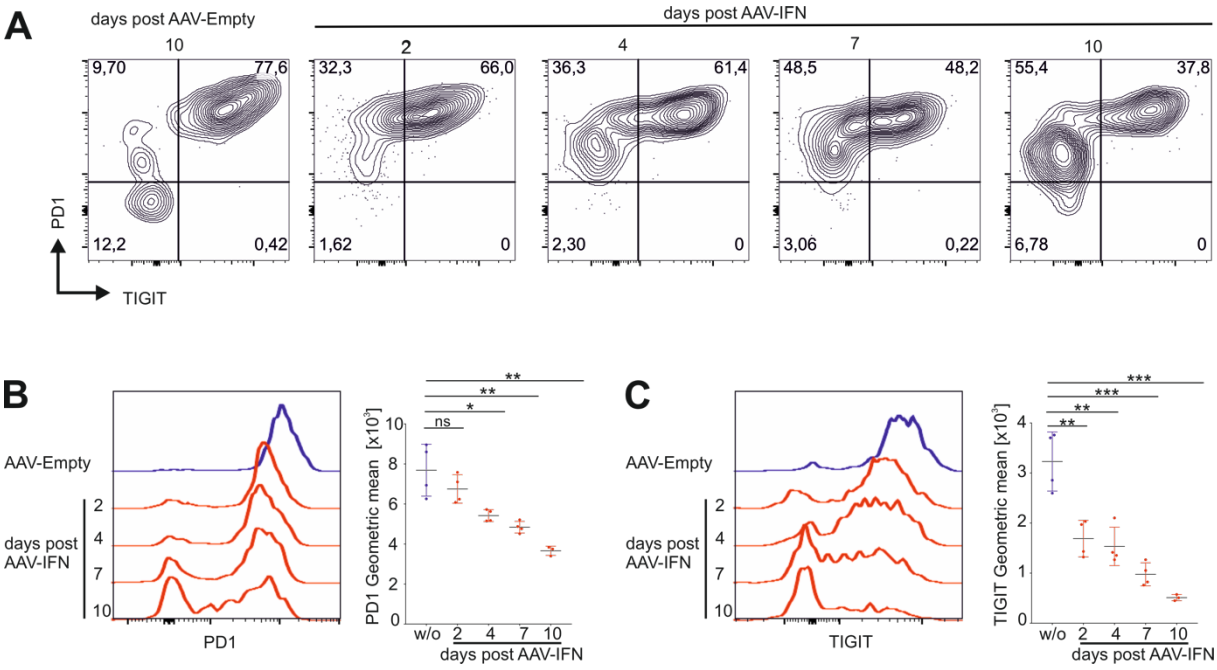

Figure 2.17| Analysis of inhibitory receptors on HBV-specific CD8$^+$ T cells in chronically Ad-HBV-Luc infected animals after AAV-IFN treatment
(A) Exemplary dot plots showing PD1 and TIGIT co-expression on intrahepatic HBV-specific CD8 T cells (gated on living CD8$^+$, CD44$^+$, C93-pentamer$^+$ T cells) at 2,4,7 and 10 days post AAV-IFN treatment compared to 10 days AAV-Empty treatment. (B) histogram plot and quantification of PD1 expression on HBV-specific CD8$^+$T cells from (A). (C) histogram plot and quantification of TIGIT expression on HBV-specific CD8$^+$ T cells from (A). Mean and SD are shown (n=3-4).

Surface expression of the cytotoxicity marker KLRG1, which was low on HBV-specific CD8$^+$ T cells in chronically infected mice treated with AAV-Empty, was strongly induced on HBV-specific CD8$^+$ T cells of mice treated with AAV-IFN already at day 2 after treatment and high expression was measured at any time point after AAV-IFN (Fig 2.18 B). Increased surface expression of the early activation marker CD69 was measured on HBV-specific CD8$^+$ T cells 2 days after AAV-IFN treatment. CD69 expression levels declined again from day 2 to day 10. However, also CD69 levels remained significantly increased over the AAV-Empty control treated mice at any time point after AAV-IFN treatment (Fig 2.18 C).

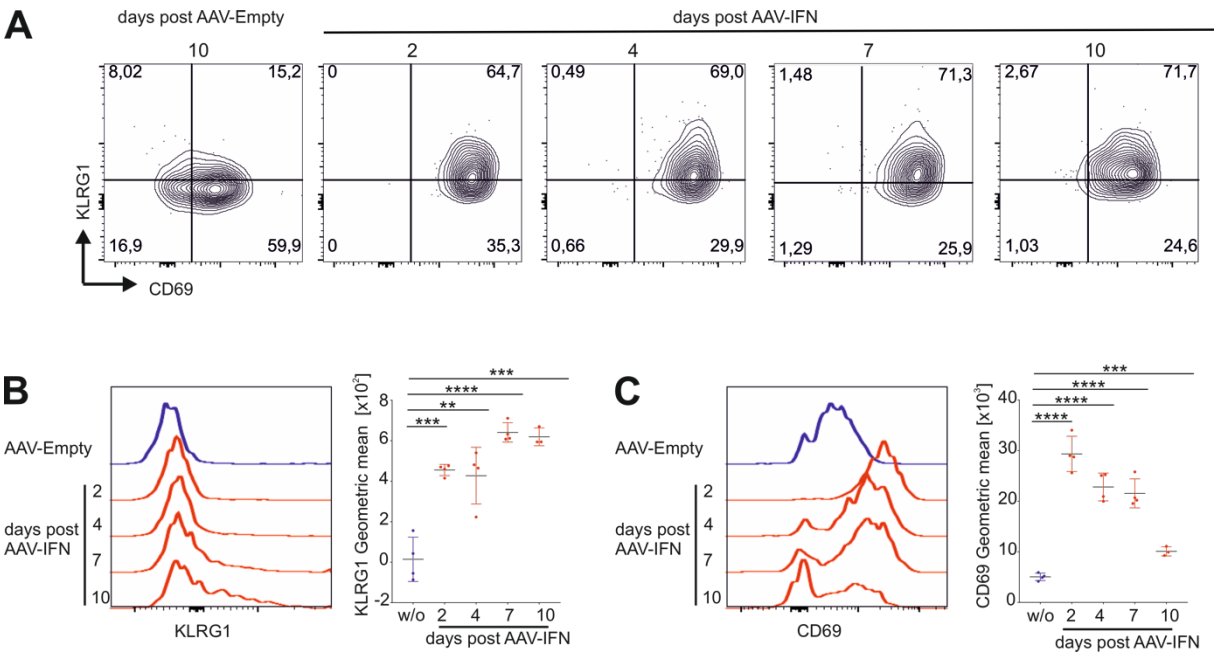

Figure 2.18| Analysis of cytotoxicity and activation marker on HBV-specific CD8⁺ T cells in chronically Ad-HBV-Luc infected animals after AAV-IFN treatment
(A) Exemplary dot plots showing KLRG1 and CD69 co-expression on intrahepatic HBV-specific CD8⁺ T cells (gated on living CD8⁺, CD44⁺, C93-pentamer⁺ T cells) at 2,4,7 and 10 days post AAV-IFN treatment compared to 10 days AAV-Empty treatment. (B) histogram plot and quantification of KLRG1 expression on HBV-specific CD8⁺ T cells from (A). (C) histogram plot and quantification of CD69 expression on HBV-specific CD8⁺ T cells from (A). Mean and SD are shown (n=3-4).

In addition, the levels of granzyme B, the proliferation marker Ki-67, and the exhaustion-associated transcription factor TOX on intrahepatic bulk CD8⁺ T cells after AAV-IFN treatment were determined. Consistent with increased levels of KLRG1, AAV-IFN treatment also induced granzyme B expression in CD8⁺ T cells (Fig 2.19 B). As the Ki-67 protein is absent in resting cells (G_0) and present during all active phases of the cell cycle (G_1, S, G_2, mitosis), we used Ki-67 protein expression as a proliferation-associated marker. AAV-IFN treatment highly induced Ki-67 already on day 2 after treatment, and levels increased until day 7. At day 10 after AAV-IFN treatment, Ki-67 levels were back to low expression levels of CD8⁺ T cells in AAV-Empty treated mice (Fig 2.19 C).

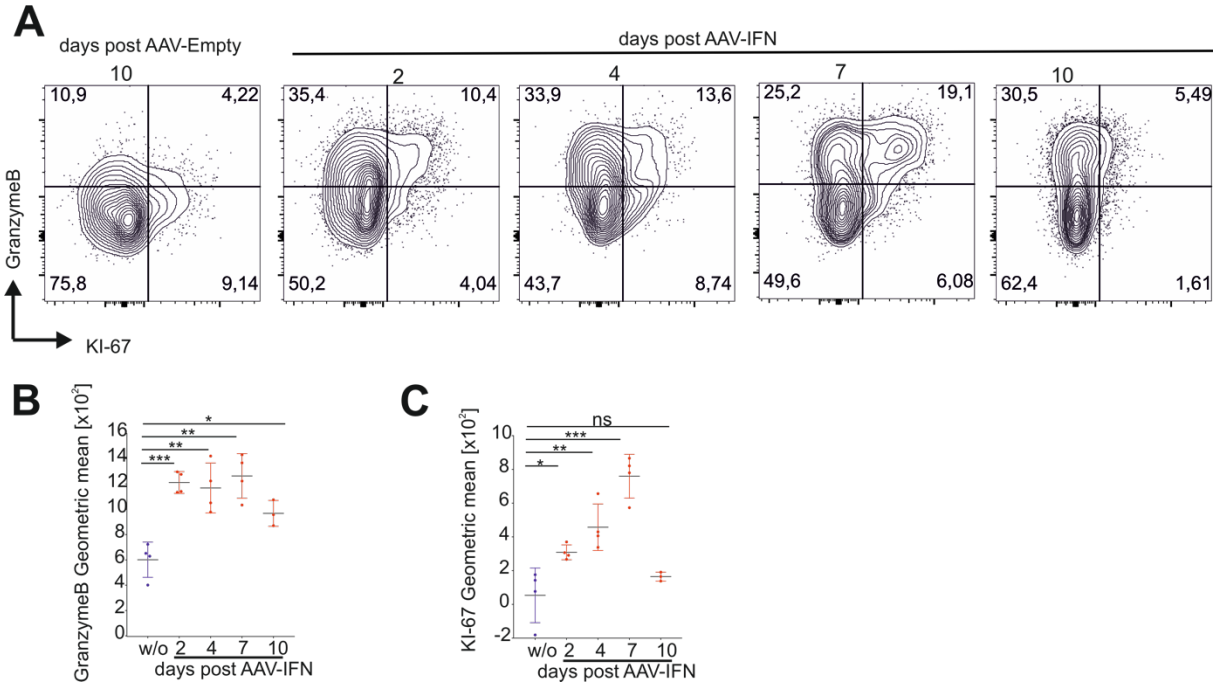

Figure 2.19| Analysis of intracellular cytotoxicity and proliferation marker in intrahepatic bulk CD8⁺ T cells in chronically Ad-HBV-Luc infected animals after AAV-IFN treatment
(A) Exemplary dot plots showing granzyme B and KI-67 co-expression in intrahepatic CD8⁺ T cells (gated on living CD8⁺ lymphocytes) at 2,4,7 and 10 days post AAV-IFN treatment compared to 10 days AAV-Empty treatment. (B) Quantification of intracellular granzyme B expression in CD8⁺ T cells from (A) (C) Quantification of KI-67 expression in CD8⁺ T cells from (A). Mean and SD are shown (n=3-4).

Treatment with AAV-IFN significantly reduces the frequency of exhausted TOX⁺PD1⁺TIGIT⁺CD8⁺ T cells in the liver. While more than 60% of intrahepatic bulk CD8⁺ T cells co-expressed TOX and PD1 in chronically infected mice, the frequency of TOX and PD1 co-expressing cells was reduced to 24.5% at day 10 after AAV-IFN treatment (Fig 2.20, A). Reduced levels of TOX were detected from day 4 onwards after AAV-IFN treatment (Fig 2.20, B).

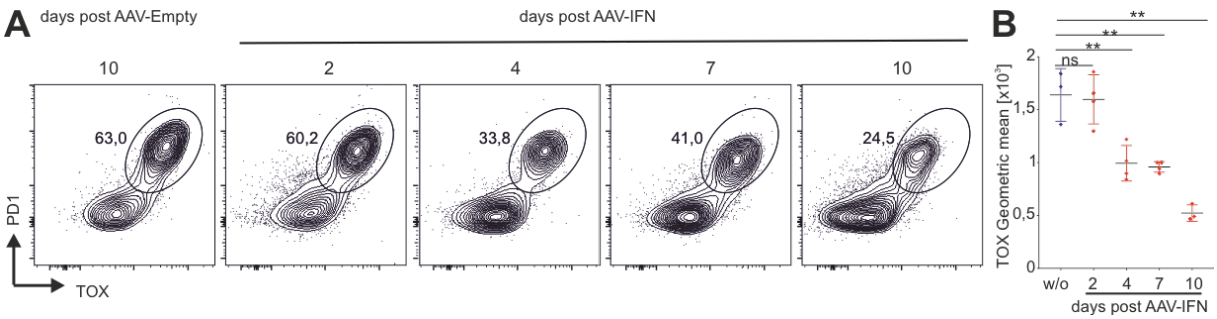

Figure 2.20| Analysis of the exhaustion-associated transcription factor TOX in intrahepatic bulk CD8⁺ T cells in chronically Ad-HBV-Luc infected animals after AAV-IFN treatment
(A) Exemplary dot plots showing TOX and PD1 co-expression in intrahepatic bulk CD8⁺ T cells (gated on living CD8⁺ lymphocytes at 2,4,7 and 10 days post AAV-IFN treatment compared to 10 days AAV-Empty treatment. (B) Quantification of TOX expression in CD8⁺ T cells from (A). Mean and SD are shown (n=3-4).

Because increased numbers of C93-specific CD8$^+$ T cells and an activated phenotype after AAV-IFN treatment suggest restored the functionality of HBV-specific CD8$^+$ T cells, an *ex vivo* kill assay was performed to prove restored functionality of HBV-specific CD8$^+$ T cells isolated from AAV-IFN treated mice. Upon co-culture with Ad-HBV1.3-infected primary murine hepatocytes, CD8$^+$ T cells isolated from animals transduced with AAV-IFN specifically killed a significantly higher number of target cells (80% specific killing) compared to CD8$^+$ T cells from animals transduced with AAV-Empty (30% specific killing) (Fig 2.21 B).

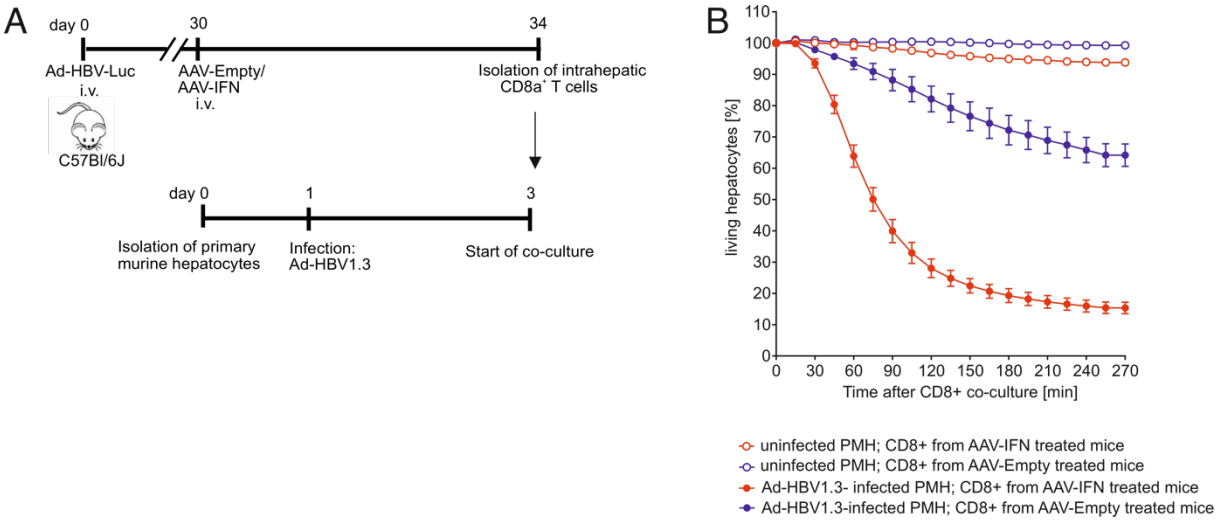

Figure 2.21| *Ex vivo* HBV-specific killing capacity of intrahepatic CD8$^+$ T cells after AAV-IFN treatment
(A) Schematic overview: HBV-specific effector CD8$^+$ T cells were generated by high-dose Ad-HBV-Luc infection at day 0 and AAV-IFN/Empty transduction at day 30. Effector CD8$^+$ T cells were isolated via untouched MACS isolation on day 4 after AAV-transduction. One day after isolation and seeding, primary murine hepatocytes (PMHs) were infected with Ad-HBV1.3 (MOI 5). 48 hours after infection, Ad-HBV1.3-infected or uninfected PMHs were co-cultured with 6 x 10^5 CD8$^+$ T cells isolated from either AAV-Empty or AAV-IFN transduced mice. (B) Normalized impedance measurement of PMH cocultured with isolated CD8$^+$ T cells as in (A) using the xCELLigence system. Mean and SD of triplicates are shown.

In conclusion, hepatocyte-specific IFNβ-expression restored quantity and functionality of C93-specific CD8$^+$ T cells in mice with an established chronic Ad-HBV-Luc infection. However, after an immune-active phase lasting for approximately 7 days, the anti-HBV immune response was terminated, although antigen was still present at a low level. The reason for the abrogation of reactivated HBV-specific CD8$^+$ T cell response and thereby incomplete control of persistent Ad-HBV-Luc infection remains to be elucidated.

2.3.3 Suppression of HBV antigen expression by HBV-specific RNA interference in an established chronic Ad-HBV-Luc infection

Another strategy to suppress HBV antigen expression is RNA interference (RNAi). RNAi was reported to suppress all HBV transcripts and proteins *in vivo* [230, 231]. As the four major HBV transcripts share a common 3' end, they are all targeted using one anti-HBV shRNA against the 3'end of all HBV RNAs. To this end, we used self-complementary AAV vectors (serotype

8) expressing an H1 promoter-driven shRNA targeting all HBV transcripts, named AAV-shHBV, or a non-coding AAV vector (AAV-shCTRL). The AAV-shHBV vector was demonstrated to efficiently knock-down secreted HBsAg, HBeAg, and HBV DNA as well as intracellular pgRNA, total HBV RNA and DNA [232]. Both vectors were provided by Thomas Michler (Institute of Virology, TUM) [222, 232].

We injected 10^{11} genome copies (gc) of AAV-shHBV or AAV-shCTRL intravenously into C57Bl/6J mice with an established chronic Ad-HBV-Luc infection at day 30 p.i. and measured bioluminescence signals, sALT, and HBeAg for 10 days after AAV-shHBV/AAV-shCTRL transduction (Fig 2.22 A). Transduction with AAV-shHBV efficiently reduces, as expected, HBeAg levels in the blood by 1 log at day 8 post transduction (Fig 2.22 B). It is important to note that the extent of serum HBeAg-level reduction of 1 log is comparable to the reduction achieved by IFN-mediated inhibition of protein synthesis and also to levels detected in mice infected with the acute infectious dose. However, neither the bioluminescence signal nor the sALT level was affected by AAV-shHBV transduction (Fig2.22 C, D). Hence, the reduction of HBV-antigen levels by RNAi fails to induce anti-HBV immunity in chronic Ad-HBV-Luc infected animals.

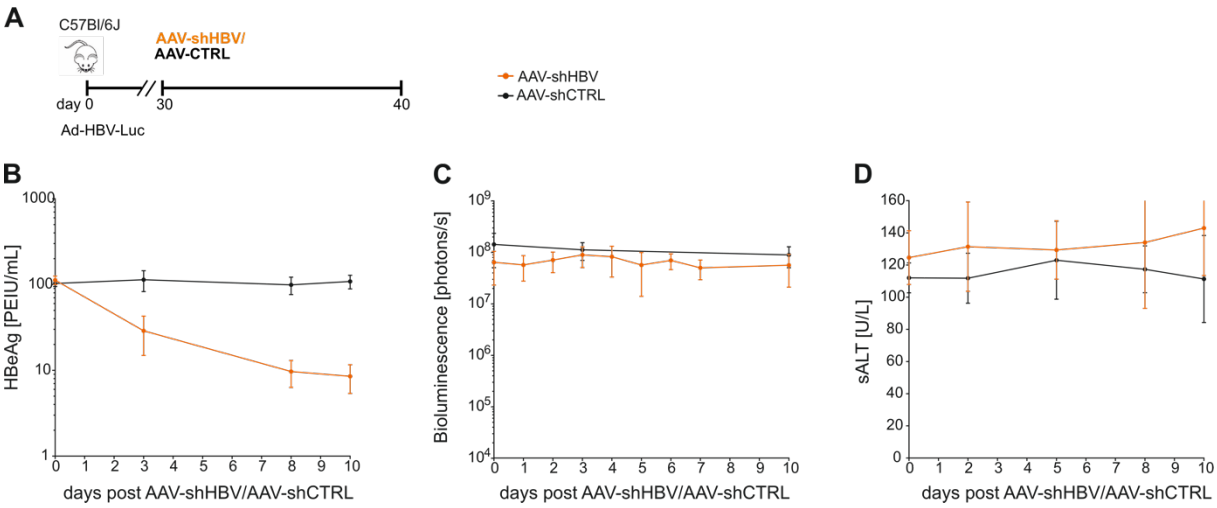

Figure 2.22| Impact of HBV-antigen reduction by HBV-specific RNAi on anti-HBV immunity
(A) Schematic overview: C57Bl/6J mice were i.v. injected with 2 x 10^8 pfu Ad-HBV-Luc. At day 30 p.i., mice were i.v. injected with 1 x 10^{11} gc of either AAV-shHBV or AAV-shCTRL. (B) HBeAg levels in the blood after AAV-shHBV or AAV-shCTRL transduction. (C) Quantification of bioluminescence signal in mice after AAV-shHBV or AAV-shCTRL transduction. (D) Serum ALT levels after AAV-shHBV or AAV-shCTRL transduction. Mean and SD are shown (n=5).

2.3.4 Effect of hepatocyte- and T cell-specific IFNAR1 knockout on the induction of anti-HBV immunity by hepatocyte-specific IFNβ expression

A recent study conducted by Michler and Kosinska *et al.* demonstrated that reduction of HBV antigen levels via RNAi prior to application of a therapeutic vaccination scheme promotes

successful induction of anti-HBV $CD8^+$ T cell immunity [222]. These data support the hypothesis that both effects elicited by IFN signaling, namely inhibition of viral protein synthesis and direct $CD8^+$ T cell stimulation, are necessary to re-activate exhausted HBV-specific $CD8^+$ T cells in an established chronic HBV infection. Therefore, both mechanisms elicited by IFN signaling were separated to determine whether the reduction of antigen load or the IFN-mediated immune stimulation is redundant. In AlbCre x $IFNAR^{fl/fl}$ mice, which lack IFNAR1 expression specifically on hepatocytes, hepatocyte-specific IFNβ expression elicits immune stimulation but fails to reduce HBV antigen load in hepatocytes. In CD4Cre x $IFNAR^{fl/fl}$ mice, which lack IFNAR1 expression on $CD4^+$ and $CD8^+$ T cells, hepatocyte-specific IFNβ expression reduces HBV antigen load in hepatocytes but IFN signaling in $CD4^+$ and $CD8^+$ T cells is not engaged.
In $IFNAR^{fl/fl}$ littermates, AAV-IFN transduction led to a 300-fold reduction of viral antigen load at day 13 post transduction (Fig 2.23 B), which is comparable to the reduction observed in wildtype C57BL/6J mice (Fig 2.13). From the 10-fold reduced viral antigen load in AAV-IFN transduced $IFNAR^{fl/fl}$ mice depleted of $CD8^+$ T cells, a 30-fold reduction of viral antigen load in the liver was deduced to be mediated by $CD8^+$ T cells. Immunohistochemical analysis of HBcAg levels in liver tissue of either AAV-IFN or AAV-Empty transduced $IFNAR^{fl/fl}$ mice revealed 19-fold less HBc+ nuclei per mm^2 liver tissue in AAV-IFN transduced mice as in AAV-Empty transduced mice (Fig 2.23 C). In AlbCre x $IFNAR^{fl/fl}$ mice, the AAV-IFN transduction led to 2-fold decreased viral antigen load measured by bioluminescence signal at day 13 post transduction (Fig 2.23 B). However, immunohistochemical quantification of HBc+ nuclei per mm^2 revealed no significant reduction (1,2-fold) in AAV-IFN transduced compared to AAV-Empty transduced mice. Interestingly, cytoplasmic HBcAg staining was only observed in AlbCre x $IFNAR^{fl/fl}$ mice transduced with AAV-Empty, which was not present in AlbCre x $IFNAR^{fl/fl}$ mice transduced with AAV-IFN (Fig 2.23 C). This observation indicates that IFNAR signaling in hepatocytes is responsible for low cytoplasmic HBcAg levels. In CD4Cre x $IFNAR^{fl/fl}$ mice, hepatocyte-specific IFNβ expression led to 11-fold reduced viral load measured via bioluminescence at day 13 post transduction, which is similar to $CD8^+$ T cell depleted $IFNAR^{fl/fl}$ littermates. Immunohistochemical quantification revealed that it is significant, but only 1,9-fold reduction of HBc+ nuclei per mm^2 in AAV-IFN transduced mice (Fig 2.23 C). These results demonstrate that in animals lacking IFNAR1 on T cells, anti-HBV immunity is either not induced at all, or only weakly induced.

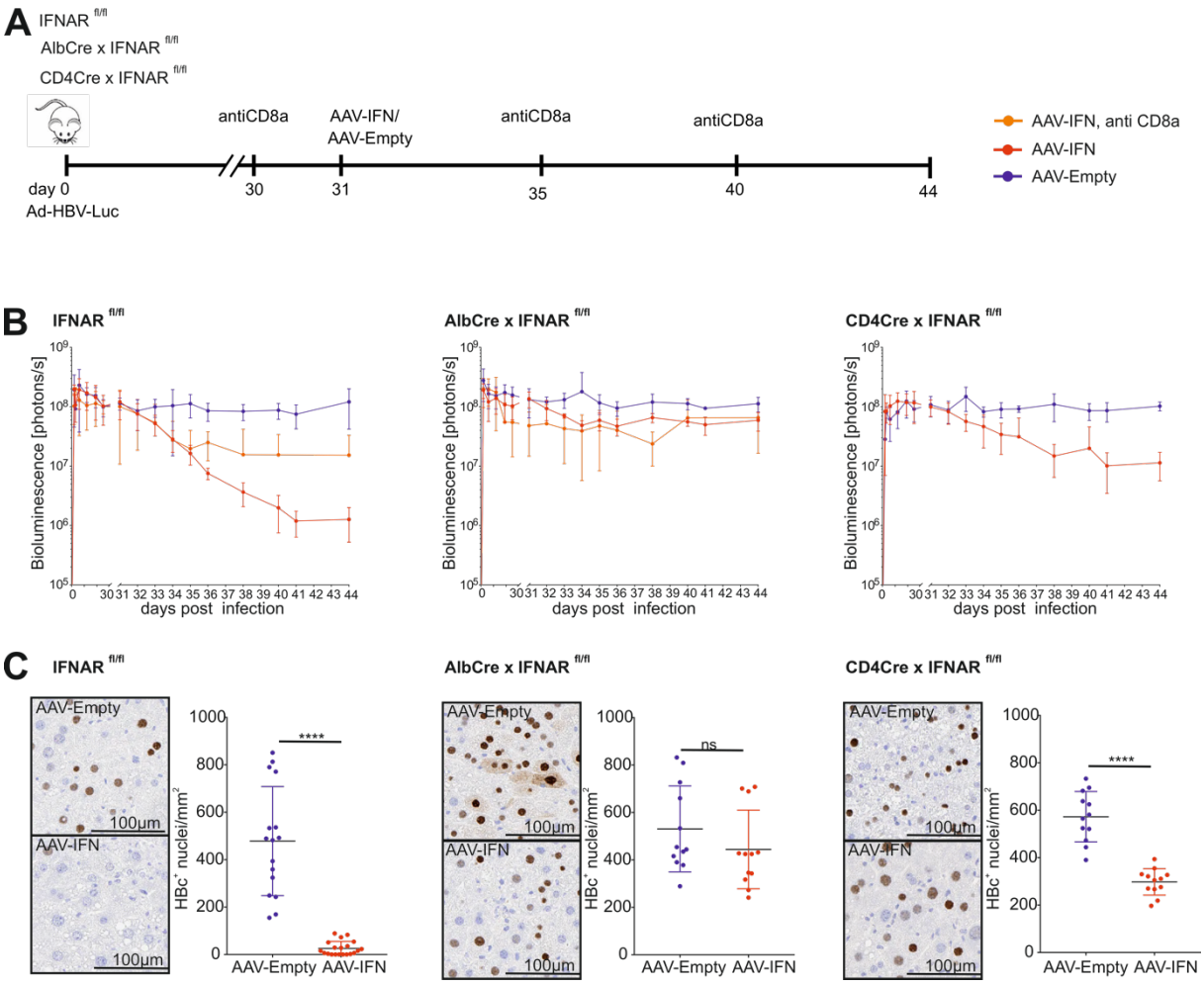

Figure 2.23| Antiviral effect of hepatocyte-specific IFNβ expression in mice lacking IFNAR1 specifically on hepatocytes or T cells
(A) Schematic overview: IFNAR $^{fl/fl}$, AlbCre x IFNAR $^{fl/fl,}$ and CD4Cre x IFNAR$^{fl/fl}$ mice were i.v. injected with 10^8 pfu Ad-HBV-Luc on day 0. On day 31 after infection, mice were i.v. Injected with 10^{11} gc AAV-IFN or AAV-Empty. In the CD8$^+$ T cell depleted groups, mice were i.v. injected with antiCD8a depleting antibody one day before, four days and 9 days after AAV-transduction. (B) Quantification of bioluminescence in mice treated as in (A). (C) Representative immunohistochemical HBcAg staining of liver sections of mice treated as in (A) at day 44. Quantification of HBc+ nuclei/mm^2. Mean and SD are shown (n= 4-9).

I also analyzed pSTAT1 levels in liver tissue of AAV-IFN, or AAV-Empty transduced IFNAR $^{fl/fl}$, AlbCre x IFNAR $^{fl/fl}$, and CD4Cre x IFNAR$^{fl/fl}$ mice at day 13 post transduction. Levels of pSTAT1 were significantly increased in AAV-IFN compared to AAV-Empty transduced mice. At this late time point post transduction, I observed only a 2-fold increase of pSTAT1 levels in IFNAR$^{fl/fl}$ control littermates transduced with AAV-IFN compared to AAV-Empty (Fig 2.24 A, B). This observation is consistent with the analysis of pSTAT1 levels in wildtype C57BL/6 mice at later time points post transduction. In CD4Cre x IFNAR$^{fl/fl}$ mice, no significant increased pSTAT1-levels in the liver of AAV-IFN over AAV-Empty transduced mice were measured at day 13 post transduction. In AlbCre x IFNAR$^{fl/fl}$ mice, pSTAT1-levels were 5-fold higher in AAV-IFN compared to AAV-Empty transduced mice at day 13 post transduction (Fig 2.24 A, B). However, in contrast to CD4Crex IFNAR$^{fl/fl}$ or IFNAR$^{fl/fl}$ mice, pSTAT1 staining was not

observed in hepatocytes of AlbCre x IFNAR$^{fl/fl}$ mice (Fig2.24 A). Interestingly, despite the absence of pSTAT1 in hepatocytes, the strength of IFN signaling, measured via staining intensity of pSTAT1, was highest in AlbCre x IFNAR$^{fl/fl}$ mice (Fig 2.24 B). An induction of OAS-1 RNA after AAV-IFN treatment compared to AAV-Empty treatment was measured in all genotypes (Fig 2.24 C). Although, the background level (AAV-Empty treated) of OAS-1 RNA in liver tissue of AlbCre x IFNAR$^{fl/fl}$ mice was lower, the induction after AAV-IFN was similar to the induction in CD4Cre x IFNAR$^{fl/fl}$ or IFNAR$^{fl/fl}$ mice (Fig 2.24 C).

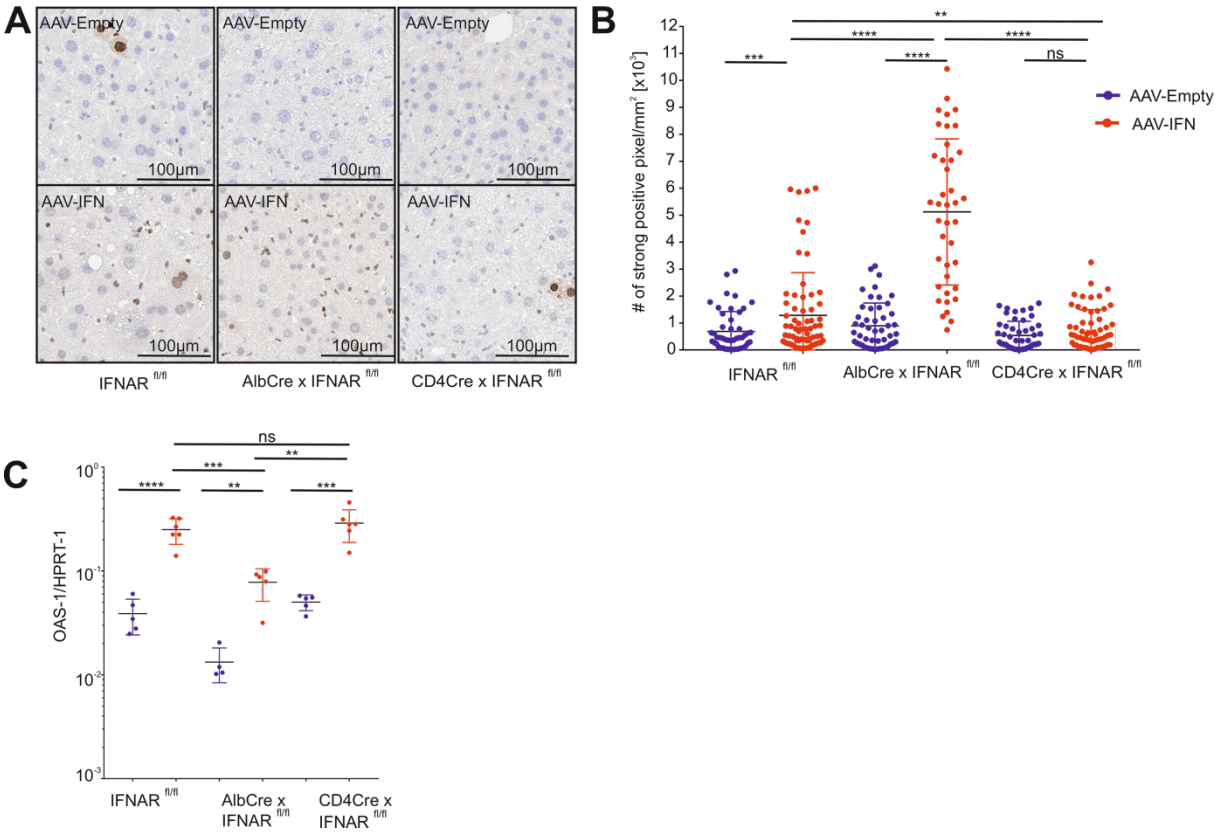

Figure 2.24| IFNAR-signaling in IFNAR $^{fl/fl}$, AlbCre x IFNAR $^{fl/fl}$, and CD4Cre x IFNAR$^{fl/fl}$ mice 13 days after AAV-IFN/Empty transduction in animals with an established chronic Ad-HBV-Luc infection
(A) Representative immunohistochemical pSTAT1 staining of liver sections of mice infected with 10^8 pfu Ad-HBV-Luc at day 44 treated with AAV-IFN or AAV-Empty at day 31. Scale bars indicate 100 µm. (B) Quantification of strong positive pixel per mm^2. 10 ROIs per liver section were analyzed. (C) OAS-1 expression in liver tissue of mice from (A) relative to HPRT-1 determined by qPCR. Mean and SD are shown (n=4-7).

In conclusion, these important results indicate that IFN-mediated restoration of HBV-specific exhausted CD8$^+$ T cells in chronic Ad-HBV-Luc infected mice depends on (1) reduction of viral antigen in hepatocytes, mediated via IFNAR-signalling in hepatocytes, and on (2) the exertion of an immunostimulatory signal for CD8$^+$ T cells, mediated via IFNAR-signalling in CD8$^+$ T cells.

2.4 Impact of length of exposure to high antigen load on mounted HBV-specific CD8$^+$ T cell immunity

Although the results demonstrated that reactivation of exhausted anti-HBV CD8$^+$ T cell immunity in an established chronic Ad-HBV-Luc infection is possible by treatment with AAV-IFN, complete viral clearance was not achieved.

There is literature suggesting that length of antigen exposure impacts the severity of CD8$^+$ T cell exhaustion[233] and thereby probably also influences the threshold for reactivation. Therefore, we aimed at investigating the impact of exposition duration on reactivation via HBV antigen load reduction.

2.4.1 Impact of length of exposure to high viral antigen load on kinetic or magnitude of reactivated anti-HBV immunity

To determine whether kinetic or magnitude of anti-HBV immunity induced by hepatocyte-specific IFNβ expression depends on the time period immune cells are exposed to high levels of HBV antigens before, we injected AAV-IFN or AAV-Empty into mice 1 day, 15 days or 30 days after Ad-HBV-Luc infection (Fig 2.25 A). In mice injected at day 15 and day 30 p.i. the extent of antigen reduction (Fig 2.25 B) and kinetic of serum ALT elevation (Fig 2.25 C) were comparable. While the magnitude and kinetics of immune response seem comparable, total antigen load was lower 10 days after treatment, and the magnitude of serum ALT elevation was lower in mice treated at day 30 compared to mice treated on day 15. These differences originate most likely from slightly different antigen load at injection time points.

In mice treated at day 1 after Ad-HBV-Luc infection, antigen load was slightly reduced at day 1 and 2 after treatment, but further reduction mediated by anti-HBV-immunity was significantly delayed starting at day 6 after treatment (Fig 2.25 B, C). Delayed induction of anti-HBV immunity is explainable by the absence of primed HBV-specific effector cells in animals treated at day 1 after Ad-HBV-Luc infection. However, despite reduced antigen load early after infection and early anti-HBV immune response, mice treated at day 1 after Ad-HBV-Luc infection did not control Ad-HBV-Luc infection later on (Data not shown).

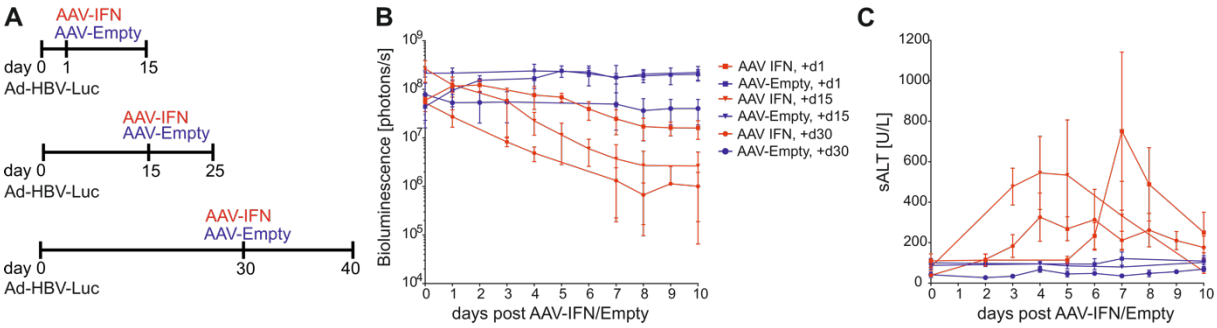

Figure 2.25| Impact of antigen exposure length on IFN-induced anti-HBV immune response
(A) Schematic overview: C57Bl/6J mice were i.v. injected with 10^8 pfu Ad-HBV-Luc on day 0. At day 1, day 15 or day 30 after infection, animals were i.v. injected with AAV-IFN or AAV-Empty. (B) Quantification of bioluminescence signal in mice after transduction with AAV-IFN/Empty (d0) of animals either injected at day 1, 15, or 30 after Ad-HBV-Luc infection. (C) Serum ALT levels of mice from (B). Mean and SD are shown (n=5).

In summary, these results do not provide any evidence of a positive impact of shorter exposition to high antigen load on the magnitude of reactivated anti-HBV immunity. The extent of viral elimination appears to depend instead on the viral load at the start of treatment, which is in this setting without re-infection lower at later time points p.i..

2.5 Investigation of TLR3-stimulation mediated reactivation of anti-HBV immunity

Hepatocyte-specific IFNβ expression was shown to induce a continuous and relatively stable strength of IFN signaling in the liver. Systemic injections of recombinant IFNα or IFNβ or their pegylated forms induce tonic type I IFN signaling depending on the frequency of injections. Because of very poor stability and short half-life of recombinant IFNα or IFNβ in the systemic circulation, tonic IFN signaling was induced via sequential injections of theTLR3-ligand polyI:C.

2.5.1 Antiviral effect of TLR3-stimulation in mice with established chronic Ad-HBV-Luc infection

We tested whether the effects of systemically applied polyI:C on the restoration of anti-HBV immunity in an established chronic Ad-HBV-Luc infection are comparable to the effects that were observed by intrahepatic production of type I IFN. To this end, 20 µg polyI:C were i.v. injected on a daily basis into mice with an established persistent Ad-HBV-Luc infection or into uninfected animals (Fig 2.26 A). The effects were monitored by bioluminescence imaging, measurement of sALT, and body weight over 12 days from the start of treatment. Kinetic and level of antigen reduction mediated via daily polyI:C injection was comparable to kinetic and level of reduction induced by AAV-IFN transduction (Fig 2.26 B) until day 8 post treatment. While in AAV-IFN treated animals, no further reduction was observed after day 8, bioluminescence levels of polyI:C treated mice were reduced to background levels until day 12 of treatment (Fig 2.26 B). In line with the reduction of antigen load in the liver, sALT levels were strongly elevated compared to untreated chronically Ad-HBV-Luc infected animals (Fig 2.26 C). The loss of body weight in the polyI:C treated group accumulated to around 8% from the start of treatment on (Fig 2.26 D).

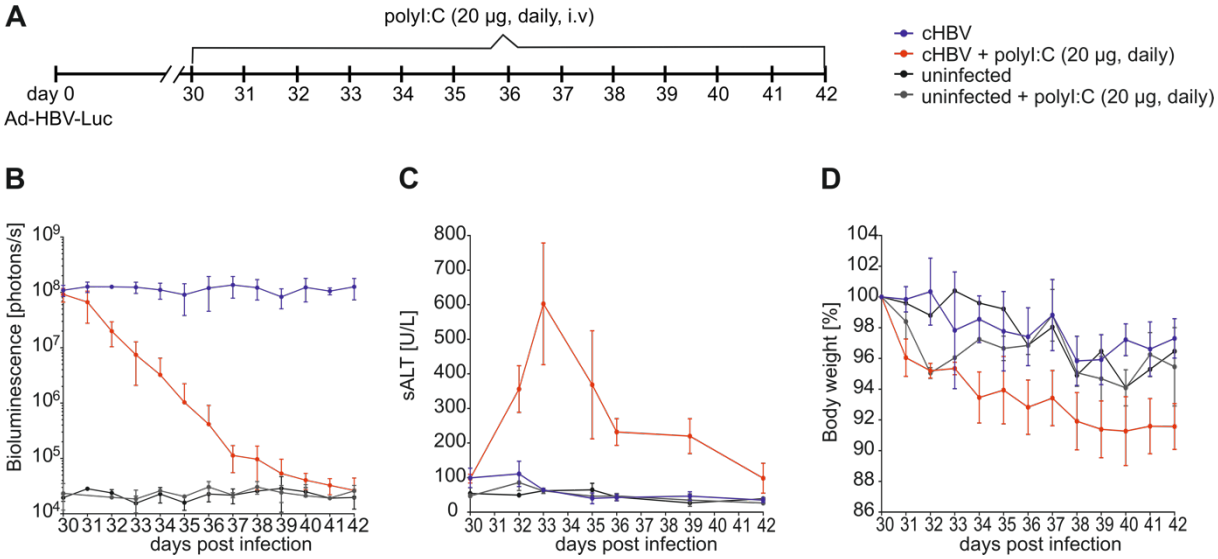

Figure 2.26| Analysis of polyI:C-induced anti-HBV immunity in animals with an established chronic Ad-HBV-Luc infection
(A) Schematic overview: C57Bl/6J mice were i.v. injected with 10^8 pfu Ad-HBV-Luc on day 0. From day 30 p.i. on, one group of mice with an established chronic Ad-HBV-Luc infection and one group of uninfected mice was injected with 20 µg polyI:C on a daily basis for 12 days. (B) Quantification of bioluminescence signal in mice from the start of polyI:C treatment onwards. (C) Serum ALT levels from the start of polyI:C treatment onwards. (D) Bodyweight change from the start of treatment in mice with an established chronic Ad-HBV-Luc infection or uninfected mice treated with polyI:C. Mean and SD are shown (n=2-5).

9 days post polyI:C treatment (d51 p.I), mice were sacrificed, and liver tissue was analyzed for pgRNA, OAS-1, and ISG15 expression levels. Levels of pgRNA expression in liver tissue were almost down to background expression levels measured in livers of uninfected mice (Fig 2.27 B). At this time, levels of interferon-stimulated genes ISG15 and OAS-1 in liver tissue of polyI:C-treated mice were not elevated over untreated mice (Fig 2.27 C, D).

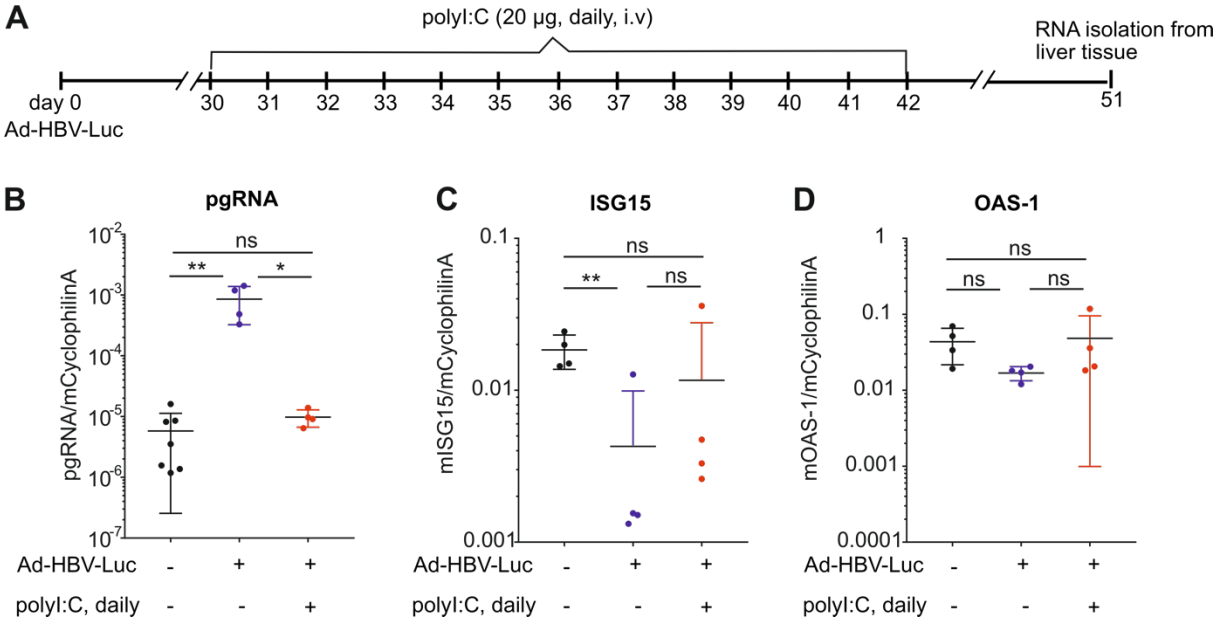

Figure 2.27| Analysis of IFN signaling and pgRNA expression after polyI:C mediated elimination of persistent Ad-HBV-Luc infection
(A) Schematic overview: C57Bl/6J mice were i.v. injected with $2x10^8$ pfu Ad-HBV-Luc on day 0. From day 30 p.i. on, one group of mice with an established chronic Ad-HBV-Luc infection and one group of uninfected mice were injected with 20 µg polyI:C on a daily basis for 12 days. From day 43 to 51, all groups were left untreated. At day 51 p.i. mice were sacrificed, and livers were removed for RNA isolation. (B) Levels of pgRNA, (C) ISG15, and (D) OAS-1 in liver tissue of mice with an established chronic Ad-HBV-Luc infection either treated with polyI:C or left untreated relative to CyclophilinA determined by qPCR. Mean and SD are shown (n=4).

In summary, systemic administration of polyI:C reduced HBV infection parameters to the detection limit. As we did not observe significant levels of pgRNA in livers of mice treated with 12 consecutive daily injections and then left untreated for 9 days before analysis was performed, I propose that elimination of Ad-HBV-Luc infected hepatocytes rather than an IFN-mediated suppression of HBV antigens or pgRNA was achieved.

2.5.2 Antiviral effects of TLR3-stimulation in AlbCre and CD4Cre IFNAR$^{fl/fl}$ mice

In order to investigate whether induction of antiviral effects by TLR3-stimulation depends on IFNAR signaling in hepatocytes and T cells, comparable with the antiviral effects induced by AAV-IFN treatment, we compared the polyI:C-mediated induction of antiviral immunity in AlbCre x IFNAR$^{fl/fl}$ mice, CD4Cre x IFNAR$^{fl/fl}$ mice, and IFNAR$^{fl/fl}$ littermates with established chronic Ad-HBV-Luc infection (Fig 2.28 A). In IFNAR$^{fl/fl}$ littermates, 10 sequential polyI:C injections efficiently reduced viral antigen (Fig 2.28 B) and increased sALT levels sustained over 10 days of treatment (Fig 2.28 C). In contrast, only a minor reduction of viral antigen in the liver (Fig 2.28 B) and transiently increase sALT levels was observed in CD4Cre- and AlbCre x IFNAR$^{fl/fl}$ mice.

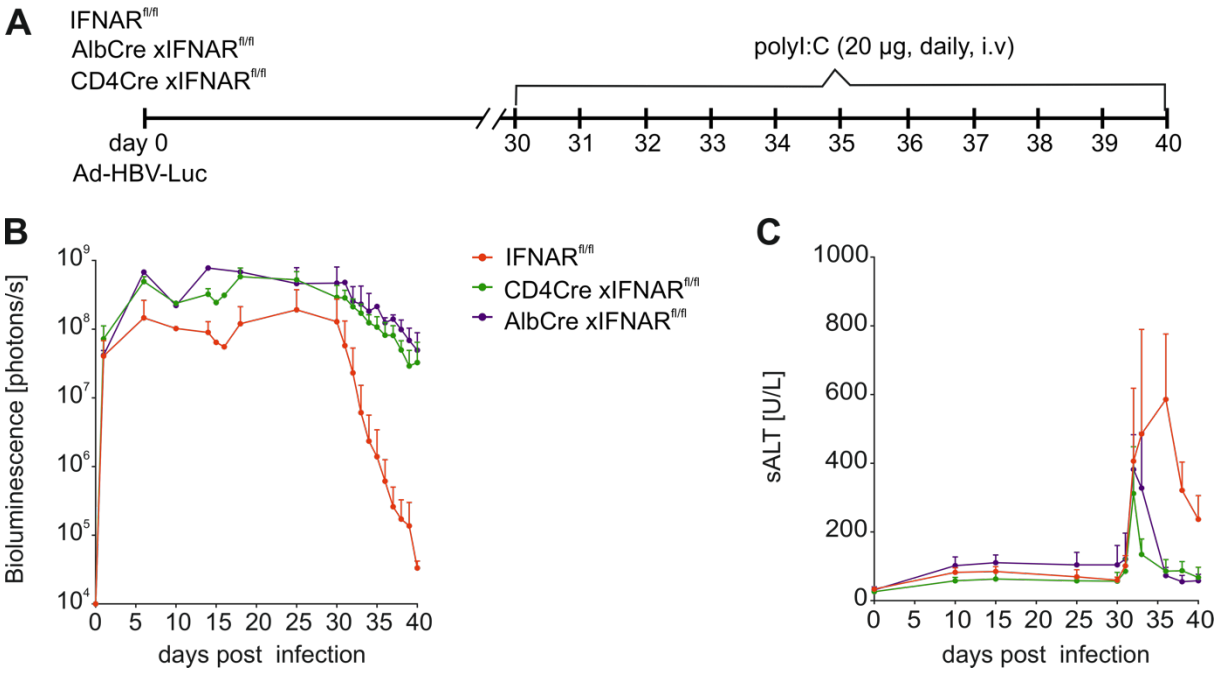

Figure 2.28| Analysis of antiviral effects induced by sequential polyI:C injections in AlbCre x IFNAR$^{fl/fl}$, CD4Cre x IFNAR$^{fl/fl}$, and IFNAR$^{fl/fl}$ mice with established chronic Ad-HBV-Luc infection
(A) Schematic overview AlbCre x IFNAR$^{fl/fl,}$ CD4Cre x IFNAR$^{fl/fl}$, and IFNAR$^{fl/fl}$ mice were i.v. injected with 10^8 pfu Ad-HBV-Luc on day 0. From day 30 p.i. onwards, mice were injected with 20 µg polyI:C on a daily basis for 10 days. B) Quantification of bioluminescence signal in mice from Ad-HBV-Luc infection onwards. (C) Serum ALT levels from Ad-HBV-Luc infection onwards. Mean and SD are shown (n=3-6).

Hence, TLR3-stimulation-induced anti-HBV immunity in mice with persistent Ad-HBV-Luc infection depends on INFAR signaling in hepatocytes and T cells. To determine whether IFNAR1 signaling in HBV-specific CD8$^+$ T cells is sufficient to rescue polyI:C-induced antiviral immunity in CD4Cre x IFNAR$^{fl/fl}$ mice, IFNAR1 competent naïve C93-specific CD8$^+$ T cells were transferred into CD4Cre x IFNAR$^{fl/fl}$ mice or IFNAR$^{fl/fl}$ littermates at day 0 shortly before Ad-HBV-Luc infection (Fig 2.29 A). In IFNAR$^{fl/fl}$ littermates, reduction of viral antigen load in the liver (Fig 2.29 B) and induction of sALT levels (Fig 2.29 C) was similar as in mice with or without adoptive transfer of IFNAR competent naïve C93-specific CD8$^+$ T cells. In CD4Cre x IFNAR$^{fl/fl}$ mice, the reduction of viral antigen load was significantly strengthened in mice with adoptive transfer (Fig 2.29 B). Further, increased sALT levels were sustained in CD4Cre x IFNAR$^{fl/fl}$ mice with adoptive transfer over mice without adoptive transfer (Fig 2.29 C). Thus, the adoptive transfer of IFNAR1 competent C93-specific CD8$^+$ T cells rescued the phenotype in CD4Cre x IFNAR$^{fl/fl}$ mice, indicating a mandatory provision of direct IFNAR signaling in HBV-specific CD8$^+$ T cells for polyI:C-mediated restoration of anti-HBV-specific CD8$^+$ T cell immunity.

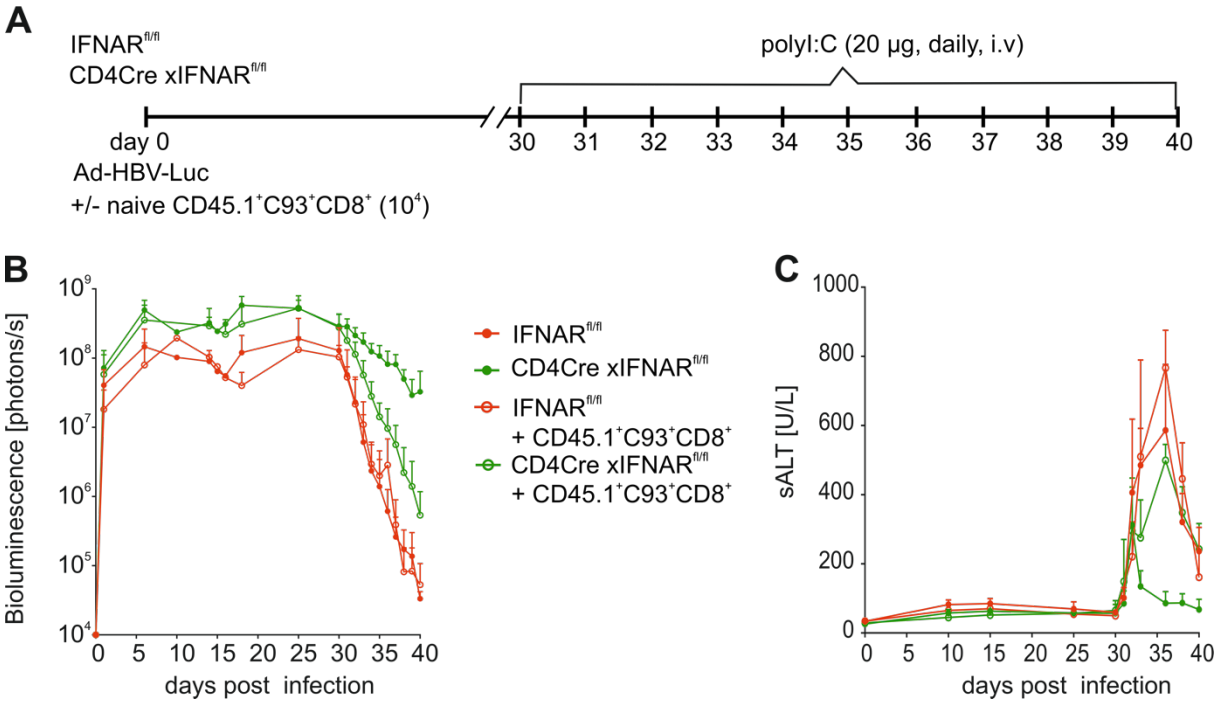

Figure 2.29| Analysis of antiviral effects induced by sequential polyI:C injections in CD4Cre x IFNAR$^{fl/fl}$ and IFNAR$^{fl/fl}$ mice with established chronic Ad-HBV-Luc infection with or without adoptive transfer of naïve IFNAR competent C93-specific CD8$^+$ T cells.
(A) Schematic overview CD4Cre x IFNAR$^{fl/fl}$ and IFNAR$^{fl/fl}$ mice were i.v. injected with 10^8 pfu Ad-HBV-Luc on day 0. Additionally, 10^4 naïve CD45.1$^+$ C93-specific CD8$^+$T cells, isolated from spleens of C93-TCR transgenic mice, were transferred at day 0. From day 30 p.i. onwards, mice were injected with 20 µg polyI:C on a daily basis for 10

days. B) Quantification of bioluminescence signal in mice from Ad-HBV-Luc infection onwards. (C) Serum ALT levels from Ad-HBV-Luc infection onwards. Mean and SD are shown (n=3-6).

2.5.3 Systemic administration of TLR3-ligand polyI:C induces expansion and activation of HBV-specific CD8$^+$ T cells

In mice with an established chronic Ad-HBV-Luc infection, two injections of polyI:C in 24-hour intervals induced a significant increase of ALT levels in the serum and a > 1 log reduction of antigen load in the liver (Fig 2.26 B, C), indicating reactivation of anti-HBV immunity. 24 hours after the second polyI:C injection, an approx. 10-fold increase of C93-specific CD8$^+$ T cells in livers of polyI:C-treated chronic Ad-HBV-Luc infected mice was detected (Fig 2.30 B, C).

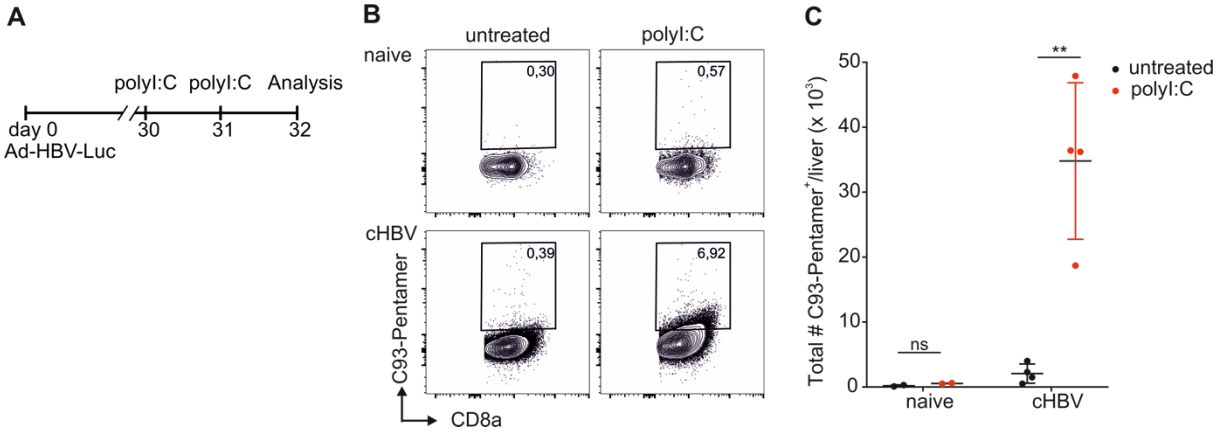

Figure 2.30| Quantification of HBV-specific CD8$^+$ T cells after polyI:C treatment of mice with an established chronic Ad-HBV-Luc infection
(A) Schematic overview: C57Bl/6J mice were i.v. injected with 10^8 pfu Ad-HBV-Luc on day 0. At day 30 and 31 p.i., the polyI:C treated group was injected with polyI:C. At day 32 p.i. liver associated lymphocytes were analyzed. (B) flow cytometric analysis and (C) quantification of C93-specific CD8$^+$ T cells (gated on living CD44$^+$ CD8$^+$ cells). Unspecific staining was determined using uninfected mice with or without polyI:C-treatment. Total numbers were calculated using counting beads. Mean and SD are shown (n=2-4).

To provide further evidence for re-activation of anti-HBV-immunity in cHBV-infected mice after two consecutive injections of polyI:C, expression of activation and cytotoxicity markers on C93-specific CD8$^+$ T cells were measured. C93-specific CD8$^+$ T cells isolated from cHBV-infected animals treated with two consecutive injections of polyI:C demonstrated substantially higher expression levels of CD69 (Fig 2.31 A), KLRG1 (Fig 2.31 B) and granzyme B (Fig 2.31 C). CD69 was shown to be directly regulated downstream of IFNα/β [234] and granzyme B and other effector molecules were demonstrated to be induced by IFN in the absence of cognate antigen [235, 236]. In order to discriminate between specific activation of HBV-specific CD8$^+$ T cells and direct measures of IFNα/β-signaling, the induction of all markers on naïve CD8$^+$ T cells and C93-specific CD8$^+$ T cells were compared. PolyI:C treatment affected CD69 and granzyme B expression levels in naïve CD8$^+$ T cells, while KLRG1 expression was not significantly affected (Fig 2.31 A-C).

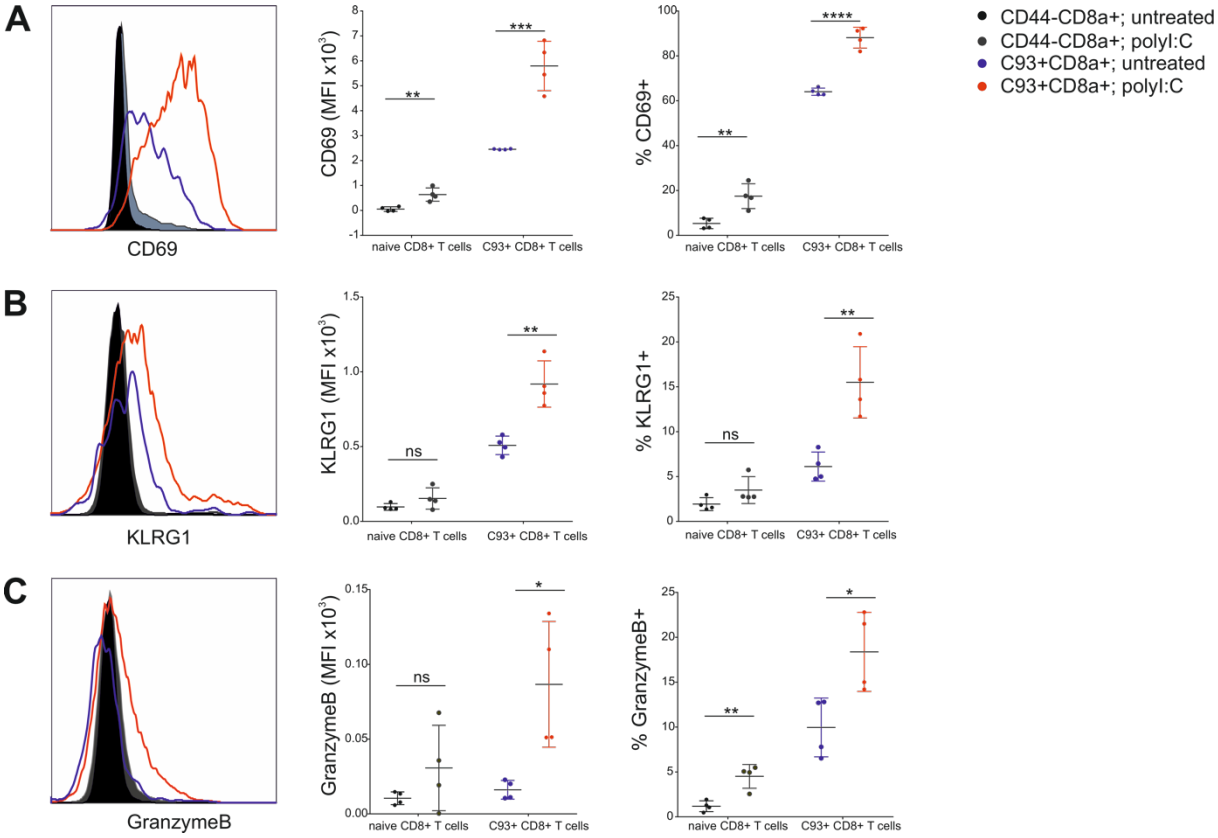

Figure 2.31| Expression of activation and cytotoxicity markers on HBV-specific CD8⁺ T cells after polyI:C treatment of mice with established chronic Ad-HBV-Luc infection
Flow cytometric analysis and quantification of CD69 (A), KLRG1 (B) and granzyme B (C) expression on HBV-specific CD8⁺ T cells (gated on living C93-specific CD8⁺) and naïve CD8⁺ T cell (gated on living CD44⁻CD8⁺) treated with 2 consecutive injections polyI:C or left untreated. Mean and SD are shown (n=4).

Although the frequency of TIGIT⁺ C93-specific CD8⁺ T cells was not affected by two injections of polyI:C, the quantity of TIGIT surface expression levels was significantly reduced (Fig 2.32 A). Already after two consecutive injections of polyI:C frequency of C93-specific CD8⁺ T cells expressing the proliferation marker Ki-67 was significantly increased, suggesting considerably more cell division of C93-specific CD8⁺ T cells in the polyI:C-treated group (Fig 2.32 B).

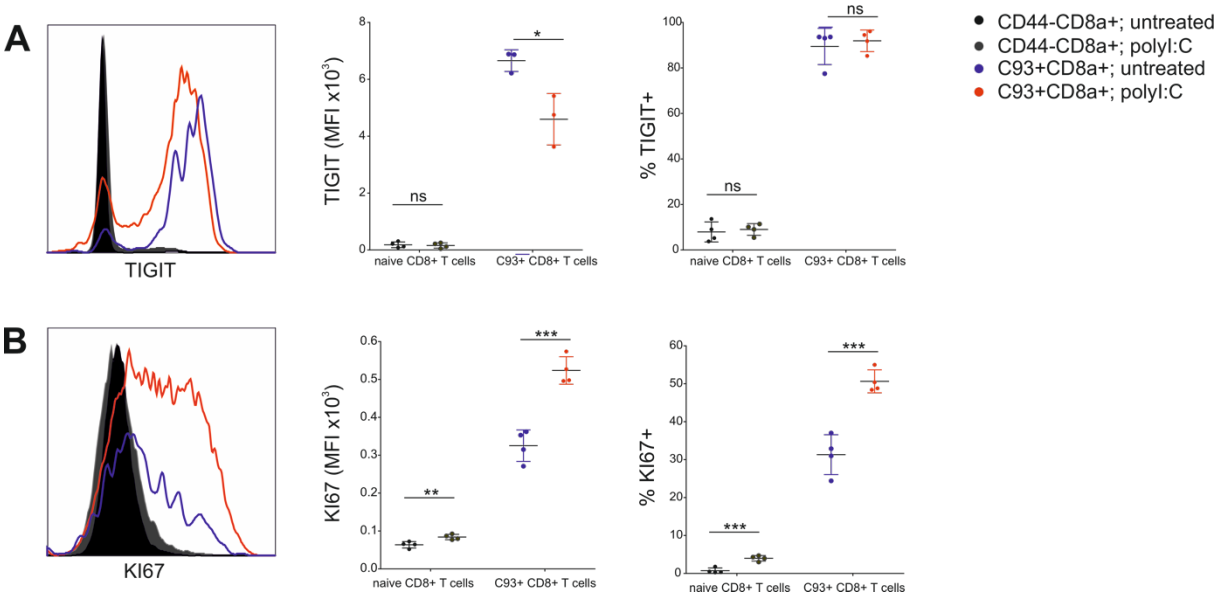

Figure 2.32| Expression of the inhibitory receptor TIGIT and the proliferation marker Ki-67 after polyI:C treatment of mice with an established chronic of Ad-HBV-Luc infection
Flow cytometric analysis and quantification of TIGIT (A) and Ki-67 (B) expression on HBV-specific $CD8^+$ T cells (gated on living C93-specific $CD8^+$) and naïve CD8 T cell (gated on living $CD44^-CD8^+$) treated with 2 consecutive injections polyI:C or left untreated. Mean and SD are shown (n=4).

Taken together, the *ex vivo* analysis of C93-specific $CD8^+$ T cell quantity and phenotype after polyI:C treatment revealed that polyI:C rescues numbers and functionality of C93-specific $CD8^+$ T cells in the liver of chronically Ad-HBV-Luc infected mice.

2.5.4 $CD4^+$ T cell help independent reactivation of HBV-specific $CD8^+$ T cells

During persistent LCMV clone13 infection, the absence of $CD4^+$ T cell help was associated with more severe functional exhaustion and deletion of virus-specific $CD8^+$ T cells and thereby reduced viral control [237, 238]. Based on these results, it is conceivable that the generation of functional virus-specific $CD8^+$ effector T cells during persistent viral infections is $CD4^+$ T cell help dependent. In order to investigate whether polyI:C-mediated reactivation of HBV-specific $CD8^+$ T cells is $CD4^+$ T cell help dependent, we depleted $CD4^+$ T cells in chronically Ad-HBV-Luc infected mice prior to polyI:C-induced reactivation (Fig 2.33 A). Strength of polyI:C-induced effector functions measured via the level of antigen reduction (Fig 2.33 B) and induction of sALT levels (Fig 2.33 C) were comparable in the $CD4^+$ T cell depleted and $CD4^+$ T cell competent group. Induction of sALT levels at day 2 and 3 post polyI:C was even slightly higher in the $CD4^+$ T cell depleted group. Further, total numbers of C93-specific $CD8^+$ T cells in the liver were significantly increased in all mice treated with polyI:C independent of $CD4^+$ T cell help (Fig 2.33 D). Furthermore, numbers of cytotoxic $KLRG1^+$ (Fig 2.33 E) and granzyme B^+ (Fig 2.33 F) C93-specific $CD8^+$ T cells were increased in livers of polyI:C treated animals independent of $CD4^+$ T cell help.

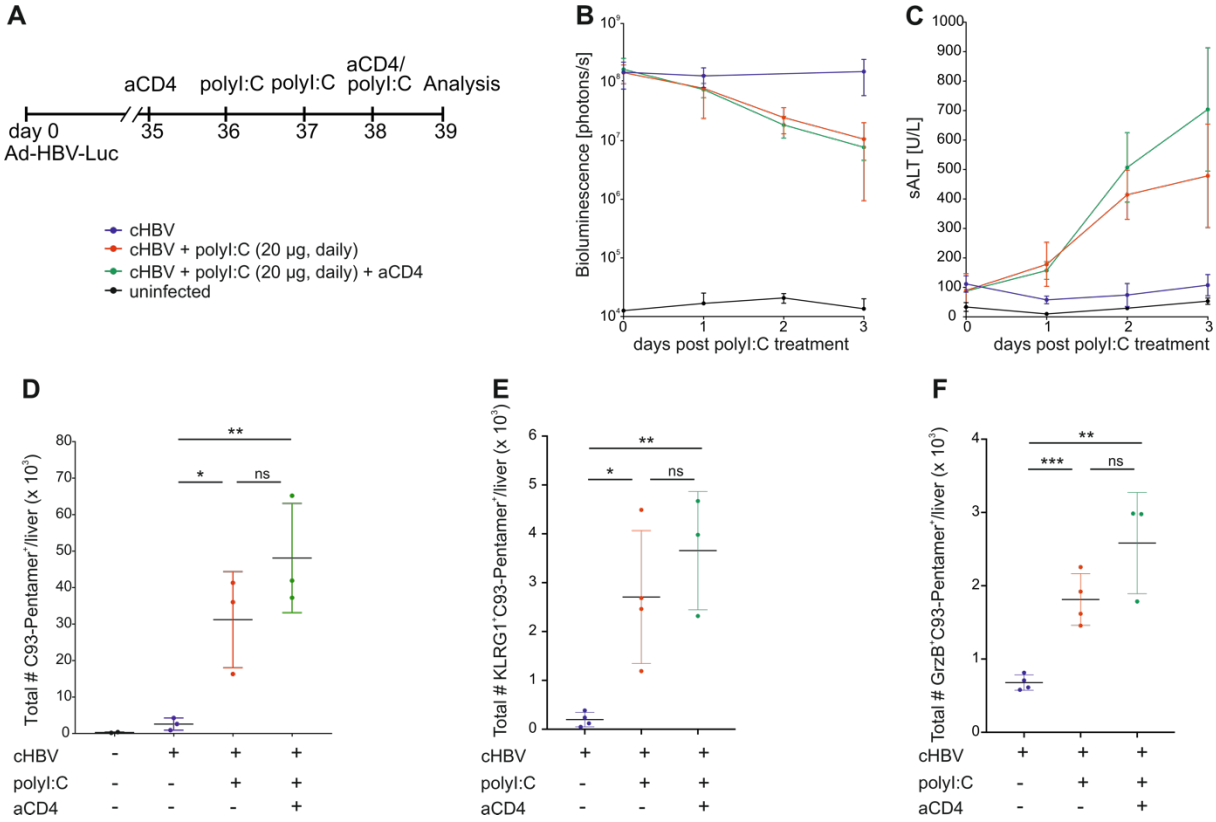

Fig 2.33| Importance of CD4⁺ T cell help for polyI:C-mediated reactivation of HBV-specific CD8⁺ T cell immunity in an established chronic Ad-HBV-Luc infection
A) Schematic overview: C57Bl/6J mice were i.v. injected with $2x10^8$ pfu Ad-HBV-Luc on day 0. At day 35 and day 38 one group was injected with an anti CD4+ T cell depleting antibody. At day 36,37 and 38 were injected with 20 µg polyI:C. (B) Quantification of bioluminescence signal in the liver from the start of polyI:C treatment onwards. (C) Serum ALT levels from the start of polyI:C treatment onwards. (D) Flow cytometric quantification of C93-specific CD8⁺ T cells *ex vivo*. Unspecific staining was determined using uninfected mice. Total numbers were calculated using counting beads. (E) Flow cytometric quantification of KLRG1⁺ C93-specific CD8⁺ T cells *ex vivo*. (F) Flow cytometric quantification of granzyme B⁺ C93-specific CD8⁺ T cells *ex vivo*. Mean and SD are shown (n=3-4).

In summary, polyI:C mediated restoration of HBV-specific CD8⁺ T cell immunity is independent of CD4⁺ T cell help.

2.6 Reactivation of exhausted HBV-specific CD8⁺ T cells

Exhausted virus-specific CD8⁺ T cells were demonstrated to provide a certain level of control and are therefore assumed not to be inert. So far, the source of emerging functional HBV-specific effector CD8⁺ T cells shortly after AAV-IFN or polyI:C treatment is unknown. As those cells arise within 48 hours after the start of treatment and their generation is independent of CD4⁺ T cell help, it is unlikely that these cells are newly primed cells. There are two sources, which are more likely: (1) They derive from the exhausted HBV-specific CD8⁺ T cell population, which is already detected in the liver before the start of treatment or (2) they derive from recently primed and activated HBV-specific CD8⁺ T cells that were not yet part of the exhausted population detected before the start of treatment.

In order to clarify the origin of the emerging functional HBV-specific CD8$^+$ T cells after treatment with polyI:C, we adoptively transferred naïve C93-specific CD8$^+$ T cells with the congenic marker CD45.1 before Ad-HBV-Luc infection and re-isolated these cells after polyI:C-mediated restoration of effector functions (Fig 2.34 A). We detected transferred CD45.1$^+$ CD8$^+$ T cells as well as endogenous CD45.1$^-$ C93-specific CD8$^+$ T cells in the liver of mice with an established chronic Ad-HBV-Luc infection independent of polyI:C treatment (Fig 2.34 B). The numbers of transferred CD45.1$^+$ CD8$^+$ T cells were 40-80-fold higher compared to endogenous cells. Even though there is a trend towards increased numbers of transferred CD45.1$^+$CD8$^+$ T cells in the polyI:C-treated group, neither total numbers of endogenous C93-specific CD8$^+$ T cells nor numbers of transferred CD45.1$^+$CD8$^+$ T cells were significantly increased after two consecutive polyI:C injections (Fig 2.34 C).

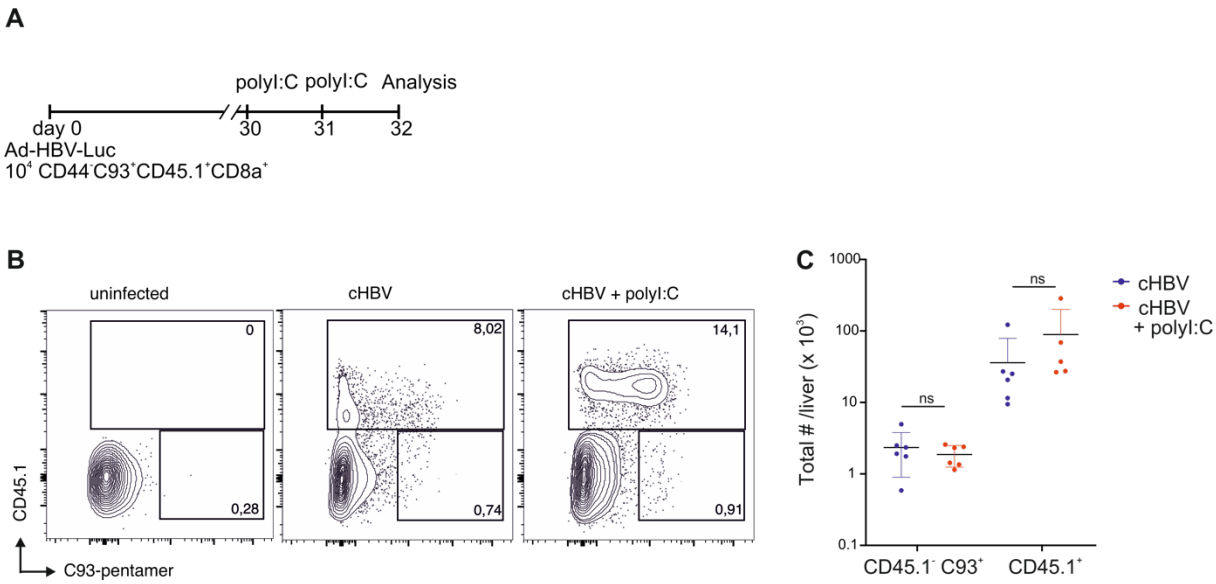

Fig 2.34| Ex vivo quantification of transferred CD45.1$^+$ and endogenous CD45.1$^-$ C93-specific CD8$^+$ T cells in the liver of chronically Ad-HBV-Luc infected mice after polyI:C treatment
A) Schematic overview: C57Bl/6J mice were i.v. injected with 10^8 pfu Ad-HBV-Luc on day 0. Additionally, 10^4 naïve CD45.1$^+$ C93-specific CD8$^+$T cells, isolated from spleens of C93 transgenic mice, were transferred at day 0. At day 30 p.i., one group was treated with 2 consecutive injections of polyI:C (d30 + d31), and liver associated lymphocytes were isolated at day 32. (B) Flow cytometric analysis of intrahepatic CD8$^+$ T cells (gated on living CD44$^+$ CD8$^+$ cells) ex vivo using C93 pentamer and antiCD45.1 antibody. (C) Quantification of intrahepatic endogenous CD45.1$^-$C93-specific CD8$^+$ T cells and transferred CD45.1$^+$ CD8$^+$ T cells from (B). Unspecific staining was determined using uninfected mice. Total numbers were calculated using counting beads. Mean and SD are shown (n=5-6).

The unchanged total numbers of transferred or endogenous C93-specific CD8$^+$ T cells after polyI:C treatment does not match the results from previously performed experiments without transfer of naïve TCR-transgenic CD8$^+$ T cells specific for the C93-epitope prior to Ad-HBV-Luc infection (Fig 2.30). After an adoptive transfer of 10^4 naïve C93-specific CD8$^+$ T cells from transgenic mice, the precursor frequency is notably increased, and therefore, comparability of absolute cell numbers between experiments with and without transfer is difficult. However, this does not explain the unchanged numbers of C93-specific CD8$^+$ T cells (endogenous or

transferred) after polyI:C treatment. A possible explanation is the observed downregulation of the T cell receptor specific for the C93 epitope in the setting of an established chronic Ad-HBV-Luc infection (Fig 2.35). Detection of C93-specific $CD8^+$ T cells via the congenic marker CD45.1 makes it possible in the first place to detect antigen-specific $CD8^+$ T cells with downregulated TCR. These results suggest that total numbers of C93-specific $CD8^+$ T cells are not necessarily increased after polyI:C treatment, but they can be detected because of increased expression levels of the C93-TCR and thereby detection via pentamer staining.

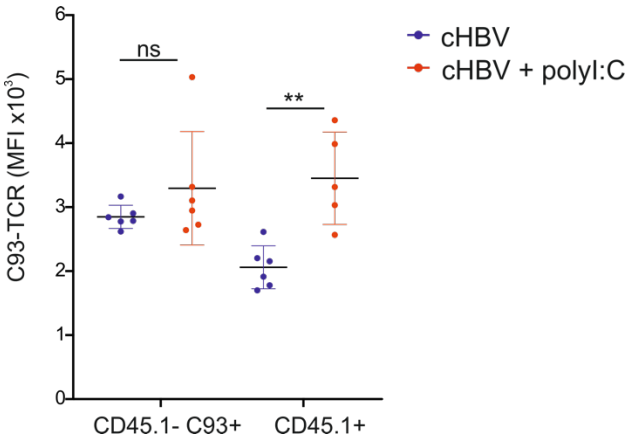

Fig 2.35| Changes in T cell receptor surface expression after polyI:C treatment
Flow cytometric analysis of TCR expression levels on intrahepatic endogenous (CD45.1-) and transferred ($CD45.1^+$) C93-specific $CD8^+$ T cells in mice with an established chronic Ad-HBV-Luc infection after two consecutive polyI:C injections.

Separated phenotypic analysis of the transferred and endogenous C93-specific $CD8^+$ T cell population revealed a significant increase of cytotoxic $KLRG1^+$ (Fig 2.36 A, B) and granzyme B^+ (Fig 2.36 C, D) effector cells in both populations. Further, levels of the early activation marker CD69 (Fig 2.36 F), the proliferation marker Ki-67 (Fig 2.36 H), and CD44 (Fig 2.36 G) were significantly higher in the transferred and endogenous C93-specific $CD8^+$ T cell population isolated from polyI:C-treated animals. Expression levels of the inhibitory surface receptor PD1 were significantly reduced in the transferred C93-specific $CD8^+$ T cell population, and a trend towards reduction was observed in the endogenous C93-specific $CD8^+$ T cell population (Fig 2.34 C).

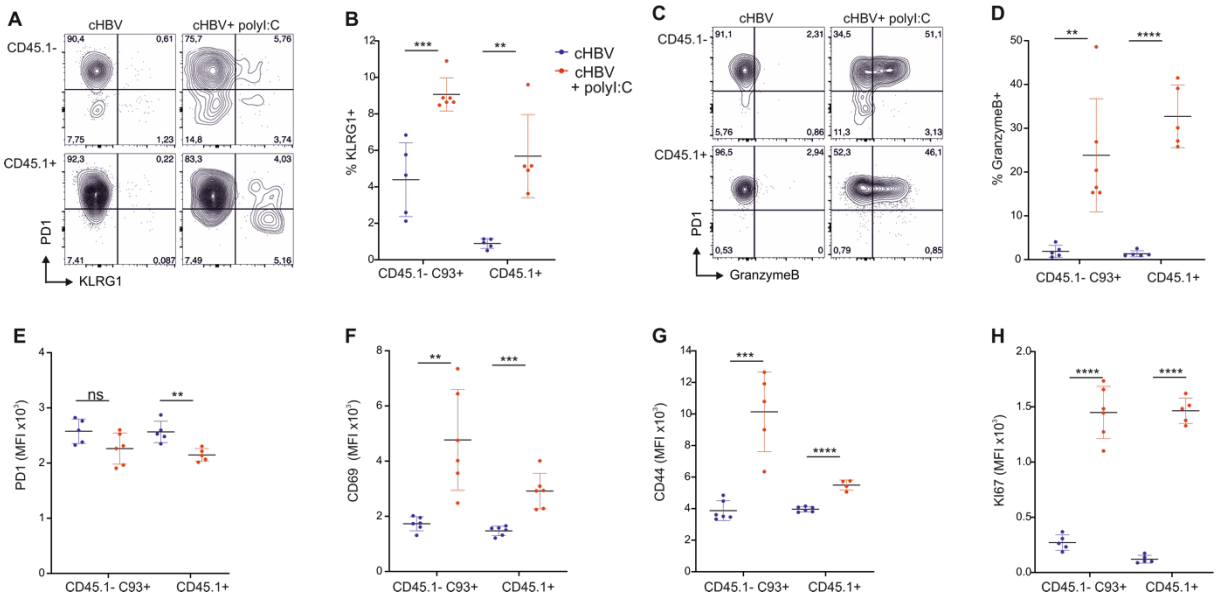

Fig 2.36| Phenotypic analysis of endogenous and transferred C93-specific CD8⁺ T cells in the liver of chronically Ad-HBV-Luc infected mice after polyI:C treatment
Flow cytometric analysis of endogenous (CD45.1⁻) and transferred (CD45.1⁺) C93-specific CD8⁺ T cells (gated on living CD8⁺CD44⁺) in the liver of chronically Ad-HBV-Luc infected mice after two consecutive polyI:C injections. (A) Co-expression of the cytotoxicity marker KLRG1 and the inhibitory receptor PD1. (B) Frequency of KLRG1⁺ C93-specific CD8⁺ T cells (transferred or endogenous). (C) Co-expression of the effector molecule granzyme B and the inhibitory receptor PD1. (D) Frequency of granzyme B⁺ C93-specific CD8⁺ T cells (transferred or endogenous). Mean fluorescence intensity (MFI) of PD1 (E), CD69 (F), CD44 (G) and Ki-67 (H) on endogenous (CD45.1⁻) or transferred (CD45.1⁺) C93-specific CD8⁺ T cells. Mean and SD are shown (n=5-6).

In summary, a switch from dysfunctional exhausted CD8⁺ T cell phenotype characterized by high expression of inhibitory receptors PD1 and TIGIT, basal expression levels of CD69 and granzyme B and a very small subpopulation of KLRG1⁺ cells to a more functional effector CD8⁺ T cell phenotype marked by high expression levels of KLRG1, granzyme B, and CD69 and slightly reduced expression of PD1 was detected in the endogenous and transferred C93-specific CD8⁺ T cell population after polyI:C treatment. The emergence of CD45.1⁺ C93-specific CD8⁺ T cells with restored phenotype revealed that the existing exhausted HBV-specific CD8⁺ T cell population is a target of IFN-mediated reactivation.

3. DISCUSSION

Currently, IFNα-based therapy is, although the response rate to therapy is estimated at only 10% [68]or 12%[67], the most effective therapy approved for the treatment of CHB[64]. The common consensus is that induction of HBV-specific adaptive immunity is crucial for control of HBV infection and therefore, the immunomodulatory effects of IFNα are thought to be crucial for sustained off-therapy response[239]. However, the mechanisms underlying the IFNα-mediated switch from inadequate and impaired HBV-specific immune response to off-therapy immune control are not understood yet[239, 240]. However, it is common sense that high viral antigen load is the primary cause and driving force of $CD8^+$ T cell exhaustion, a possible causal link between IFN-mediated reduction of viral antigen load and induction of functional anti-HBV immunity has not been demonstrated so far. In this thesis, the complex interplay between HBV antigen load and HBV-specific $CD8^+$ T cell immunity was investigated using a newly generated vector Ad-HBV-Luc to establish acute, self-limiting, or persistent HBV infection in mice.

3.1 High HBV antigen load leads to functional impaired exhausted anti-HBV $CD8^+$ T cell immunity resulting in viral persistence

The absence of a functional and effective adaptive immune response against viruses that establish persistent infections in humans can be associated with either very low or very high viral load[241]. Several important pathogens in humans, namely HBV, HCV, or HIV, express high amounts of potential antigenic viral proteins resulting in continuous antigenic stimulation of the host's immune system[111]. Such high viremic persistent infections in patients or in various animal models are associated with exhausted $CD8^+$ T cell immunity. Specifically, in CHB patients, excess of viral antigen correlates with hyporesponsive, exhausted T cells[62, 242]. As patients are usually diagnosed after the incubation phase of HBV when clinical symptoms occur, it is almost impossible to figure out whether high antigen load is cause or consequence of $CD8^+$ T cell exhaustion in patients. To tackle this question, animal models of HBV infection that can be experimentally infected with defined doses are of particular importance. Comparable to the results in this thesis for mice infected with a high or low dose of Ad-HBV-Luc, Dusseaux *et al.* demonstrated that humanized mice equipped with a human immune system controlled HBV infection more efficiently when infected with lower doses (10^7 GE) of HBV compared to higher doses of HBV (10^9 GE)[243]. The HBeAg levels achieved with the low dose, approx. 10 PEIU/mL, and with the high dose, approx. 100 PEIU/ml, were roughly similar to HBeAg levels achieved with a low or high dose of Ad-HBV-Luc. Even though their data emphasize that antigen load impacts anti-HBV immunity, the study is inconclusive regarding the effect of high antigen load on the functionality of HBV-specific $CD8^+$ T cells due to HLA-

mismatch present in their humanized mice. Also in chimpanzees, the size of HBV inoculum was shown to determine the outcome of infection[60]. It was demonstrated that intermediate inoculum size (10^4 to 10^7 GEs) led to a limited spread to 0.1% of hepatocytes, followed by abrupt viral elimination. In contrast, infection with a very low dose (10^0 or 10^1 GE), or a high dose (10^{10} GE) led to a massive spread of the virus to virtually 100% of hepatocytes and to viral persistence or delayed viral clearance. The highest investigated dose in chimpanzees (10^{10} GE) led to delayed induction of anti-HBV immunity but was still controlled. In contrast, the highest investigated dose of Ad-HBV-Luc (10^8 pfu) establishes a persistent infection in mice. However, it seems difficult to define a common range for low, moderate and high infectious doses for natural HBV infection and adenoviral mediated genome transfer and for different species as kinetic of viral parameters vary greatly in those different settings. Therefore, it is conceivable, that the highest investigated dose in chimpanzees is at the upper boundary of dosage window within which the virus is controlled and that an even higher dose (> 10^{10} GE) would establish a persistent infection comparable with the high-dose Ad-HBV-Luc infection in mice. In a study conducted by Asabe *et al.*, an early and efficient control of HBV infection was associated with early $CD4^+$ T cell priming before or early during onset of detectable viral spread that seemed to result in effective HBV-specific $CD8^+$ T cell response. A study in mice using the OT1-Ovalbumin system determined the threshold for generation of a functional $CD8^+$ T cell response. Based on their results, initial antigen expression in more than 25% of hepatocytes resulted in $CD8^+$ T cell exhaustion[244]. In line with this study, there is evidence from our lab that a high dose Ad-CMV-GOL (10^9 pfu) infection establishes a chronic infection in immunocompetent wildtype C57BL/6J mice (unpublished data). The acute self-limiting infectious dose of Ad-HBV-Luc results in initial antigen expression in less than 5% of hepatocytes and the persistent infectious dose of Ad-HBV-Luc results in initial antigen expression in around 20% of hepatocytes, which is slightly below the threshold of T cell exhaustion determined in the study of Tay *et al.*. However, it is not unlikely that the threshold deviates slightly in different infection settings depending on various parameters such as TCR-pMHC-I affinity, expression strength per cell, the sensitivity of detection, and inflammatory stimuli.

Consistent with data on HBV-specific $CD8^+$ T cells isolated from chronically infected patients, C93-specific $CD8^+$ T cells isolated from mice infected with the high dose of Ad-HBV-Luc exhibited an exhausted phenotype. In detail, they permanently express high levels of the inhibitory receptors PD1 and TIGIT as it was also reported for HBV-specific $CD8^+$ T cells in CHB patients[62, 209, 245, 246]. Additionally, the HMG-box transcription factor TOX, which correlates with the presence of exhausted T cells during persistent LCMV infection in mice and HCV infection in humans and which is critically involved in development and maintenance of

exhausted CD8$^+$ T cells[247, 248], was permanently highly expressed on C93-specific CD8$^+$ T cells isolated from mice infected with the high dose of Ad-HBV-Luc.

3.2 Appearance of functional HBV-specific effector CD8$^+$ T cells early during persistent Ad-HBV-Luc infection

As patients infected with HBV are usually diagnosed after the development of clinical symptoms, the availability of data in the early phase of CHB, when exhausted HBV-specific CD8$^+$ T cells develop, is very limited. In the literature, massive expansion of virus-specific CD8$^+$ T cells and acquisition of effector functions early after an infection has been described for persistent LCMV infection in mice or HIV infection in humans, suggesting the generation of functional virus-specific CD8$^+$ T cells takes place at the beginning of persistent infections[127, 129, 130, 131]. Additionally, Brooks *et al.* showed by adoptive transfer experiments in the LCMV model that dysfunctionality of virus-specific CD8$^+$ T cells is not irreversible imprinted during priming, but that functionality of virus-specific CD8$^+$ T cells is determined by their environment [127]. However, as there are major differences regarding kinetic and magnitude of the antiviral immune response against HBV, the transferability of concepts applicable for LCMV or HIV infection to HBV is questionable. The non-invasive monitoring of intrahepatic viral antigen using the Ad-HBV-Luc vector offers the advantage of the exact determination of the onset of HBV-specific effector function during acute, self-limiting infection. Due to monitoring intrahepatic antigen load in close intervals, we observed contraction of functional HBV-specific CD8$^+$ effector T cells occurring immediately after the exertion of effector function. Therefore, detection and phenotyping of functional HBV-specific effector CD8$^+$ T cells is only possible in a very narrow time frame that can be precisely determined by monitoring intrahepatic antigen load. During exertion of effector functions in acute, self-limiting infection, HBV-specific CD8$^+$ T cell express transiently high levels of the inhibitory receptors PD1 and TIGIT and exhibit increased expression of KLRG1 and granzyme B. Phenotyping of HBV-specific CD8$^+$ T cells at three different time points during persistent Ad-HBV-Luc infection indicated generation of functional HBV-specific CD8$^+$ T cells early during chronic HBV infection. At day 10 post infection, the earliest investigated time point, relatively high numbers of C93-specific CD8$^+$ T cells expressing partially the cytotoxicity marker KLRG1 and high levels of granzyme B were detected in livers of mice infected with the persistent dose of Ad-HBV-Luc. Comparable with data gathered from the LCMV model[120, 127, 128, 249], a decline in the quantity of intrahepatic C93-specific CD8$^+$ T cells and loss of cytotoxicity and activity marker observed at subsequent time points after day 10 p.i., suggest a progressive loss of CD8$^+$ T cell functionality during persistent Ad-HBV-Luc infection.

When intrahepatic antigen load, measured via bioluminescence imaging, is applied on a linear scale, there is a slight decline observed from day 2 until day 30, which is more distinct at early

time points. Further, during persistent Ad-HBV-Luc infection, a slight but constant elevation of ALT levels is measured in the serum, indicating a constant ongoing low level of effector functions during persistent Ad-HBV-Luc infection.

However, already at day 10 p.i, when quantity is highest, and cytotoxicity markers are not entirely lost, frequency of IFNy$^+$ and TNF$^+$ CD8$^+$ T cells detected in the chronic setting are low compared to frequencies measured during the effector phase of acute, self-limiting Ad-HBV-Luc infection (day 15 p.i.). Possibly, the peak of functionality is already missed at day 10 p.i. and functionality is already decreasing, or HBV-specific CD8$^+$ T cells generated during persistent infection never reached functionality of HBV-specific CD8$^+$ T cells generated during acute, self-limiting infection.

3.3 IFNβ expression in the liver induces anti HBV-specific CD8$^+$ T cell immunity

The HBV genome was demonstrated to persist as an integrated genome and/or as episomal cccDNA and therefore, it is suggested that off-treatment control is only achieved via strong activation of the host's adaptive anti-HBV immunity[250]. Further, viral elimination was shown to depend on CD8$^+$ T cells[44], which makes them the most promising target of therapy.

Already in 1962, an early study using the LCMV model demonstrated that established persistent infections could be controlled entirely by the adoptive transfer of functional virus-specific T cells[151, 242]. The concept of reactivation of dysfunctional CD8$^+$ T cell immunity as a therapeutic intervention in persistent infections was further supported by the successful restoration of antiviral T cell immunity via immune checkpoint inhibition[113]. However, so far, results with anti-PD1 blockade using nivolumab in patients with CHB were disappointing[210, 211].

Also, for standard therapies, either PEG-IFNα or NAs, successful reactivation of HBV-specific CD8$^+$ T cells *in vivo* was not demonstrated so far[183, 187]. In contrast, Micco *et al.* illustrated that PEG-IFNα treatment of CHB patients even reduced numbers of circulating effector CD8$^+$ T cells, including HBV-specific CD8$^+$ T cells, and did not rescue the exhausted CD8$^+$ T cell phenotype. In this study, they instead reported restoration of NK cell response, suggesting a direct involvement of NK cells to the IFNα-mediated antiviral effects[183].

The data obtained in the Ad-HBV-Luc model demonstrated that a substantial reduction of viral load after expression of IFNβ in the liver was achieved by a combination of direct antiviral effects and immune-mediated elimination of infected hepatocytes. In contrast to the study by Micco *et al.,* we could not confirm a significant involvement of NK cells in the immune-mediated elimination induced by IFNβ expression. Instead, the immune-mediated antiviral effect induced by IFN treatment was utterly dependent on CD8$^+$ T cells, as CD8$^+$ T cell depletion prevented immune-mediated effects. Unlike the findings in two studies analyzing effects of PEG-IFNα on circulating HBV-specific CD8$^+$ T cells in HBeAg negative CHB patients[183, 187], we observed a

rescue of quantity and phenotype of C93-specific CD8$^+$ T cells in the liver of AAV-IFN treated mice. We demonstrated that as early as 48 hours after induction of IFN signaling, numbers of C93-specific CD8$^+$ T cells in the liver were significantly increased and acquired an activated effector T cell phenotype with high expression levels of KLRG1 and CD69. These cells exhibited superior cytolytic effector functions against Ad-HBV1.3 infected hepatocytes *ex vivo* compared to T cells isolated from animals with an untreated established persistent Ad-HBV-Luc infection. The re-acquired effector CD8$^+$ T cell phenotype was maintained, and surface expression levels of inhibitory receptors decreased steadily together with declining antigen load. Moderately increased ALT levels in the serum lasting for 7 days (day 3 to 10 post AAV-IFN) indicate long-lasting effector function of reactivated HBV-specific CD8$^+$ T cells. These very different findings concerning the recovery of HBV-specific CD8$^+$ T cells in response to IFN-based therapies might be caused by two reasons. Possibly, HBV-specific CD8$^+$ T cells with recovered phenotype are efficiently retained in the liver and are therefore not detectable in the circulation. It is also conceivable that effects induced by hepatocyte-specific expression of IFNβ, which is so far not feasible in patients, is not comparable to effects induced by systemic administration of PEG-IFNα.

3.4 Reduction of HBV antigen load failed to restore the functionality of HBV-specific CD8$^+$ T cell response

In patients with chronic HBV infection, the appearance of exhausted, hyporesponsive HBV-specific CD8$^+$ T cells correlates with high viral and high antigen loads[62, 242]. Further, high antigen load was demonstrated in studies using the LCMV model to be the cause and major driver of CD8$^+$ T cell exhaustion[132, 136, 137, 138]. Several studies in humans demonstrated that therapeutic suppression of viral replication causes an increase in antiviral T cell activity[251, 252, 253, 254, 255, 256, 257]. A study in the OT-1-Ovalbumin system conducted by Tay *et al.* demonstrated that the functionality of antigen-specific CD8$^+$ T cells inversely correlated with the number of antigen-expressing hepatocytes[244]. Another study performed the OT-1-Ovalbumin system revealed that the number of antigen expressing hepatocytes is decisive for the outcome of T cell responses in the liver even under sterile conditions, which indicate that the described adenoviral vector dose-dependent effect does not depend on infection-associated effects such as inflammation[139]. It was further demonstrated via adoptive transfer experiments in the OT-1-Ovalbumin system[244] and in the LCMV infection model[127, 128] that CD8$^+$ T cell exhaustion in the setting of high numbers of infected hepatocytes is not irreversibly imprinted in the initial phase of T cell activation. Rescue of CD8$^+$ T cell function after adoptive transfer from high dose infection setting into low dose infection setting in the OT-1-Ovalbumin and the LCMV infection model led to the hypothesis that a dysfunctional HBV-specific CD8$^+$ T cell response in the high-dose Ad-HBV-Luc infection could be rescued by reduction of HBV antigen load only. Reduction

of viral antigen load in high-dose Ad-HBV-Luc infected animals was therefore thought to improve the functionality of exhausted HBV-specific $CD8^+$ T cells and thereby lead to immune-mediated control. However, using RNA interference to reduce HBeAg to levels in the low-dose in acute, self-limiting infection setting demonstrated that antigen reduction alone failed to restore HBV-specific $CD8^+$ T cell response after prolonged antigen exposure at day 30 post infection. This finding confirms the results achieved in CHB patients treated with NAs, which efficiently suppresses HBV replication and thereby reduce HBV antigens, but fail to induce immune-mediated control of HBV[258, 259, 260].

Together, these data indicate that reduction of viral antigen load in chronic HBV infection is not sufficient to restore dysfunctional anti-HBV $CD8^+$ T cell immunity. Even though the adoptive transfer experiments performed in the LCMV and OT-1-Ovalbumin system were not performed in the Ad-HBV-Luc model due to low numbers of HBV-specific $CD8^+$ T cells that can be re-isolated from the high-dose infection setting, it is not unlikely that requirements for restoration of $CD8^+$ T cell immunity differ between LCMV infection or the OT1-Ovalbumin system and HBV infection. Possibly, antigen expressing cell type, cross-presentation, co-stimulatory signals, and TCR-pMHC-I affinity are not only decisive for initial priming of $CD8^+$ T cells[244], but also for their reactivation.

3.5 Combined reduction of viral antigen load and IFNAR signaling in T cells is mandatory to restore exhausted HBV-specific $CD8^+$ T cell immunity

IFNα-based therapy, which induces immune-mediated off-therapy control of HBV more frequently, provides an immunomodulatory stimulus in addition to the reduction of HBV antigen load. The reduction of HBV antigen load alone was shown to be not sufficient to restore HBV-specific $CD8^+$ T cell immunity. Although this finding is supported by the fact that (1) NA-therapy in patients does not lead to off-therapy control and (2) magnitude of antigen reduction induced by AAV-IFN and AAV-shHBV is comparable, it cannot be excluded that IFN-mediated HBV antigen reduction differs from AAV-shHBV antigen reduction and is thereby sufficient to restore dysfunctional HBV-specific $CD8^+$ T cell immunity.

Even though it was not analyzed in detail, the pattern of intracellular antigen reduction in the liver differs between AAV-shHBV and AAV-IFN treatment. Suppression of HBV antigen via RNAi occurs exclusively in co-transduced hepatocytes as the trans-signaling effect of IFN on Ad-HBV-Luc single infected hepatocytes does not exist. This suggests a more uniform antigen reduction in the liver in the AAV-IFN system, which is probably weaker on single hepatocyte level. In order to test whether IFN-mediated antigen reduction is sufficient to restore HBV-specific $CD8^+$ T cell immunity, we performed experiments in CD4Cre x IFNAR $^{fl/fl}$ mice, which lack IFNAR1 on $CD4^+$ and $CD8^+$ T cells. In CD4Cre x IFNAR $^{fl/fl}$ mice with an established chronic Ad-HBV-Luc infection, magnitude and kinetic of HBV antigen reduction measured via

bioluminescence measurements in the liver were comparable to the induced reduction in IFNAR $^{fl/fl}$ littermates. However, termination of further antigen reduction after day 4 post AAV-IFN transduction in CD4Cre x IFNAR $^{fl/fl}$ mice compared to ongoing antigen reduction in IFNAR $^{fl/fl}$ littermates indicate failed induction of HBV-specific CD8$^+$ T cell immunity. As we lack the CD8$^+$ T cell depleted group for CD4Cre x IFNAR$^{fl/fl}$ animals, it is so far unclear if the slight 1,9-fold reduction of HBc$^+$ nuclei at termination of the experiment was due to CD8$^+$ T cell mediated elimination of virus-infected hepatocytes or due to nuclei under the detection limit due to inhibition of protein synthesis. Notwithstanding, even if the reduction of HBc$^+$ nuclei were due to HBV-specific CD8$^+$ T cell immunity, the efficiency of restoration would be very low. These data provide evidence that IFN-mediated reduction of HBV antigens alone is not sufficient to restore dysfunctional anti-HBV immunity and thereby support the assumption that the immunomodulatory stimulus provided by IFNAR signaling on T cells is mandatory.

To further elucidate whether IFN-mediated antigen reduction is redundant for the restoration of anti-HBV-immunity, we analyzed the induction of HBV-specific immunity after IFN treatment in AlbCre x IFNAR $^{fl/fl}$ mice, which lack IFNAR1 specifically on hepatocytes. In AlbCre x IFNAR $^{fl/fl}$ mice with an established chronic Ad-HBV-Luc infection, AAV-IFN treatment did not significantly reduce HBV antigen load and antigen reduction in the CD8$^+$ T cell competent group was not superior over the reduction in the CD8$^+$ T cell depleted group indicating failed restoration of HBV-specific CD8$^+$ T cell immunity.

These results demonstrate that neither reduction of antigen load nor IFN-mediated immune stimulation is redundant for the IFN-induced switch from dysfunctional to functional HBV-specific immune response.

3.6 Shortened time of exposure to high antigen fails to improve restoration of HBV-specific CD8$^+$ T cell immunity

In the present thesis, I demonstrated that reactivation of exhausted anti-HBV CD8$^+$ T cell immunity in an established chronic Ad-HBV-Luc infection is feasible by treatment with AAV-IFN. However, complete viral clearance was not achieved.

Prolonged exposure to persistent antigen stimulation in chronically infected animals, which exceeded 3 weeks, was reported to prevent differentiation to normal functional CD8$^+$ T cells after transfer into uninfected mice [128]. These data suggest that prolonged exposure to high antigen load increases the severity of T cell exhaustion and thereby potentially increases the threshold for the restoration of CD8$^+$ T cell effector function. To determine whether shortened exposure to high antigen load lowers this threshold for functional restoration and thereby increases the efficiency of restored HBV-specific CD8$^+$ T cell response, AAV-IFN was applied at early time points during persistent Ad-HBV-Luc infection.

However, we did not observe an improved efficiency of effector functions at earlier treatment time points (day 1 and day 15) over treatment at day 30 p.i.. Instead, induced HBV-specific $CD8^+$ T cell immunity was reduced after early treatment time points. The slightly reduced efficiency of HBV-specific $CD8^+$ T cell immunity when treated at day 15 p.i. compared to day 30 p.i. may be due to slightly higher viral load at the start of treatment at day 15 compared to day 30 p.i.. The further reduced efficiency when treated at day 1 p.i. could be mediated by IFN-mediated augmentation of T cell responses, which was reported to occur when IFNAR signaling precedes TCR engagement[107].

3.7 Systemic administration of TLR3-ligand polyI:C mediates control of an established persistent Ad-HBV-Luc infection

In this thesis, restoration of HBV-specific $CD8^+$ T cell immunity by continuous hepatocyte-specific expression of IFNβ induced by transduction of AAV-IFN was demonstrated. For a reason not understood yet, AAV-IFN induced anti-HBV immune response was terminated at day 9 after AAV-IFN transduction, although low numbers of Ad-HBV-Luc infected hepatocytes were still present. The shortened time of exposure to high antigen load was not shown to not prevent termination of anti-HBV immune response prior to complete elimination.

As several studies demonstrated adverse effects of continuous type I IFN on T cell maintenance and antiviral immune response during persistent viral infections[103, 104, 261, 262, 263], we aimed at investigating whether tonic type I IFN signaling similarly restores anti-HBV specific $CD8^+$ T cell immunity comparably and further maintains anti-HBV $CD8^+$ T cell response until final elimination of Ad-HBV-Luc. Induction of tonic type I IFN signaling via sequential injections of recombinant IFNα or IFNβ is limited due to their poor stability and short half-life in systemic circulation[264]. For this reason, we injected the synthetic double-stranded RNA analog polyI:C, which is a potent inducer of type I IFNs, every 24 hours in order to induce tonic type I IFN signaling. In a mouse model of HBV infection, hydrodynamic injection of polyI:C was reported to mediate IFN-dependent elimination of HBV previously[207]. Already after two consecutive polyI:C injections, when a significant increase of sALT levels was detected, we observed a restored HBV-specific $CD8^+$ T cell immunity. The numbers of C93-specific $CD8^+$ T cells were significantly increased and exhibited an activated effector cell phenotype. Thus, the induction of a functional HBV-specific $CD8^+$ T cell response in established persistent Ad-HBV-Luc infection is comparable between AAV-IFN and polyI:C treatment early after initiation of IFN signaling. After twelve consecutive injections of polyI:C in mice with an established chronic Ad-HBV-Luc infection, levels of intrahepatic antigen measured via bioluminescence imaging were reduced to background levels measured in uninfected mice. Additionally, pgRNA, which is considered as a marker for active HBV replication, was not detectable anymore. Hence, in contrast to sustained IFNβ expression by AAV-IFN transduction, HBV-specific $CD8^+$ T cell

response was maintained until complete elimination of detectable HBV parameters during polyI:C treatment regime. In line with a study performed by Wu *et al.*, which demonstrates that hydrodynamically injected polyI:C induces IFN-dependent clearance of HBV infection[207], I demonstrated that polyI:C mediated restoration of anti-HBV immunity depends on IFNAR1 signaling in both hepatocytes and HBV-specific $CD8^+$ T cells. Even though polyI:C-mediated effects are IFN-dependent, it is still possible that the superior control of chronic Ad-HBV-Luc infection by polyI:C treatment regime over AAV-IFN treatment is due to (1) induction of additional inflammatory cytokines, chemokines or co-stimulatory signals by TLR3 stimulation or (2) beneficial effects of tonic over continuous IFN signaling. Further investigations are needed to determine the cause for beneficial long-term maintenance of HBV-specific $CD8^+$ effector T cell response induced by polyI:C treatment regime over AAV-IFN transduction.
Taken together, these data indicate the existence of a sensitive balance between beneficial and detrimental effects elicited by type I IFN signaling, probably depending on the magnitude, kinetic, and tonicity of induced IFN signaling. Thus, I provide a possible explanation for the low response rates observed in patients as there are probably high variations in the magnitude and the kinetic of induced IFN-signaling in patients.

3.8 IFN type I signaling targets exhausted HBV-specific $CD8^+$ T cells

Type I IFNs are generally regarded as proinflammatory cytokines that promote activation and maturation of DCs and act as a potent third signal promoting the cross presentation of viral antigen and priming and clonal expansion of virus-specific $CD8^+$ T cells [265, 266]. Therefore, it seemed possible that type I IFN signaling promotes priming and clonal expansion of newly generated naïve HBV-specific $CD8^+$ T cells instead of restoring the function of already present exhausted HBV-specific $CD8^+$ effector cells. However, the rescue of antiviral immunity induced by polyI:C injection in CD4Cre x $IFNAR^{fl/fl}$ mice with established persistent Ad-HBV-Luc infection by adoptive transfer of IFNAR1 competent naïve HBV-specific $CD8^+$ T cells before infection, indicate that polyI:C-induced functional HBV-specific $CD8^+$ T cells originate from HBV-specific $CD8^+$ T cells present for 30 days in those animals. In line with this data, $CD45.1^+$ $CD8^+$ T cells
that originate from adoptively transferred naïve $CD45.1^+$ C93-specific $CD8^+$ T cells before Ad-HBV-Luc infection, exhibit a functional effector phenotype ($KLRG1^+$ and granzyme B^+) after polyI:C treatment at day 30 post infection. Further, the observation that polyI:C-mediated restoration of HBV-specific $CD8^+$ T cells was $CD4^+$ T cell help independent supports this conclusion because priming of new HBV-specific $CD8^+$ T cells depends on $CD4^+$ T cell help. Thus, the data obtained in the present study demonstrate that type I IFN targets HBV-specific $CD8^+$ T cells already present in chronically Ad-HBV-Luc infected mice rather than promoting a new generation of HBV-specific $CD8^+$ T cells. Almost all $CD45.1^+$ $CD8^+$ with functional effector

phenotype appearing after 2 consecutive polyI:C injections were stained KI-67$^+$, suggesting that type I IFN signaling targets a precursor population of HBV-specific CD8$^+$ T cells and promotes proliferation and differentiation to functional HBV-specific effector CD8$^+$ T cells rather than the conversion of already differentiated exhausted HBV-specific CD8$^+$ T cells. In future experiments, sort on the basis of for example their TCF1 expression, different populations of the intrahepatic exhausted HBV-specific CD8$^+$ T cell pool could be extracted to perform adoptive transfer experiments and evaluate which subpopulations of exhausted intrahepatic HBV-specific CD8+ T cells are targeted by type I IFN.

4. MATERIAL AND METHODS

4.1 Materials

4.1.1 Devices

Product	Supplier
Architect™ i1000SR platform	Abbott Laboratories, USA
Analytical Balance Sartorius CP224S-OCE	Sartorius, Germany
Analytical Balance ABS	Kern & Sohn GmbH, Germany
Automacs® pro Seperator	Miltenyi Biotec, Germany
Bondmax Rxm system	Leica Microsystems, Germany
Balance LSM2000	PCE Deutschland GmbH,Germany
Cage ventilation ScanClime Mini^{ECO}	Scanbur A/S, Denmark
Centrifuge Rotana 460 RC	Andreas Hettich GmbH & Co. KG, Germany
Centrifuge Heraeus® Fresco17	Thermo Fisher Scientific, USA
Centrifuge Heraeus® multifuge X3R	Thermo Fisher Scientific, USA
Flow Cytometer LSR Fortessa™	BD Biosciences, USA
Flow Cytometer SP6800 Spectral Analyzer	Sony Biotechnology Inc., USA
Fluorescence microscope Eclicpse TE2000s	Nicon Imaging Japan Inc., Japan
Gel-imaging system Chemidoc™ XRS	Bio-Rad Laboratories, Germany
Incubator Heracell 150i	Thermo Fisher Scientific, USA
IVIS® Lumina LT Series III (in vivo imaging system)	Perkin Elmer, USA
Leica Bond MAX system	Leica Microsystems, Germany
LightCycler® 480 II	Roche Diagnostics, Switzerland
Light microscope Axiovert25	Carl Zeiss AG, Germany
MACS separator MultiStand	Miltenyi Biotec, Germany
Magnet column LS	Miltenyi Biotec, Germany
Neubauer improved hemocytometer	Brand, Germany
PCR System ProFlex	Applied Biosystems, USA
Perfusion pump Masterflex®	Cole Parmer, USA
Ph-meter inoLab® pH 7110	WTW (Xylem Analytics), Germany
Photometer Biodrop	Serva, Germany
Pipettes	Eppendorf, Germany
Power supply PowerPac™ Basic	Bio-Rad Laboratories, Germany

Shaking incubator hood TH15	Edmund Bühler GmbH, Germany
Sterile hood Heraeus® HERASafe®	Thermo Fisher Scientific, USA
Reflotron® Plus	Roche Diagnostics, Switzerland
Table-top centrifuge 5417R	Eppendorf, Germany
Thermo mixer F1.5	Eppendorf, Germany
Tissue processor Leica ASP300 S	Leica Microsystems, Germany
Ultracentrifuge Avanti J25-I	Beckman Coulter, USA
Water bath WN45	Memmert GmbH + Co. KG, Germany
xCelligence RTCA	ACEA Biosciences, USA

4.1.2 Consumables

Product	**Supplier**
24-well plate	TPP Techno Plastic Products AG, Switzerland
96-Well-Platte, V-bottom	Greiner Bio-one, Germany
96-Well-Platte, F-bottom	TPP Techno Plastic Products AG, Switzerland
Butterfly canula	Sarstedt AG & Co. KG, Germany
Blood lancets SUPRA	megro GmbH & Co. KG, Germany
Capillary HIRSCHMANN® ringcaps® Li-Heparin 32 µl	Hirschmann Laborgeräte GmbH & Co. KG, Germany
Cell culture flasks, dishes, plates	TPP Techno Plastic Products AG, Switzerland
Cell strainer 70 µm, 100µm	Miltenyi Biotec, Germany
E-plate 96-well	ACEA Biosystems, USA
Falcon tubes 15ml/50ml	Greiner Bio-one, Germany
Filter tips	Greiner Bio-one, Germany
Individually Ventilated Cage GM500 Mouse IVC Green Line	Scanbur A/S, Denmark
Insulin Syringes Omnican® U-100	Braun, Germany
MACS separation columns (MS, LS)	Miltenyi Biotec, Germany
Microvette 500 LH-Gel	Sarstedt AG & Co. KG, Germany
Needles	Braun, Germany
LightCycler® 480 Multiwell Plate 384, white	Roche Diagnostics, Switzerland

Reflotron ALT (GPT) stripes	Roche Diagnostics, Switzerland
Reaction tubes 1.5ml, 2ml	Greiner Bio-one, Germany
Sterile filters 0.2µm	Sarstedt AG & Co. KG, Germany
Surgical Disposable Scalpels	Braun, Germany
Syringes	Braun, Germany
Pipettes (disposable) 2, 5, 10, 25, 50ml	Greiner Bio-one, Germany

4.1.3 Chemicals and reagents

Product	**Supplier**
Bioluminescene Imaging	
Isoflurane CP 1 ml/ml	CP-Pharma, Germany
ViviRen™ In Vivo Renilla Luciferase Substrate	Promega, USA
XenoLight D-luciferin - K+ Salt Bioluminescent Substrate	PerkinElmer, USA
Flow Cytometry	
Count Bright absolute counting beads (FACS)	Invitrogen, USA
eBioscience™ Brefeldin A Solution (1000x)	Invitrogen, USA
eBioscience™ Cell Stimulation Cocktail (500x)	Invitrogen, USA
Fixable viability dye eF780	Invitrogen, USA
UltraComp eBeads™ Compensation Beads	Thermo Fisher Scientific, USA
Hepatocyte Isolation	
Heparin	Braun, Germany
Ketamin 10 %	MEDISTAR, Germany
Xylazin, 20 mg/ml (Rompun 2%)	Bayer AG, Germany
Immunohistochemistry	
Paraformaldehyde solution (4 %)	AppliChem GmbH, Germany
Antibody Diluent (IHC)	Thermo Fisher Scientific, USA
IHC Antigen Retrieval Solution	Thermo Fisher Scientific, USA
Cloning	
Agarose	Sigma-Aldrich, USA

Ethanol	Thermo Fisher Scientific, USA
Isopropanol	Thermo Fisher Scientific, USA
Methanol	Sigma-Aldrich, USA
Midori Green Advanced DNA dye	Nippon Genetics Europe GmbH, Germany
Lymphocyte Isolation	
Pancoll, human	PAN-Biotech GmbH, Germany
Percoll™	GE Healthcare, Chicago
Cell culture	
Bovines Serumalbumine (BSA)	AppliChem GmbH, Germany
Dimethylsulfoxid (DMSO)	Sigma-Aldrich, USA
Dulbecco's Modified Eagle's Medium (DMEM)	Thermo Fisher Scientific, USA
Fetal calf serum (FCS)	Sigma-Aldrich, USA
Glucose solution, 50 mM	Sigma-Aldrich, USA
L-Glutamine, 200mM	Sigma-Aldrich, USA
HEPES, 1M	Sigma-Aldrich, USA
Hydrocortisone	Rotexmedica GmbH, Germany
Insulin	Novo Nordisk Pharma GmbH, Germany
Lipofectamine 2000	Invitrogen, USA
Penicillin/Streptomycin, 10 000 U/mL	Biochrome GmbH, Germany
RPMI (Glutamaxx)	Gibco, Life Technologies, USA
Selenium, Transferin, Insulin	Sigma-Aldrich, USA
Trypan Blue	Invitrogen, USA
Trypsin-EDTA	Invitrogen, USA
Williams E medium (w: L-Glutamine)	PAN-Biotech, Germany
Others	
Polyinosinic-polycytidylic acid (Poly I:C) HMV	Invivogen, USA
NaCL 0,9%	Deltamedica GmbH, Germany
GBSS	PAN Biotech, USA
PBS	Biochrom, Germany

4.1.4 Buffers and solutions

Buffer/Solution	Ingredients	Concentration
ACK lysis buffer (pH:7,4)	NH_4Cl	150 mM

	$KHCO_3$	10 mM
	Na_2EDTA	0,1 mM
AAV Production		
Benzonase Buffer (pH: 8,5)	Tris-HCL	50mM
	NaCL	150 mM
	$MgCl_2$	2mM
PBS-MK	PBS	1x
	$MgCl_2$	1mM
	KCl	2,5 mM
PBS-MK-NaCL	PBS-MK	
	NaCL	1M
Adenovirus Production		
Cäsiumchloride buffer 1	Virus buffer	1,25 M
	CsCl	
Cäsiumchloride buffer 2	Virus buffer	1,34 M
	CsCl	
Cäsiumchloride buffer 3	Virus buffer	1,4 M
	CsCl	
Dialysis buffer (10x)	H_2O	
	Sucrose	30%
	NaCL	1,5 M
	$MgCl_2$	0,1 M
	Tris-HCL	0,1M
Virus buffer (pH: 7,8)	H_2O	
	Tris-HCL	10 mM
	$MgCl_2$	20 mM
Hepatocyte isolation		
EGTA buffer (Buffer A)	Glucose solution: 62 mL KH buffer: 10 mL HEPES buffer I: 10 mL Amino acid solution:15 mL L-Glutamine (200 mM): 0,24 mL EGTA solution: 0,4 mL	
Collagenase buffer (Buffer B)	Glucose solution: 38,75 mL KH buffer: 6,25 mL HEPES buffer I: 6,25 mL	

	Amino acid solution :7,5 mL $CaCl_2$ solution: 0,95 mL $MgCl_2$ solution: 1,55 mL L-Glutamine (200 mM): 0,15 mL Collagenase NB 4G	 0,46 g/mL
Suspension buffer (Buffer C)	Glucose solution: 124 mL KH Buffer: 20 mL HEPES buffer II: 20 mL Amino acid solution: 30 mL L-Glutamine (200 mM): 0,479 mL $CaCl_2$ solution: 1,6 mL $MgSO_4$ solution: 0,8 mL BSA: 340 mg	
Aminoacid solution (pH:7,6)	L-Alanin	0,27 g/L
	L-Asparaginsäure	0,14 g/L
	L-Asparagin	0,4 g/L
	Citrullin	0,27 g/L
	L-Cystein	0,14 g/L
	L-Histidin	1 g/L
	L-Glutaminsäure	1 g/L
	L-Glycin	1 g/L
	L-Isoleucin	0,4 g/L
	L-Leucin	0,8 g/L
	L-Lysin	1,3 g/L
	L-Methionin	0,55 g/L
	L-Ornithin	0,65 g/L
	L-Phenylalanin	0,55 g/L
	L-Prolin	0,55 g/L
	L-Serin	0,64 g/L
	L-Threonin	1,35 g/L
	L-Tryptophan	0,65 g/L
	L-Tyrosin	0,55 g/L
	L-Valin	0,8 g/L
$CaCl_2$ solution	$CaCl_2 \times 2H_2O$	0,13 M
EGTA solution (pH: 7,6)	EGTA	125 mM
Glucose solution	Glucose monohydrate	50 mM
HEPES buffer I (pH: 8,5)	HEPES	0,25 M
HEPES buffer II (pH: 7,6)	HEPES	0,25M

KH buffer (pH: 7,4)	NaCL	1 M
	KCL	23,5 mM
	KH_2PO_4	12 mM
$MgCl_2$ solution	$MgCl_2$ x 6 H_2O	0,13 M
$MgSO_4$ solution	$MgSO_4$ x 7 H_2O	0,1 M

4.1.5 Kits

Kit	**Supplier**
ARCHITECT HBeAg Reagent Kit	Abbott Laboratories, USA
AAVpro® Titration Kit	Takara Bio Inc., Japan
BOND Polymer Refine Detection Kit	Leica Microsystems, Germany
eBioscience™ Foxp3 / Transcription Factor Staining Buffer Set	Invitrogen, USA
eBioscience™ IC Fixation and Permeabilization Buffer set	Invitrogen, USA
GeneJet™ Plasmid Miniprep Kit	Thermo Fisher Scientific, USA
Naïve $CD8^+$ T cell isolation Kit, Maus	Miltenyi Biotec, Germany
NucleoBond® Xtra high-copy Midi Kit	Macherey-Nagel GmbH, Germany
NucleoSpin ® RNA	Macherey-Nagel GmbH, Germany
Nucleospin® Gel and PCR Clean-up Kit	Macherey-Nagel GmbH, Germany
NucleoSpin® Tissue Kit	Macherey-Nagel GmbH, Germany
REDTaq® ReadyMix™ PCR Reaction Mix	Sigma-Aldrich, USA
Sensifast™ cDNA synthesis Kit	Bioline, UK
True Nuclear™ Transcription Factor buffer set	Biolegend, USA

4.1.6 Enzymes and Peptides

Enzyme	**Supplier**
Benzonase	Sigma-Aldrich, USA
Collagenase Type II	Worthington Biochemical Corporation, USA
Collagenase Type NB 4G	SERVA, Germany
Gateway® LR Clonase® Enzyme mix	Thermo Fisher Scientific, USA
Gateway® Proteinase K-solution	Thermo Fisher Scientific, USA
GeneRuler 1 kb DNA Ladder	Thermo Fisher Scientific, USA

T4-DNA-Ligase (5 U/µL)	Thermo Fisher Scientific, USA
TakyonTM No Rox SYBR® MasterMix dTTP Blue	Eurogentec, Belgium
Peptide	
C93 (specific for HBcAg, Amino acid sequence: MGLKFRQL, presented on MHC-I)	JPT Peptide Technologies, Germany
SIINFEKL (specific for OVAS8L, Amino acid sequence: SIINFEKL, presented on MHC-I	Iba Lifesciences, Germany

4.1.7 Primer

Name	**Sequence (5'-3')**
Adeno fw	TAA GCG ACG GAT GTG G
Adeno rev	CCA CGT AAA CGG TCA AAG
Cyclophiline fw	ATGGTCAACCCCACCGTGT
Cyclophiline rev	TTCTGCTGTCTTTGGAACTTTGTC
HPRT fw	TCA GTC AAC GGG GGA CAT AAA
HPRT rev	GGG GCT GTA CTG CTT AAC CAG
ISG 15 fw	TGA CTG TGA GAG CAA GCA GC3
ISG 15 rev	CCC CAG CAT CTT CAC CTT TA
MX-1 fw	TCT GAG GAG AGC CAG ACG AT
MX-1 rev	ACT CTG GTC CCC AAT GAC AG
OAS1 fw	GCT GTG GTA CCC ATG TTT TAT GAA
OAS1 rev	AC CAC CGT CGG CAC ATC
pgRNA fw	GAGTGTGGATTCGCACTCC
pgRNA rev	GAGGCGAGGGAGTTCTTCT

4.1.8 Cell culture media

Medium	**Ingredients**	**Concentration**
Hepatocyte maintenance medium	William's E medium (with L-Glutamine)	
	L-Glutamine	240 µM
	HEPES (pH 7.4)	23 mM
	Penicillin/Streptomycin	100 U/mL
	Gentamycin	0,5 mg/mL

	Hydrocortisone	40 ng/mL
	Insulin	5 µg/mL
	DMSO	1,6 %
Hepatocyte attachment medium	Hepatocyte maintenance medium + FCS	10%
Hepatocyte over-night medium	Hepatocyte maintenance medium + FCS	1%
T cell medium	RPMI GlutaMAX	
	FCS	10%
	L-Glutamine	1%
	Penicillin/Streptomycin	1%
	β-Mercaptoethanol	50 µM
HEK293 Medium	DMEM	
	FCS	10%
	L-Glutamine	1%
	Penicillin/Streptomycin	1%

4.1.9 Mouse strains

Mouse Strain	**Description**	**Source**
C57BL/6J	Wildtype C57Bl/6J	Janvier Labs, France
CD45.1 OT-I	C57BL/6-Tg(TcraTcrb)1100Mjb/Crl	Charles River Laboratories, USA
CD45.1 COR93	B6.Cg-Ptprc^{a} Pepc^{b} Tg(TcraBC10 TcrbBC10) 3Chi/J	The Jackson Laboratory, USA
AlbCre x IFNAR$^{fl/fl}$	C57BL/6- LoxP-flanked ifnar1(IFNAR$^{fl/fl}$) mice were bred with mice that express Cre recombinase specifically in hepatocytes (Alb-Cre)	Ulrich Kalinke, TWINCORE, Germany
CD4Cre x IFNAR$^{fl/fl}$	C57BL/6- LoxP-flanked ifnar1(IFNAR$^{fl/fl}$) mice were bred with mice that express Cre recombinase specifically in T cells (CD4-Cre)	Ulrich Kalinke, TWINCORE, Germany
IFNAR$^{fl/fl}$	LoxP-flanked ifnar1(IFNAR$^{fl/fl}$) mice	Ulrich Kalinke, TWINCORE, Germany

4.1.10 Viral vectors

All adeno-associated viral vectors (AAVs) in this study are AAVs serotype 2 packed with an

AAV serotype 8 capsid resulting in liver-specificity. All adenoviral vectors (Ad) were of serotype 5 (Ad 5) backbone with deletions of E1A/E1B and E3.

Vector name	Abbreviation	Source
Ad-HBV1.3	Ad-HBV	Generated by U. Protzer, produced by K. Manske/ D. Wohlleber
Ad-HBV-Luc	-	Generated + produced by K. Manske/ D. Wohlleber
Ad-CMV-GOL	-	Generated + produced by K. Manske/ D. Wohlleber
AAV-CMV-IFNβ-RL	AAV-IFNRL	Generated + produced by A. Schneider
AAV-CMV-GFP-RL	AAV-GRL	Generated + produced by A. Schneider
AAV-TTR-IFNβ	AAV-IFN	Generated by A. Schneider, produced by M. Anton
AAV-TTR-Empty	AAV-Empty	Generated by A. Schneider, produced by M. Anton

4.1.11 Antibodies

Antibody	Clone	Supplier
Depletion Antibodies		
Anti-mouse CD4	GK1.5	Bio X Cell, USA
Anti-mouse CD8a	2.43	Bio X Cell, USA
Anti-mouse NK1.1	PK136	Bio X Cell, USA
Flow Cytometry		
anti-CD19	6D5	Invitrogen, USA
anti-CD4	RM4-5	Invitrogen, USA
anti-CD44	IM7	BioLegend Inc., USA
anti-CD45.1	A20	Invitrogen, USA
anti-CD62L	MEL-14	BioLegend Inc., USA
anti-CD69	H1.2F3	BioLegend Inc., USA
anti-CD8a	53-6.7	BioLegend Inc., USA
anti-CD8a	KT15	ProImmune, UK
anti-human Granzyme B	GB11	Invitrogen, USA
Anti-H2K^{b} bound to SIINFEKL	25-D1.16	BioLegend Inc., USA
anti-IFNγ	XMG1.2	BioLegend Inc., USA
anti-KLRG-1	2F1/KLRG1	BD Biosciences, USA

anti-KI-67	16A8	BioLegend Inc., USA
anti-LAG3 (CD223)	C9B7W	BioLegend Inc., USA
anti-MHC Class I ($H2K^b$)	AF6-88.5	BioLegend Inc., USA
anti-NK1.1	PK136	BioLegend Inc., USA
anti-PD1	J43	Invitrogen, USA
anti-PD1	29F.1A12	BioLegend Inc., USA
anti-TCF1/TCF7	C63D9	Cell Signaling Technology, Inc., USA
anti-TIGIT	1G9	BioLegend Inc., USA
anti-TIGIT	4D4	BioLegend Inc., USA
anti-Tim3	RMT3-23	BioLegend Inc., USA
anti-TNF	MP6-XT22	Invitrogen, USA
anti-TOX	TXRX10	Invitrogen, USA
aRabbit IgG, BV421 gekoppelt	Poly4064	BioLegend Inc., USA
aRabbit IgG, BV510 gekoppelt	Poly4064	BioLegend Inc., USA
Immunohistochemistry		
HbcAg rabbit polyclonal antibody		Origene, USA
PhosphoSTAT1 rabbit polyclonal antibody		Cell Signaling Technology, Inc., USA

4.1.12 Multimers

Pentamers are a subgroup of multimers consisting of five MHC I-peptide headgroups. All of the five headgroups can contact the $CD8^+$ T cell and they are connected via flexible linkers to a multimerization domain, which is coupled to five fluorescent or biotin tags.

Epitope	Tag	Supplier
C93: MGLKFRQL	APC	ProImmune, UK
C93: MGLKFRQL	PE	ProImmune, UK
C93: MGLKFRQL	Biotin	ProImmune, UK

4.1.13 Software

Product	Supplier
Adobe Illustrator CS6	Adobe Systems Software Ireland Limited, Ireland
Adobe® Acrobat® XI Version 11.0.23	Adobe Acrobat, USA
Aperio Image Scope	Leica Biosystems, Germany
ChemiDoc™ XRS	Bio-Rad Laboratories, Germany
EndNote X9	Clarivate, USA
FlowJo 10.5.3	Becton, USA

Image Lab Software 5.2.1	Bio-Rad Laboratories, Germany
Lightcycler 480 Software 1.5.1.62 SP2	Roche Diagnostics, Switzerland
Living Image® 4.5	PerkinElmer, USA
Microsoft® Excel für Mac Version 16.38	Microsoft Corporation, USA
Microsoft® Word für Mac Version 16.38	Microsoft Corporation, USA
Prism für Mac OS X Version 7.0	GraphPad Software, USA
Prism für Mac OS X Version 8.0	GraphPad Software, USA
SnapGene® Viewer 5.0.4	GSL Biotech LLC, USA
SP6800 Spectral Analyzer	Sony Biotechnology Inc, USA

4.2 Methods

4.2.1 Molecular biological methods

4.2.1.1 Polymerase chain reaction (PCR)

PCRs for genotyping were performed using the REDTaq® ReadyMix™ PCR 2x Reaction Mix (Sigma) according to the manufacturer´s instructions. In brief, 1 µl of each Primer (10 µM), 1µl DNA (10-100 ng/µl) and 12,5 µl 2x Mastermix were mixed with 7,5 µl H20. Amplification of gene of interested was performed using the following program:

	Temperature [°C]	Time [sec]	Cycles
Denaturation	95	180	1
Denaturation	95	30	30
Annealing	55-65 (depending on primers)	30-60	
Elongation	72	30 per 1 kb	
Elongation	72	120	1
Cooling	4	∞	1

4.2.1.2 Restriction enzyme digestion

Restriction enzyme digestion was used to obtain fragments of plasmids for cloning or to control plasmid DNA after its isolation on the basis of fragment sizes.
Per digestion reaction, 200 ng for analytical digests or 3 µg for preparative digests of Plasmid DNA was mixed with 2 µl FastDigest Green Buffer (10x) and up to 1 µl of the appropriate FastDigest restriction enzyme. H_20 was added to a total reaction volume of 20 µl with subsequent incubation at 37°C for 10 – 60 minutes. If restriction digests were implemented to obtain a plasmid backbone for the following ligation, 1 µl FastAP for dephosphorylation of 5’

and 3' ends was added in order to prevent self-ligation without an insert. Inactivation of enzymes was performed according to the manufacturer's instructions.

4.2.1.3 DNA gel electrophoresis and gel extraction

Plasmid DNA or PCR productions were analyzed depending on their size on a 1-2 % agarose gel prepared with TAE buffer (1x) and 5 µl Midori green advanced DNA dye per 50 ml total volume. Samples and a DNA ladder, used to determine the size of DNA fragments, were run at 70 – 120 mV until the desired separation of fragments had been reached. DNA Fragments needed for further molecular cloning steps were cut out from the agarose gel using a scalpel. Subsequently, DNA was extracted using the Nucleospin® gel and PCR clean-up kit (Machery Nagel) according to the manufacturer's instructions.

4.2.1.4 Ligation

For ligation, 100 ng of DNA fragments were ligated in a molar ratio of 3:1 (insert: backbone) with 2 µl T4 ligase buffer and 1 µl T4 ligase. H_20 was added to a total reaction volume of 20 µl with subsequent incubation at RT for 30 minutes.

4.2.1.5 Transformation of E.coli

E.coli Top10 or E.coli STBL3 (only used for AAV plasmids) were thawed on ice and 5 µl of the ligation reaction or 1 ng plasmid DNA was added to 50 µl bacteria and incubated for 20 minutes on ice. Cell permeabilization via heat shock was performed for 45- 90 sec at 42°C. Bacteria were chilled on ice for 2 – 3 minutes before 500 µl SOC medium was added and bacteria shook for one hour at 225 rpm. Next, bacteria were spun down at 500g for 5 minutes, resuspended in 100 µl of SOC medium and spread on antibiotic-resistance (50 µg/ml Kanamycin or 100 µg/ml Ampicillin) LB plates. After overnight incubation at 37°C, single E. coli colonies were selected and multiplied in LB-medium for plasmid DNA preparation.

4.2.1.6 Isolation of Plasmid DNA

Single colonies of E. coli Top10 or STBL3 transformed with respective plasmids were amplified in overnight cultures in LB medium supplemented with either 100 µg/ml ampicillin or 50 µg/ml kanamycin (depending on the resistance gene on the plasmid) at 37°C, 185 rpm. Bacteria cultures were centrifuged (3400 xg, 10 min, 4°C) after they had reached a maximal absorbance of 1.5 (OD600). Plasmid DNA was isolated using the GeneJet™ Plasmid Miniprep Kit or the

Nucleobond™ Xtra high-copy midi kit depending on culture size according to the manufacturer's instructions.

4.2.1.7 Sequencing

For sequencing, samples were diluted to a concentration of 30 – 100 ng/µl and 20 µl sample as well as 20 µl primer (10 µM) were sent to the external provider GATC Biotech (Konstanz, Germany). Sequencing results were downloaded for subsequent analysis using Serial Cloner 2.6.1.

4.2.1.8 DNA/RNA isolation

DNA from tissue or serum was extracted using the Nucleospin® Tissue Kit according to the manufacturer's instructions for tissue or serum. If available, 200 µl of serum was applied (or serum was filled up to 200 µl with PBS). RNA from tissue was isolated using the Nucleospin® RNA Kit according to the manufacturer's instructions for tissue. Plasmid and genomic DNA, as well as RNA concentrations, were determined on a NanoDrop using an appropriate buffer solution as a blank.

4.2.1.9 cDNA synthesis

Isolated DNA was transcribed into complementary DNA (cDNA) using the SensiFAST™ cDNA Synthesis Kit (Bioline Reagents) according to the manufacturer's instructions. Thereby, 1 µg isolated DNA was transcribed at 42°C in a reaction volume of 20 µl by adding 5x TransAmp Buffers and reverse transcriptase.

4.2.1.10 Quantitative PCR

Quantitative PCR was performed to determine the total intracellular adenovirus DNA or HBV DNA using an external plasmid standard or for relative quantification of pgRNA, OAS-1, MX-1, HPRT, or cyclophilin-1 from cDNA from liver tissue. Relative quantification of pgRNA, OAS-1, or MX-1 was achieved by normalization to the housekeeping gene HPRT or cyclophilin-1 measured in the same sample. Per reaction, 0.5 µl of each primer (stock: 20 µM), 5 µl LightCycler480 SYBR green master mix and 1 µl H_20 were mixed with 3 µl sample. All PCRs were performed with the following program:

4.2.2 General cell culture methods

All primary cells and cell lines were cultured under sterile conditions and only handled under a clean hood with laminar airflow. Cells were incubated at 37°C, 5% CO_2 and 95% humidity.

4.2.2.1 Maintenance of cell lines

Adherent cell lines (HEK293, HEK293T) were cultured in DMEM full medium. Depending on confluency, cells were passaged 1:5 or 1:10 every two to four days. Cells were detached using Trypsin (5-10 min, 37°C).

4.2.2.2 Counting cells

After harvesting, a single cell suspension was obtained by vigorous resuspension and manually diluted 1:1 to 1:10 with Trypan blue to stain dead cells. Afterwards, cells were counted on a Neubauer improved hemocytometer under a light microscope.

4.2.2.3 Freezing/Thawing of cells

For freezing, cells were harvested and centrifuged at 450g for 5 minutes and pelleted cells were resuspended in 1 mL freezing medium per cryo vial. Subsequently, cryo vials were transferred into a freezing device and stored at -80°C for slow temperature decline. After 1 or 2 days, cryo vials were transferred to liquid nitrogen.
In order to thaw cells, cryo vials were slowly thawed by panning within a 37°C water bath. Just before the solution was completely thawed, the solution was transferred into a falcon containing 15 mL prewarmed medium. Cells were pelleted (450g, 5 min, RT) and seeded in an appropriate cell culture flask with the respective medium.

4.2.3 Viral vector production

4.2.3.1 Adenoviral vectors

Recombinant, replication-deficient serotype 5 adenoviral vectors of the second-generation (with deletion of the E1 and E3 proteins) were generated using the Gateway®-technology (Thermo Fisher Scientific). The expression cassettes with the respective transgenes (Ad-CMV-GOL: eGFP, Ovalbumin, CBG99-Luciferase; Ad-HBV.1.3: HBV1.3 overlength construct; Ad-HBV-Luc: HBV1.3 overlength construct, CBG99-Luciferase) were synthesized and cloned into the Gateway® pENTR™ 11 dual selection vector. Once we obtained the pENTR™ 11 vectors with respective expression cassettes, an LR recombination reaction with the pAd/PL-DEST™ Gateway® vector was performed according to the manufacturer's instructions. The pAd/PL-

DEST™ bearing the respective expression cassette was linearized via PacI digestion. Thereby, all genes needed for vector propagation in bacteria were removed.HEK293 cells, which were grown until ~50% confluent, were transfected with the linearized construct using Lipofectamine 2000. In detail, 3 µg linearized vector was diluted in 500 µl DMEM medium and in another Eppendorf tube, 7,5 µl Lipofectamine 2000 (2,5 µg/1µg vector DNA) was diluted in 500 µl DMEM medium. Subsequently, both solutions were mixed, incubated for 20 minutes at room temperature and added dropwise to HEK293 cells in transfection medium (DMEM,3%FCS). After transfection, cells were monitored daily until they had a round shape and were partly detached. Then, cells were carefully detached by tapping, harvested within the medium and exposed to three freezing-thawing cycles (-80°C- 37°C) to break down cell membranes. Next, cell debris was pelleted (3360 g, 10 min, RT) and the supernatant was used for infection of 15cm^2 dishes. Supernatant from one T175 flask was distributed to 20 15 cm^2 dishes grown with HEk293 cells (80% confluency). Around 48 hours after infection, when cells started to detach, cells were harvested, pelleted (840 g, 5 min, RT), and resuspended in 6 mL of virus-buffer (for 20 dishes). Again, cells were exposed to three freezing-thawing cycles (-80°C- 37°C) to release intracellular viruses. The cell debris was removed by centrifugation (3360 g, 10 min, RT) and the viral particles in the supernatant were purified via Cesium-chloride (CsCL) density gradient centrifugation. Therefore, a CsCL gradient consisting of a 3,5 mL 1.4 CsCL-solution and 3,5 mL 1,25 CsCL-solution, was overlaid with the virus-containing solution (filled up to 8,5 mL with virus-buffer) and centrifuged at 30000 rpm for 1 h at 10°C under vacuum (brake and acceleration set to “low”). After centrifugation, the blue-appearing layer containing the viral particles was collected using a syringe. For the second ultracentrifugation step, 11 mL of a 1.34 CsCL-solution were overlaid with 5 mL of virus-solution (filled up to 5 mL with virus-buffer). The second ultracentrifugation step was performed at 30000 rpm for 18 hours at 10°C under vacuum (brake and acceleration set to “low”). Again, the blue-appearing layer containing the viral particles was collected using a syringe. Next, the residual CsCL was removed from the collected virus solution via dialysis. Therefore, virus-solution was transferred to a dialyze cell and stored in 1L of dialysis buffer. After the first dialysis step for 30 minutes at 4°C (stirring), the buffer was exchanged, and 4 further dialysis steps were performed for 1 hour with fresh dialysis buffer each. Finally, virus-solution was removed from the dialysis cell and stored at -80°C in small aliquots. Virus titer was determined via hexon titration. Therefore, HEK293 cells were seeded into poly-Lysin coated 24-well plates (2,5 x 10^5 cells/well) in DMEM with 10% FCS and 1% Glutamine. One hour after seeding, virus-solution was added in different solutions. In detail, using the medium as a diluent, a 10-fold serial dilution of virus-solution was prepared (duplicate). The dilutions 10^{-6}, $10^{-7,}$ and 10^{-8} were used for titration. Duplicate of solutions were again added onto cells in duplicates. After incubation of ~ 36 hours at 37°C in 5 % CO_2, cells were fixed by adding ice-cold 100 %

methanol to each well and incubated at -20°C for 20 minutes. Next, cells were washed three times with 1%BSA in PBS and anti-Hexon antibody was added (1:200 in 1%BSA/PBS). After incubation for 1h at RT, cells were washed three times with PBS and DAB-solution diluted in DAB-buffer (Agilent Technologies) was added. After 10 minutes of incubation at RT, DAB-solution was removed, and the reaction was stopped by washing three times with PBS. Finally, the brown/black positive cells were counted under the microscope and thereby infectious units per mL virus-solution were determined.

4.2.3.2 Adeno-associated viral vectors

Adeno-associated virus (AAV) serotype 2 packed with an AAV serotype 8 capsid were produced in HEK293T cells. HEK293T cells were seeded in a total number of 4 x 10^6 cells per 15 cm^2 dish and grown 48 hours until confluency of ~80%. At 80% confluency, a triple transfection with Adeno-Helper DNA, Capsid DNA, and viral vector DNA was performed. Therefore, a DNA mix and a PEI mix were prepared separately: For the DNA mix 14,7 µg of Adeno-Helper DNA, Capsid-DNA and viral vector DNA each was mixed with 0,79 mL of H20 and NaCL each (amounts and volumes/1 dish). For the PEI mix 0,44 mL H20 was mixed with 0,35 mL PEI and 0,79 mL NaCL (volumes/1 dish). Subsequently, DNA solution was added to PEI solution and vortexed vigorously. After 10 minutes of incubation at room temperature, 3,2 mL of transfection solution per dish was added dropwise and slowly. 72 hours after transfection, cells were harvested and pelleted (500xg, 15 min, RT). The supernatant was removed and pellets were dried to remove the remaining medium and resuspend in 5 mL Benzonase-buffer (pellets of 40 petri-dishes; 0,125 mL/1 dish). Next, the solution was vortexed vigorously, exposed to five freezing-thawing cycles (-80°C- 37°C), treated with ultrasound for 80s (ultrasound waterbath), and finally treated with 50U/mL benzonase for 1h at 37°C (inverted every 10 min). Vector stocks were purified by an iodixanol gradient: 60% iodixanol was diluted to 15, 25 and 40% in PBS-MK (25%, 40%) or PBS-MK-NaCL (15%). A 2,5 µl volume of 0,5% phenolred per mL was added to the 60% and 25% iodixanol solutions to facilitate easier distinguishing of the phase boundaries within the gradient. Using a Pasteur pipette total volume of processed cell layer (~5 mL) was underlaid with 1,5 mL 15%, followed by 25%, 40%, and 60% of iodixanol solutions. After centrifugation in a 70.1 Ti rotor for 2 hours at 50000 rpm at 4°C, AAVs were collected from the fractions obtained from the 40% phase. Viral genome titers were determined by qPCR using the AAVpro® Titration Kit following the manufacturer's instructions. AAV stocks were stored at -80°C.

4.2.4 Isolation of primary cells

4.2.4.1 Isolation of murine hepatocytes

Approximately 20 minutes before starting isolation of primary murine hepatocytes, mice were i.p. injected with 150 µl Heparin (2000 U/mL) to ensure anticoagulation. 10 minutes after Heparin injection, mice were narcoticized via i.p injection of 200 µl Ketamin (5%)/Xylazin (20mg/mL) (3:1). After the loss of reflexes, mice were opened to access the internal organs. The cannula was inserted into the portal vein and the liver was perfused with EGTA Buffer (~6 mL/min; 7-8 min). Once, cannulation was confirmed to be successful, the inferior vena cava was cut. Next, EGTA Buffer was exchanged to collagenase-buffer and pumping speed was reduced to 4 mL/min. After perfusion with 45 mL collagenase-buffer, the liver was excised, and gallbladder was removed. Using scalpels and forceps, cells were gently removed from the liver capsule and filtered through a 100 µM filter to remove cell clumps and obtain a single-cell suspension. Cells were washed with two times with 50 mL suspension buffer (50g, 2min, 4°C) and resuspended in 5 mL of PBS-buffered 50% Percoll. Next, the cell-Percoll suspension was underlaid with 5,5 mL of PBS-buffered 80% Percoll and centrifuged (600g, 20 min, RT; acceleration 7; brake 1). After centrifugation, the dead cells on top were removed and remaining living hepatocytes were washed two times with suspension buffer (50g, 2min, 4°C) and resuspended in 3 to 5 mL maintenance medium. Finally, hepatocytes were counted (using 1:3 or 1:5 ratio trypan blue) and adjusted to respective cell numbers in attachment-medium (maintenance medium + 10% FCS) for culture or in PBS (+ BSA/FCS) for staining. For culture, hepatocytes were seeded on plates (96-well: 10000/well; 24-well: 1 x 10^5/well; 12-well: 2x10^5/well) coated with CollagenR solution. After four to five hours, when cells were attached, attachment-medium was exchanged to overnight-medium (maintenance-medium + 1% FCS). The next day, hepatocytes were washed twice with cold PBS and were then cultured in maintenance-medium for up to four days.

4.2.4.2 Isolation of murine splenocytes

To isolate splenocytes of mice, spleens were crushed through 100 µm cell strainers using a plunger of a 5 mL syringe. Cell strainer was repeatedly flushed with cold PBS and collected cells were pelleted (1500 rpm, 5min, 4°C). Next, erythrocytes were lysed in 2 mL ACK lysis buffer for 2 min at RT. The reaction was stopped by adding 40 mL of PBS, splenocytes were pelleted (1500 rpm, 5min, 4°C), filtered through a 70 µm cell filter to obtain a single-cell solution, centrifuged and resuspended in a suitable volume of T cell medium for culture or PBS (+ BSA/FCS) for staining.

4.2.4.3 Isolation of murine liver-associated lymphocytes

To isolate murine liver-associated lymphocytes, livers were perfused for ~ 45 s with PBS in order to remove non-liver-associated lymphocytes. Then, livers were crushed through 100 µm

cell strainers using a plunger of a 5 mL syringe. Cell strainer was repeatedly flushed with cold PBS and collected cells were pelleted (1500 rpm, 5min, 4°C). Cell pellets were resuspended in 8 mL GBSS containing 0,125 U/mL Collagenase Type II and digested for 10 minutes at 37°C (water bath) with repeated shaking. After an additional washing step with 40 mL PBS, pellets were resuspended in 3 mL PBS-buffered 40% Percoll, carefully layered onto 3 mL PBS-buffered 80% Percoll in a 15 mL Falcon tube and centrifuged at 1400 g for 20 minutes at room temperatures (acceleration and brakes set “low”). Lymphocytes located between Percoll layers were collected, washed with PBS, filtered through a 70 µm cell filter to obtain a single-cell solution, centrifuged and resuspended in either PBS (+ BSA/FCS) for staining or T cell medium for culture.

4.2.4.4 Isolation of murine PBMCs

10 µl of heparinized whole blood collected in heparinized capillary tubes was transferred to a 1,5 mL Eppendorf tube containing 0,5 mL PBS. Cells were pelleted (500g, 2 min, 4°C) and erythrocytes were lysed in 0,75 mL ACK lysis buffer. After 10 minutes of incubation at RT, the reaction was stopped adding 0,75 mL PBS, cells were pelleted (500g, 2 min, 4°C) and washed again using 1 mL PBS. Thereafter, PBMCs were resuspended in PBS(+BSA/FCS) for staining.

4.2.4.5 Isolation of lymphocytes from hepatic lymphnodes

Lymphnodes were meshed through 100 µm cell strainer using a plunger of a 5 mL syringe. Cell strainer was repeatedly flushed with cold PBS. Collected cell suspension was filtered through a 70 µm filter to obtain a single-cell solution and pelleted (1500 rpm, 5min, 4°C). Thereafter, cells were resuspended in PBS(+BSA/FCS) for staining.

4.2.5 Infection of primary cells

4.2.5.1 Infection of primary hepatocytes with adenoviral vectors

After attachment, hepatocytes were washed with PBS and adenoviral vectors were added in maintenance medium at a MOI of 1 to 10 depending on the experimental setup. Before, adenoviral vectors were pre-diluted 1:10 in murine plasma, incubated for 2 minutes at RT and further diluted in maintenance medium to the desired concentration. 24 hours after infection, the medium was exchanged.

4.2.6 Mouse experiments

Mouse experiments were conducted in accordance with the German regulations fo the Society for Laboratory Animal Science (GV-SOLAS) and the European Health Law of Federation of Laboratory Animal Science Associations (FELASA). Experiments were approved by the local Animal Care and Use Committee of Upper Bavaria. Animals were kept in a pathogen-free (SPF) facility and experiments were performed during the light phase of the day.

4.2.6.1 Injections

For intravenous (i.v.) injections, mice were fixed into a retainer and the injection site was disinfected using 70% ethanol. For intraperitoneal (i.p.) injections, mice were manually restrained in a supine position with the head tightly toward the ground. The injection site was in the animal's lower right quadrant of the abdomen to avoid damage to the urinary bladder, cecum, and other abdominal organs. For all injection's insulin syringes (30G*1/2" (0,3mm x 12 mm) needle (U-100 Insulin) were used.

4.2.6.1.1 Adenoviral/Adenovirus associated vector injection

All adenoviral vectors were injected intravenously (i.v.) in 100 or 200 µl 0,9%-NaCl into the tail vein of mice. All AAVs were injected intravenously (i.v.) in 200 µl PBS into the tail vein of mice.

4.2.6.1.2 Antibody-mediated depletion

Endogenous $CD8^+$ T cells were depleted via i.v. injection of 5 µg of the anti-CD8a depleting Antibody (clone 2.43) in 100 µl PBS. In order to maintain depletion, the injection was repeated if not stated differently every 6 to 7 days. Endogenous $NK1.1^+$ cells were depleted via i.p. injection of 300 µg of the anti-NK1.1 antibody (clone PK136) in 100 µl PBS. In order to maintain depletion, the injection was repeated if not stated differently every 6 to 7 days. Endogenous $CD4^+$ T cells were depleted via i.v. injection of 300 µg of the anti-CD4 depleting Antibody (clone GK1.5) in 100 µl PBS. In order to maintain depletion, the injection was repeated if not stated differently every 3 to 4 days.

4.2.6.2 Adoptive T cell transfer

For adoptive T cell Transfer, naïve $CD8^+$ T cells from spleens of transgenic CD45.1 C93 mice were isolated using the naïve $CD8a^+$ T cell isolation kit (Miltenyi). Per mouse, 10000 naïve C93-specific $CD8^+$ T cells were injected in 100 µl PBS intravenously.

4.2.6.3 Bioluminescence imaging

In mice that were injected with vectors expressing CBG99-Luciferase or Renilla-Luciferase, luciferase expression can be measured non-invasive and daily in the IVIS Imaging System (Perkin Elmer). For measurement of CBG99-Luciferase, mice were i.p. injected with D-Luciferin potassium salt (50 mM, 10 mg/kg bodyweight) 5 minutes before measurement. For measurement of Renilla-Luciferase, mice were i.v. injected with Coelenterazine (ViviRen™ Live cell Substrate; 1,5 mg/kg bodyweight) in 100 µl PBS 30-60 seconds before measurement. Mice were anesthetized using 2% isoflurane before in vivo imaging. For quantification, regions of interest (ROI) were selected and quantified as photons/second using Living Image® software.

4.2.6.4 Bleeding

Mice were bled from the cheek at different time points after infection or vector transduction. To analyze serum parameters (HBsAg/HBeAg), isolate PBMCs or isolate DNA from serum, blood was collected in Microvette 1,1 m Z-Gel tubes. Small volumes of blood (sALT measurements) were obtained by puncture of the tail vein.

4.2.6.5 sALT

Serum alanine aminotransferase (ALT) activity was measured (undiluted or diluted 1:1, 1:5 or 1:10 in PBS) directly from whole blood obtained by puncture of the tail vein or obtained from the cheek using the Reflotron® GPT/ALT test.

4.2.6.6 Serum analysis

Whole blood collected in Microvette 1,1 mL Z-Gel tubes was centrifuged at 10000g for 5 minutes at RT. The serum located above the gel matrix was collected and transferred into a new reaction tube for further analysis or storage at -80°C.

4.2.6.6.1 HBsAg/HBeAg

Serum HBsAg and HBeAg levels were quantified on an Architect™ platform using the quantitative HBsAg test (Ref.: 6C36-44; Cutoff: 0.25 IU/mL) or the HBeAg Reagent Kit (Ref.: 6C32-27) with HBeAg Quantitative Calibrators (Ref.: 7P24-01; Cutoff: 0.20 PEIU/mL).

4.2.6.6 Dissection and processing of organs

Mice were sacrificed and opened to access the internal organs. Blood was drawn with a 23 G syringe from the vena cava and collected in a Microvette 1,1 mL Z-Gel tube. In order to remove, non-liver associated lymphocytes, the liver was perfused with PBS through the portal vein until

the complete liver was well-perfused indicated by blanching. The gallbladder was removed before excising the liver. Moreover, if necessary, the spleen and lymph nodes were removed and both organs were store in PBS on ice until further processing. Tissue from the liver was used for extraction of DNA, RNA or for histological analysis and was therefore cut into cubic pieces of ~5mm edge length with a clean scalpel. For RNA and DNA analysis, tissue was immediately frozen to -80°C. For histological analysis, tissue was fixed in 4% paraformaldehyde (PFA) for 48 hours and transferred to a PBS container until paraffin embedding.

4.2.7 Immunohistochemistry

Immunohistochemistry was performed by the group of M. Heikenwälder or the Comparative experimental Pathology (CeP) supervised by K. Steiger. Tissue pieces from the left liver lobe and the lobus caudatus were fixed for 48 hours in 4% Paraformaldehyde (PFA) and stored in PBS until dehydration and paraffin-embedding were performed. Liver sections (2µm) were stained with hematoxylin/eosin (HE), anti-HBcAg, or anti-pSTAT1. Immunohistochemical staining was performed using a Leica BondMax Rx^{m} and tissue slides were scanned using a SCN 400 scanner or an Aperio AT2 slide scanner. For quantification, tissue slides were analyzed using the Aperio Image Scope software.

4.2.8 Ex vivo peptide stimulation

For ex vivo peptide stimulation, up to 5 x 10^6 splenocytes or LALs were plated in a U-bottom-96-well plate and stimulated with indicated peptides in a final concentration of 1 µg/mL. After 1 hour at 37°C, Brefeldin A was added and stimulation was continued at 37°C for either further 5 hours or further 15 hours until cells were harvested and an ICS was performed.

4.2.9 Real-time viability: xCelligence

The xCelligence system was used to determine the cell-viability of target cells during co-culture experiments. Adherent target cells were seeded on E-plate 96 microtiter plates, which contain interdigitated gold microelectrodes to noninvasively measure the electrical impedance. The electrical impedance is displayed as cell index (CI) values and reflect attachment/detachment and morphology of target cells. In Experiments with primary murine hepatocytes as target cells, 1 x 10^4 target cells were seeded per well. 24 hours after attachment, cells were infected with adenoviral vectors or left untreated and then cultured for further 48 hours until co-culture with T cells was started. At the start of co-culture, maintenance medium was carefully removed and T cells were added in 100 µl of T cell medium. The effector to target ratios (E:T) were titrated

and are always stated in the according experiments. Cell viability is illustrated as cell index normalized to start of co-culture.

4.2.10 Flow cytometry

4.2.10.1 Surface staining

For surface staining, up to 1 x 10^7 cells were transferred to a V-bottom 96-well plate and washed once with PBS before the first staining step (Lymphocytes: 1600 rpm, 2min, 4°C ; Hepatocytes: 50 x g, 2min, 4°C). Subsequently, cells were stained in a volume of 30 µl (Lymphocytes) to 100 µl (Hepatocytes) per well with respective antibodies diluted in PBS (+ BSA + FCS). After incubation of 20 minutes at 4°C in the dark, cells were washed twice with PBS (+ BSA + FCS). Finally, cells were resuspended in either PBS or FACS buffer for immediate analysis (Hepatocytes) or cells were fixed for flow cytometry (see: 4.2.11.2), or it was proceeded with intracellular or intranuclear staining (see: 4.2.11.3/4). Samples were analyzed on a Sony SP6800 or Cytoflex S flow cytometer. Data analysis was performed using FlowJo software.

4.2.10.2 Fixation for Flow cytometric analysis

After surface staining, cells for flow cytometric were resuspended in 200 µl IC Fixation buffer, mixed well and incubated for 30 minutes at RT. Thereafter, cells were washed once in PBS (+ BSA/FCS) and then resuspended in 100 to 200 µl FACS Buffer or PBS for analysis. Since cells change shape during fixation, speed and time centrifugation was increased from 1600 rpm for 2 minutes to 1800 rpm for 3 minutes.

4.2.10.3 Pentamer staining

Pro5® MHC Pentamers were used to stain for HBV-specific TCRs. Labeled Pro5® MHC Pentamers presents five MHC peptide complexes in a plane at one end of their pentameric coiled-coil core and five detection tags in a second plane at the opposite end of the core. 3µl of Pentamer per sample (up to 1 x 10^7 cells/well) were added in a total volume of 30 µl PBS (+FCS/BSA). After 40 min on ice, a surface antibody-mastermix was added in another 30 µl volume of PBS (+FCS/BSA). Cells were resuspended and stained for further 20 minutes at 4°C following the protocol for standard surface staining.

4.2.10.4 Intracellular cytokine staining (ICS)

For intracellular cytokine staining, cells have to be permeabilized. Cells were exposed to regular cell surface staining, washed twice and fixed according to section 4.2.11.2.

Subsequently, cells were washed twice with 200 µl Perm/Wash Buffer (according to manufacturers protocol 1:10 in H20) at 1800 rpm for 3 minutes and then incubated in 50 µl of intracellular antibody mastermix. Instead of diluting the antibodies in PBS (+FCS/BSA), antibodies were diluted in Perm/Wash Buffer. After 30 minutes of incubation at 4°C, cells were washed 3 times with 200 µl Perm/Wash Buffer at 1800 rpm for 3 minutes and then resuspended in 100 to 200 µl PBS for analysis.

4.2.10.5 Intranuclear staining

4.2.11.5.1 Intranuclear staining according to Foxp3/Transcription Factor™ Buffer Set (eBioscience)

After standard multimer and surface staining procedure (4.2.11.1/4.2.11.3), cells were resuspended in 200 Foxp3 Fixation/permeabilization working solution and incubated for 60 minutes at RT. Thereafter, cells were centrifuged at 1800 rpm for 3 minutes and cells were washed with 200 µl of 1x Permeabilization Buffer. Next, 50 µl of intranuclear mastermix, namely intranuclear antibodies diluted in 1 x Permeabilization Buffer, was added and incubated for 60 minutes at 4°C. If not using directly fluorochrome-labeled antibodies, primary antibodies were also diluted in 1 x Permeabilization Buffer and cells were incubated for 30 minutes at 4°C, washed twice and then incubated with intranuclear mastermix containing secondary antibodies for further 60 minutes at 4°C. Finally, cells were washed twice and since the TCF1 antibody interaction was rather unstable, cells were fixed according to section 4.2.11.2 after the intranuclear staining procedure before resuspended for analysis.

4.2.10.5.2 True-Nuclear™ Transcription Factor Staining Buffer Set (BD)

After standard multimer and surface staining procedure (4.2.11.1/4.2.11.3), cells were resuspended in 200 µl of True-Nuclear™ 1x Fix concentrate and incubated for 60 minutes at RT. Thereafter, cells were centrifuged at 1800 rpm for 3 minutes and cells were washed with 200 µl of True-Nuclear™ 1x Perm-Buffer three times. Next, 50 µl of intranuclear mastermix, namely intranuclear antibodies diluted in True-Nuclear™ 1x Perm-Buffer, was added and incubated for 60 minutes at 4°C. If not using directly fluorochrome labeled antibodies, primary antibodies were also diluted in True-Nuclear™ 1x Perm-Buffer and cells were incubated for 30 minutes at 4°C, washed twice and then incubated with intranuclear mastermix containing secondary antibodies for further 60 minutes at 4°C. Finally, cells were washed twice and since the TCF1 antibody interaction was rather unstable, cells were fixed according to section 4.2.11.2 after the intranuclear staining procedure before resuspended for analysis.

4.2.10.6 determination of absolute cell count by flow cytometry

To determine absolute numbers of cells, 10 µl CountBright™ absolute Counting Beads were added to the cell suspension directly before measurement on the flow cytometer. The absolute input of cell count was calculated with the following formula:

Input cells = measured cells x input beads/measured beads

The obtained value for input cells was extrapolated to the concentration in blood or to the whole organ, considering the proportion of the organ that was used for staining.

4.2.12 Statistical analysis

Data are presented as individual values plus mean with standard deviation (SD). Statistical significance was calculated as stated in individual figures using Graphpad prism software. Statistical significance was calculated with the unpaired t test, ns= not significant, * $p<0.05$, ** $p < 0.01$, *** < 0.001, **** $p< 0.0001$.

TABLE OF FIGURES

REFERENCES

1. Dane, D.S., Cameron, C.H. & Briggs, M. Virus-like particles in serum of patients with Australia-antigen-associated hepatitis. *Lancet* **1**, 695-698 (1970).

2. Hu, J. & Liu, K. Complete and Incomplete Hepatitis B Virus Particles: Formation, Function, and Application. *Viruses* **9** (2017).

3. Fung, S.K. & Lok, A.S. Hepatitis B virus genotypes: do they play a role in the outcome of HBV infection? *Hepatology* **40**, 790-792 (2004).

4. Guirgis, B.S., Abbas, R.O. & Azzazy, H.M. Hepatitis B virus genotyping: current methods and clinical implications. *Int J Infect Dis* **14**, e941-953 (2010).

5. Kramvis, A. Genotypes and genetic variability of hepatitis B virus. *Intervirology* **57**, 141-150 (2014).

6. Liaw, Y.F., Brunetto, M.R. & Hadziyannis, S. The natural history of chronic HBV infection and geographical differences. *Antivir Ther* **15 Suppl 3**, 25-33 (2010).

7. Wieland, S.F. The chimpanzee model for hepatitis B virus infection. *Cold Spring Harb Perspect Med* **5** (2015).

8. Ganem, D. Assembly of hepadnaviral virions and subviral particles. *Curr Top Microbiol Immunol* **168**, 61-83 (1991).

9. Nassal, M. HBV cccDNA: viral persistence reservoir and key obstacle for a cure of chronic hepatitis B. *Gut* **64**, 1972-1984 (2015).

10. Yan, H. *et al.* Sodium taurocholate cotransporting polypeptide is a functional receptor for human hepatitis B and D virus. *Elife* **1**, e00049 (2012).

11. Seeger, C. & Mason, W.S. Molecular biology of hepatitis B virus infection. *Virology* **479-480**, 672-686 (2015).

12. Glebe, D. & Urban, S. Viral and cellular determinants involved in hepadnaviral entry. *World J Gastroenterol* **13**, 22-38 (2007).

13. Ko, C., Michler, T. & Protzer, U. Novel viral and host targets to cure hepatitis B. *Curr Opin Virol* **24**, 38-45 (2017).

14. Institute of Medicine Committee on the, P. & Control of Viral Hepatitis, I. In: Colvin, H.M. & Mitchell, A.E. (eds). *Hepatitis and Liver Cancer: A National Strategy for Prevention and Control of Hepatitis B and C*. National Academies Press (US)
Copyright 2010 by the National Academy of Sciences. All rights reserved.: Washington (DC), 2010.

15. Peeridogaheh, H. *et al.* Current concepts on immunopathogenesis of hepatitis B virus infection. *Virus Res* **245**, 29-43 (2018).

16. Maini, M.K. *et al.* Direct ex vivo analysis of hepatitis B virus-specific CD8(+) T cells associated with the control of infection. *Gastroenterology* **117**, 1386-1396 (1999).

17. Bertoletti, A. & Gehring, A.J. The immune response during hepatitis B virus infection. *J Gen Virol* **87**, 1439-1449 (2006).

18. Bertoletti, A. *et al.* Cytotoxic T lymphocyte response to a wild type hepatitis B virus epitope in patients chronically infected by variant viruses carrying substitutions within the epitope. *J Exp Med* **180**, 933-943 (1994).

19. Shepard, C.W., Simard, E.P., Finelli, L., Fiore, A.E. & Bell, B.P. Hepatitis B virus infection: epidemiology and vaccination. *Epidemiol Rev* **28**, 112-125 (2006).

20. Pollicino, T., Saitta, C. & Raimondo, G. Hepatocellular carcinoma: the point of view of the hepatitis B virus. *Carcinogenesis* **32**, 1122-1132 (2011).

21. European Association for the Study of the Liver. Electronic address, e.e.e. & European Association for the Study of the, L. EASL 2017 Clinical Practice Guidelines on the management of hepatitis B virus infection. *J Hepatol* **67**, 370-398 (2017).

22. Terrault, N.A. *et al.* Update on Prevention, Diagnosis, and Treatment of Chronic Hepatitis B: AASLD 2018 Hepatitis B Guidance. *Clin Liver Dis (Hoboken)* **12**, 33-34 (2018).

23. Fanning, G.C., Zoulim, F., Hou, J. & Bertoletti, A. Author Correction: Therapeutic strategies for hepatitis B virus infection: towards a cure. *Nat Rev Drug Discov* (2020).

24. Maini, M.K. & Gehring, A.J. The role of innate immunity in the immunopathology and treatment of HBV infection. *J Hepatol* **64**, S60-S70 (2016).

25. Wieland, S., Thimme, R., Purcell, R.H. & Chisari, F.V. Genomic analysis of the host response to hepatitis B virus infection. *Proc Natl Acad Sci U S A* **101**, 6669-6674 (2004).

26. Wieland, S.F. & Chisari, F.V. Stealth and cunning: hepatitis B and hepatitis C viruses. *J Virol* **79**, 9369-9380 (2005).

27. Suslov, A., Boldanova, T., Wang, X., Wieland, S. & Heim, M.H. Hepatitis B Virus Does Not Interfere With Innate Immune Responses in the Human Liver. *Gastroenterology* **154**, 1778-1790 (2018).

28. Stacey, A.R. *et al.* Induction of a striking systemic cytokine cascade prior to peak viremia in acute human immunodeficiency virus type 1 infection, in contrast to more modest and delayed responses in acute hepatitis B and C virus infections. *J Virol* **83**, 3719-3733 (2009).

29. Hosel, M. *et al.* Not interferon, but interleukin-6 controls early gene expression in hepatitis B virus infection. *Hepatology* **50**, 1773-1782 (2009).

30. Dunn, C. *et al.* Temporal analysis of early immune responses in patients with acute hepatitis B virus infection. *Gastroenterology* **137**, 1289-1300 (2009).

31. Fisicaro, P. *et al.* Early kinetics of innate and adaptive immune responses during hepatitis B virus infection. *Gut* **58**, 974-982 (2009).

32. McClary, H., Koch, R., Chisari, F.V. & Guidotti, L.G. Relative sensitivity of hepatitis B virus and other hepatotropic viruses to the antiviral effects of cytokines. *J Virol* **74**, 2255-2264 (2000).

33. Guidotti, L.G. *et al.* Interferon-regulated pathways that control hepatitis B virus replication in transgenic mice. *J Virol* **76**, 2617-2621 (2002).

34. Wu, M. *et al.* Hepatitis B virus polymerase inhibits the interferon-inducible MyD88 promoter by blocking nuclear translocation of Stat1. *J Gen Virol* **88**, 3260-3269 (2007).

35. Christen, V. *et al.* Inhibition of alpha interferon signaling by hepatitis B virus. *J Virol* **81**, 159-165 (2007).

36. Fernandez, M., Quiroga, J.A. & Carreno, V. Hepatitis B virus downregulates the human interferon-inducible MxA promoter through direct interaction of precore/core proteins. *J Gen Virol* **84**, 2073-2082 (2003).

37. Visvanathan, K. *et al.* Regulation of Toll-like receptor-2 expression in chronic hepatitis B by the precore protein. *Hepatology* **45**, 102-110 (2007).

38. Chen, Z. *et al.* Expression profiles and function of Toll-like receptors 2 and 4 in peripheral blood mononuclear cells of chronic hepatitis B patients. *Clin Immunol* **128**, 400-408 (2008).

39. Xie, Q. *et al.* Patients with chronic hepatitis B infection display deficiency of plasmacytoid dendritic cells with reduced expression of TLR9. *Microbes Infect* **11**, 515-523 (2009).

40. Wu, J. *et al.* Hepatitis B virus suppresses toll-like receptor-mediated innate immune responses in murine parenchymal and nonparenchymal liver cells. *Hepatology* **49**, 1132-1140 (2009).

41. Lebosse, F. *et al.* Intrahepatic innate immune response pathways are downregulated in untreated chronic hepatitis B. *J Hepatol* **66**, 897-909 (2017).

42. Chisari, F.V., Isogawa, M. & Wieland, S.F. Pathogenesis of hepatitis B virus infection. *Pathol Biol (Paris)* **58**, 258-266 (2010).

43. Rehermann, B. Pathogenesis of chronic viral hepatitis: differential roles of T cells and NK cells. *Nat Med* **19**, 859-868 (2013).

44. Thimme, R. *et al.* CD8(+) T cells mediate viral clearance and disease pathogenesis during acute hepatitis B virus infection. *J Virol* **77**, 68-76 (2003).

45. Koup, R.A. *et al.* Temporal association of cellular immune responses with the initial control of viremia in primary human immunodeficiency virus type 1 syndrome. *J Virol* **68**, 4650-4655 (1994).

46. Rentenaar, R.J. *et al.* Development of virus-specific CD4(+) T cells during primary cytomegalovirus infection. *J Clin Invest* **105**, 541-548 (2000).

47. Webster, G.J. *et al.* Incubation phase of acute hepatitis B in man: dynamic of cellular immune mechanisms. *Hepatology* **32**, 1117-1124 (2000).

48. Fong, T.L. *et al.* High levels of viral replication during acute hepatitis B infection predict progression to chronicity. *J Med Virol* **43**, 155-158 (1994).

49. Korba, B.E. *et al.* Natural history of woodchuck hepatitis virus infections during the course of experimental viral infection: molecular virologic features of the liver and lymphoid tissues. *J Virol* **63**, 1360-1370 (1989).

50. Murray, J.M., Wieland, S.F., Purcell, R.H. & Chisari, F.V. Dynamics of hepatitis B virus clearance in chimpanzees. *Proc Natl Acad Sci U S A* **102**, 17780-17785 (2005).

51. Phillips, S. *et al.* CD8(+) T cell control of hepatitis B virus replication: direct comparison between cytolytic and noncytolytic functions. *J Immunol* **184**, 287-295 (2010).

52. Ando, K. *et al.* Class I-restricted cytotoxic T lymphocytes are directly cytopathic for their target cells in vivo. *J Immunol* **152**, 3245-3253 (1994).

53. Guidotti, L.G. *et al.* Intracellular inactivation of the hepatitis B virus by cytotoxic T lymphocytes. *Immunity* **4**, 25-36 (1996).

54. Robek, M.D., Wieland, S.F. & Chisari, F.V. Inhibition of hepatitis B virus replication by interferon requires proteasome activity. *J Virol* **76**, 3570-3574 (2002).

55. Robek, M.D., Boyd, B.S., Wieland, S.F. & Chisari, F.V. Signal transduction pathways that inhibit hepatitis B virus replication. *Proc Natl Acad Sci U S A* **101**, 1743-1747 (2004).

56. Wieland, S.F., Eustaquio, A., Whitten-Bauer, C., Boyd, B. & Chisari, F.V. Interferon prevents formation of replication-competent hepatitis B virus RNA-containing nucleocapsids. *Proc Natl Acad Sci U S A* **102**, 9913-9917 (2005).

57. Heise, T., Guidotti, L.G., Cavanaugh, V.J. & Chisari, F.V. Hepatitis B virus RNA-binding proteins associated with cytokine-induced clearance of viral RNA from the liver of transgenic mice. *J Virol* **73**, 474-481 (1999).

58. Wieland, S.F., Spangenberg, H.C., Thimme, R., Purcell, R.H. & Chisari, F.V. Expansion and contraction of the hepatitis B virus transcriptional template in infected chimpanzees. *Proc Natl Acad Sci U S A* **101**, 2129-2134 (2004).

59. Trautmann, T. *et al.* CD4+ T-cell help is required for effective CD8+ T cell-mediated resolution of acute viral hepatitis in mice. *PLoS One* **9**, e86348 (2014).

60. Asabe, S. *et al.* The size of the viral inoculum contributes to the outcome of hepatitis B virus infection. *J Virol* **83**, 9652-9662 (2009).

61. Rehermann, B. *et al.* The cytotoxic T lymphocyte response to multiple hepatitis B virus polymerase epitopes during and after acute viral hepatitis. *J Exp Med* **181**, 1047-1058 (1995).

62. Boni, C. *et al.* Characterization of hepatitis B virus (HBV)-specific T-cell dysfunction in chronic HBV infection. *J Virol* **81**, 4215-4225 (2007).

63. European Association For The Study Of The, L. EASL clinical practice guidelines: Management of chronic hepatitis B virus infection. *J Hepatol* **57**, 167-185 (2012).

64. Konerman, M.A. & Lok, A.S. Interferon Treatment for Hepatitis B. *Clin Liver Dis* **20**, 645-665 (2016).

65. Lau, G.K. *et al.* Peginterferon Alfa-2a, lamivudine, and the combination for HBeAg-positive chronic hepatitis B. *N Engl J Med* **352**, 2682-2695 (2005).

66. Liaw, Y.F. *et al.* Shorter durations and lower doses of peginterferon alfa-2a are associated with inferior hepatitis B e antigen seroconversion rates in hepatitis B virus genotypes B or C. *Hepatology* **54**, 1591-1599 (2011).

67. Marcellin, P. *et al.* Hepatitis B surface antigen levels: association with 5-year response to peginterferon alfa-2a in hepatitis B e-antigen-negative patients. *Hepatol Int* **7**, 88-97 (2013).

68. Kwon, H. & Lok, A.S. Hepatitis B therapy. *Nat Rev Gastroenterol Hepatol* **8**, 275-284 (2011).

69. Rijckborst, V., Sonneveld, M.J. & Janssen, H.L. Review article: chronic hepatitis B - anti-viral or immunomodulatory therapy? *Aliment Pharmacol Ther* **33**, 501-513 (2011).

70. Boyd, A. *et al.* Decay of ccc-DNA marks persistence of intrahepatic viral DNA synthesis under tenofovir in HIV-HBV co-infected patients. *J Hepatol* **65**, 683-691 (2016).

71. Carosi, G. *et al.* Treatment of chronic hepatitis B: update of the recommendations from the 2007 Italian Workshop. *Dig Liver Dis* **43**, 259-265 (2011).

72. von Weizsacker, F. *et al.* The tupaia model for the study of hepatitis B virus: direct infection and HBV genome transduction of primary tupaia hepatocytes. *Methods Mol Med* **96**, 153-161 (2004).

73. Wang, Q. *et al.* Experimental chronic hepatitis B infection of neonatal tree shrews (Tupaia belangeri chinensis): a model to study molecular causes for susceptibility and disease progression to chronic hepatitis in humans. *Virol J* **9**, 170 (2012).

74. Protzer, U. Viral hepatitis: The bumpy road to animal models for HBV infection. *Nat Rev Gastroenterol Hepatol* **14**, 327-328 (2017).

75. Guidotti, L.G., Matzke, B., Schaller, H. & Chisari, F.V. High-level hepatitis B virus replication in transgenic mice. *J Virol* **69**, 6158-6169 (1995).

76. Guo, W.N., Zhu, B., Ai, L., Yang, D.L. & Wang, B.J. Animal models for the study of hepatitis B virus infection. *Zool Res* **39**, 25-31 (2018).

77. Huang, L.R. *et al.* Transfer of HBV genomes using low doses of adenovirus vectors leads to persistent infection in immune competent mice. *Gastroenterology* **142**, 1447-1450 e1443 (2012).

78. Dion, S., Bourgine, M., Godon, O., Levillayer, F. & Michel, M.L. Adeno-associated virus-mediated gene transfer leads to persistent hepatitis B virus replication in mice expressing HLA-A2 and HLA-DR1 molecules. *J Virol* **87**, 5554-5563 (2013).

79. Yan, Z. *et al.* HBVcircle: A novel tool to investigate hepatitis B virus covalently closed circular DNA. *J Hepatol* **66**, 1149-1157 (2017).

80. Dandri, M., Lutgehetmann, M. & Petersen, J. Experimental models and therapeutic approaches for HBV. *Semin Immunopathol* **35**, 7-21 (2013).

81. Pestka, S., Krause, C.D. & Walter, M.R. Interferons, interferon-like cytokines, and their receptors. *Immunol Rev* **202**, 8-32 (2004).

82. Ali, S. *et al.* Sources of Type I Interferons in Infectious Immunity: Plasmacytoid Dendritic Cells Not Always in the Driver's Seat. *Front Immunol* **10**, 778 (2019).

83. Stetson, D.B. & Medzhitov, R. Type I interferons in host defense. *Immunity* **25**, 373-381 (2006).

84. Sun, L., Wu, J., Du, F., Chen, X. & Chen, Z.J. Cyclic GMP-AMP synthase is a cytosolic DNA sensor that activates the type I interferon pathway. *Science* **339**, 786-791 (2013).

85. Kumar, H. *et al.* Essential role of IPS-1 in innate immune responses against RNA viruses. *J Exp Med* **203**, 1795-1803 (2006).

86. Stetson, D.B. & Medzhitov, R. Recognition of cytosolic DNA activates an IRF3-dependent innate immune response. *Immunity* **24**, 93-103 (2006).

87. Platanias, L.C. Mechanisms of type-I- and type-II-interferon-mediated signalling. *Nat Rev Immunol* **5**, 375-386 (2005).

88. Majoros, A. *et al.* Canonical and Non-Canonical Aspects of JAK-STAT Signaling: Lessons from Interferons for Cytokine Responses. *Front Immunol* **8**, 29 (2017).

89. Ivashkiv, L.B. & Donlin, L.T. Regulation of type I interferon responses. *Nat Rev Immunol* **14**, 36-49 (2014).

90. Stark, G.R., Kerr, I.M., Williams, B.R., Silverman, R.H. & Schreiber, R.D. How cells respond to interferons. *Annu Rev Biochem* **67**, 227-264 (1998).

91. Harding, H.P., Calfon, M., Urano, F., Novoa, I. & Ron, D. Transcriptional and translational control in the Mammalian unfolded protein response. *Annu Rev Cell Dev Biol* **18**, 575-599 (2002).

92. Balachandran, S. *et al.* Alpha/beta interferons potentiate virus-induced apoptosis through activation of the FADD/Caspase-8 death signaling pathway. *J Virol* **74**, 1513-1523 (2000).

93. Madera, S. *et al.* Type I IFN promotes NK cell expansion during viral infection by protecting NK cells against fratricide. *J Exp Med* **213**, 225-233 (2016).

94. Lee, C.K. *et al.* Distinct requirements for IFNs and STAT1 in NK cell function. *J Immunol* **165**, 3571-3577 (2000).

95. Nguyen, K.B. *et al.* Coordinated and distinct roles for IFN-alpha beta, IL-12, and IL-15 regulation of NK cell responses to viral infection. *J Immunol* **169**, 4279-4287 (2002).

96. Le Bon, A. *et al.* Cross-priming of CD8+ T cells stimulated by virus-induced type I interferon. *Nat Immunol* **4**, 1009-1015 (2003).

97. Montoya, M. *et al.* Type I interferons produced by dendritic cells promote their phenotypic and functional activation. *Blood* **99**, 3263-3271 (2002).

98. Rouzaut, A. *et al.* Dendritic cells adhere to and transmigrate across lymphatic endothelium in response to IFN-alpha. *Eur J Immunol* **40**, 3054-3063 (2010).

99. Longhi, M.P. *et al.* Dendritic cells require a systemic type I interferon response to mature and induce CD4+ Th1 immunity with poly IC as adjuvant. *J Exp Med* **206**, 1589-1602 (2009).

100. Simmons, D.P. *et al.* Type I IFN drives a distinctive dendritic cell maturation phenotype that allows continued class II MHC synthesis and antigen processing. *J Immunol* **188**, 3116-3126 (2012).

101. Kolumam, G.A., Thomas, S., Thompson, L.J., Sprent, J. & Murali-Krishna, K. Type I interferons act directly on CD8 T cells to allow clonal expansion and memory formation in response to viral infection. *J Exp Med* **202**, 637-650 (2005).

102. Marrack, P., Kappler, J. & Mitchell, T. Type I interferons keep activated T cells alive. *J Exp Med* **189**, 521-530 (1999).

103. Teijaro, J.R. *et al.* Persistent LCMV infection is controlled by blockade of type I interferon signaling. *Science* **340**, 207-211 (2013).

104. Wilson, E.B. *et al.* Blockade of chronic type I interferon signaling to control persistent LCMV infection. *Science* **340**, 202-207 (2013).

105. Wilson, E.B. *et al.* Emergence of distinct multiarmed immunoregulatory antigen-presenting cells during persistent viral infection. *Cell Host Microbe* **11**, 481-491 (2012).

106. Crouse, J., Kalinke, U. & Oxenius, A. Regulation of antiviral T cell responses by type I interferons. *Nat Rev Immunol* **15**, 231-242 (2015).

107. van Boxel-Dezaire, A.H., Rani, M.R. & Stark, G.R. Complex modulation of cell type-specific signaling in response to type I interferons. *Immunity* **25**, 361-372 (2006).

108. Brierley, M.M. & Fish, E.N. Stats: multifaceted regulators of transcription. *J Interferon Cytokine Res* **25**, 733-744 (2005).

109. Tanabe, Y. *et al.* Cutting edge: role of STAT1, STAT3, and STAT5 in IFN-alpha beta responses in T lymphocytes. *J Immunol* **174**, 609-613 (2005).

110. Gimeno, R., Lee, C.K., Schindler, C. & Levy, D.E. Stat1 and Stat2 but not Stat3 arbitrate contradictory growth signals elicited by alpha/beta interferon in T lymphocytes. *Mol Cell Biol* **25**, 5456-5465 (2005).

111. Virgin, H.W., Wherry, E.J. & Ahmed, R. Redefining chronic viral infection. *Cell* **138**, 30-50 (2009).

112. Wherry, E.J., Blattman, J.N., Murali-Krishna, K., van der Most, R. & Ahmed, R. Viral persistence alters CD8 T-cell immunodominance and tissue distribution and results in distinct stages of functional impairment. *J Virol* **77**, 4911-4927 (2003).

113. Barber, D.L. *et al.* Restoring function in exhausted CD8 T cells during chronic viral infection. *Nature* **439**, 682-687 (2006).

114. Blackburn, S.D. *et al.* Coregulation of CD8+ T cell exhaustion by multiple inhibitory receptors during chronic viral infection. *Nat Immunol* **10**, 29-37 (2009).

115. Crawford, A. & Wherry, E.J. The diversity of costimulatory and inhibitory receptor pathways and the regulation of antiviral T cell responses. *Curr Opin Immunol* **21**, 179-186 (2009).

116. Brooks, D.G. *et al.* Interleukin-10 determines viral clearance or persistence in vivo. *Nat Med* **12**, 1301-1309 (2006).

117. Ejrnaes, M. *et al.* Resolution of a chronic viral infection after interleukin-10 receptor blockade. *J Exp Med* **203**, 2461-2472 (2006).

118. Blackburn, S.D. & Wherry, E.J. IL-10, T cell exhaustion and viral persistence. *Trends Microbiol* **15**, 143-146 (2007).

119. Tinoco, R., Alcalde, V., Yang, Y., Sauer, K. & Zuniga, E.I. Cell-intrinsic transforming growth factor-beta signaling mediates virus-specific CD8+ T cell deletion and viral persistence in vivo. *Immunity* **31**, 145-157 (2009).

120. Wherry, E.J. T cell exhaustion. *Nat Immunol* **12**, 492-499 (2011).

121. Schmitz, J.E. *et al.* Control of viremia in simian immunodeficiency virus infection by CD8+ lymphocytes. *Science* **283**, 857-860 (1999).

122. Jin, X. *et al.* Dramatic rise in plasma viremia after CD8(+) T cell depletion in simian immunodeficiency virus-infected macaques. *J Exp Med* **189**, 991-998 (1999).

123. Bowen, D.G. & Walker, C.M. Adaptive immune responses in acute and chronic hepatitis C virus infection. *Nature* **436**, 946-952 (2005).

124. Rehermann, B. Hepatitis C virus versus innate and adaptive immune responses: a tale of coevolution and coexistence. *J Clin Invest* **119**, 1745-1754 (2009).

125. Cornberg, M. *et al.* Clonal exhaustion as a mechanism to protect against severe immunopathology and death from an overwhelming CD8 T cell response. *Front Immunol* **4**, 475 (2013).

126. McLane, L.M., Abdel-Hakeem, M.S. & Wherry, E.J. CD8 T Cell Exhaustion During Chronic Viral Infection and Cancer. *Annu Rev Immunol* **37**, 457-495 (2019).

127. Brooks, D.G., McGavern, D.B. & Oldstone, M.B. Reprogramming of antiviral T cells prevents inactivation and restores T cell activity during persistent viral infection. *J Clin Invest* **116**, 1675-1685 (2006).

128. Angelosanto, J.M., Blackburn, S.D., Crawford, A. & Wherry, E.J. Progressive loss of memory T cell potential and commitment to exhaustion during chronic viral infection. *J Virol* **86**, 8161-8170 (2012).

129. McMichael, A.J., Borrow, P., Tomaras, G.D., Goonetilleke, N. & Haynes, B.F. The immune response during acute HIV-1 infection: clues for vaccine development. *Nat Rev Immunol* **10**, 11-23 (2010).

130. Gallimore, A. *et al.* Induction and exhaustion of lymphocytic choriomeningitis virus-specific cytotoxic T lymphocytes visualized using soluble tetrameric major histocompatibility complex class I-peptide complexes. *J Exp Med* **187**, 1383-1393 (1998).

131. Zajac, A.J. *et al.* Viral immune evasion due to persistence of activated T cells without effector function. *J Exp Med* **188**, 2205-2213 (1998).

132. Mueller, S.N. & Ahmed, R. High antigen levels are the cause of T cell exhaustion during chronic viral infection. *Proc Natl Acad Sci U S A* **106**, 8623-8628 (2009).

133. Rehr, M. *et al.* Emergence of polyfunctional CD8+ T cells after prolonged suppression of human immunodeficiency virus replication by antiretroviral therapy. *J Virol* **82**, 3391-3404 (2008).

134. Streeck, H. *et al.* Antigen load and viral sequence diversification determine the functional profile of HIV-1-specific CD8+ T cells. *PLoS Med* **5**, e100 (2008).

135. Day, C.L. *et al.* Functional capacity of Mycobacterium tuberculosis-specific T cell responses in humans is associated with mycobacterial load. *J Immunol* **187**, 2222-2232 (2011).

136. Utzschneider, D.T. *et al.* High antigen levels induce an exhausted phenotype in a chronic infection without impairing T cell expansion and survival. *J Exp Med* **213**, 1819-1834 (2016).

137. Richter, K., Brocker, T. & Oxenius, A. Antigen amount dictates CD8+ T-cell exhaustion during chronic viral infection irrespective of the type of antigen presenting cell. *Eur J Immunol* **42**, 2290-2304 (2012).

138. Bucks, C.M., Norton, J.A., Boesteanu, A.C., Mueller, Y.M. & Katsikis, P.D. Chronic antigen stimulation alone is sufficient to drive CD8+ T cell exhaustion. *J Immunol* **182**, 6697-6708 (2009).

139. Ochel, A. *et al.* Effective intrahepatic CD8+ T-cell immune responses are induced by low but not high numbers of antigen-expressing hepatocytes. *Cell Mol Immunol* **13**, 805-815 (2016).

140. Wherry, E.J. & Kurachi, M. Molecular and cellular insights into T cell exhaustion. *Nat Rev Immunol* **15**, 486-499 (2015).

141. Shankar, P. *et al.* Impaired function of circulating HIV-specific CD8(+) T cells in chronic human immunodeficiency virus infection. *Blood* **96**, 3094-3101 (2000).

142. El-Far, M. *et al.* T-cell exhaustion in HIV infection. *Curr HIV/AIDS Rep* **5**, 13-19 (2008).

143. Harty, J.T. & Badovinac, V.P. Shaping and reshaping CD8+ T-cell memory. *Nat Rev Immunol* **8**, 107-119 (2008).

144. Stelekati, E. *et al.* Bystander chronic infection negatively impacts development of CD8(+) T cell memory. *Immunity* **40**, 801-813 (2014).

145. Brooks, D.G. *et al.* IL-10 and PD-L1 operate through distinct pathways to suppress T-cell activity during persistent viral infection. *Proc Natl Acad Sci U S A* **105**, 20428-20433 (2008).

146. Wilson, E.B. & Brooks, D.G. The role of IL-10 in regulating immunity to persistent viral infections. *Curr Top Microbiol Immunol* **350**, 39-65 (2011).

147. Paley, M.A. *et al.* Progenitor and terminal subsets of CD8+ T cells cooperate to contain chronic viral infection. *Science* **338**, 1220-1225 (2012).

148. Utzschneider, D.T. *et al.* T Cell Factor 1-Expressing Memory-like CD8(+) T Cells Sustain the Immune Response to Chronic Viral Infections. *Immunity* **45**, 415-427 (2016).

149. Utzschneider, D.T. *et al.* T cells maintain an exhausted phenotype after antigen withdrawal and population reexpansion. *Nat Immunol* **14**, 603-610 (2013).

150. Chen, Z. *et al.* TCF-1-Centered Transcriptional Network Drives an Effector versus Exhausted CD8 T Cell-Fate Decision. **51**, 840-855 e845 (2019).

151. Volkert, M. Studies on immunological tolerance to LCM virus. A preliminary report on adoptive immunization of virus carrier mice. *Acta Pathol Microbiol Scand* **56**, 305-310 (1962).

152. Velu, V. *et al.* Enhancing SIV-specific immunity in vivo by PD-1 blockade. *Nature* **458**, 206-210 (2009).

153. Fuller, M.J. *et al.* Immunotherapy of chronic hepatitis C virus infection with antibodies against programmed cell death-1 (PD-1). *Proc Natl Acad Sci U S A* **110**, 15001-15006 (2013).

154. Gardiner, D. *et al.* A randomized, double-blind, placebo-controlled assessment of BMS-936558, a fully human monoclonal antibody to programmed death-1 (PD-1), in patients with chronic hepatitis C virus infection. *PLoS One* **8**, e63818 (2013).

155. Nakamoto, N. *et al.* Functional restoration of HCV-specific CD8 T cells by PD-1 blockade is defined by PD-1 expression and compartmentalization. *Gastroenterology* **134**, 1927-1937, 1937 e1921-1922 (2008).

156. Blackburn, S.D., Shin, H., Freeman, G.J. & Wherry, E.J. Selective expansion of a subset of exhausted CD8 T cells by alphaPD-L1 blockade. *Proc Natl Acad Sci U S A* **105**, 15016-15021 (2008).

157. Darvin, P., Toor, S.M., Sasidharan Nair, V. & Elkord, E. Immune checkpoint inhibitors: recent progress and potential biomarkers. *Exp Mol Med* **50**, 165 (2018).

158. Blattman, J.N. *et al.* Therapeutic use of IL-2 to enhance antiviral T-cell responses in vivo. *Nat Med* **9**, 540-547 (2003).

159. Pellegrini, M. *et al.* IL-7 engages multiple mechanisms to overcome chronic viral infection and limit organ pathology. *Cell* **144**, 601-613 (2011).

160. Brooks, D.G., Lee, A.M., Elsaesser, H., McGavern, D.B. & Oldstone, M.B. IL-10 blockade facilitates DNA vaccine-induced T cell responses and enhances clearance of persistent virus infection. *J Exp Med* **205**, 533-541 (2008).

161. Maris, C.H., Chappell, C.P. & Jacob, J. Interleukin-10 plays an early role in generating virus-specific T cell anergy. *BMC Immunol* **8**, 8 (2007).

162. Vezys, V. *et al.* Continuous recruitment of naive T cells contributes to heterogeneity of antiviral CD8 T cells during persistent infection. *J Exp Med* **203**, 2263-2269 (2006).

163. Wherry, E.J., Barber, D.L., Kaech, S.M., Blattman, J.N. & Ahmed, R. Antigen-independent memory CD8 T cells do not develop during chronic viral infection. *Proc Natl Acad Sci U S A* **101**, 16004-16009 (2004).

164. Shin, H. & Wherry, E.J. CD8 T cell dysfunction during chronic viral infection. *Curr Opin Immunol* **19**, 408-415 (2007).

165. Siddiqui, I. *et al.* Intratumoral Tcf1(+)PD-1(+)CD8(+) T Cells with Stem-like Properties Promote Tumor Control in Response to Vaccination and Checkpoint Blockade Immunotherapy. *Immunity* **50**, 195-211 e110 (2019).

166. Lau, G.K. *et al.* Clearance of hepatitis B surface antigen after bone marrow transplantation: role of adoptive immunity transfer. *Hepatology* **25**, 1497-1501 (1997).

167. Ilan, Y. *et al.* Adoptive transfer of immunity to hepatitis B virus after T cell-depleted allogeneic bone marrow transplantation. *Hepatology* **18**, 246-252 (1993).

168. Sato, S. *et al.* The RNA sensor RIG-I dually functions as an innate sensor and direct antiviral factor for hepatitis B virus. *Immunity* **42**, 123-132 (2015).

169. Lucifora, J. *et al.* Specific and nonhepatotoxic degradation of nuclear hepatitis B virus cccDNA. *Science* **343**, 1221-1228 (2014).

170. Sagnelli, E. *et al.* HBV superinfection in hepatitis C virus chronic carriers, viral interaction, and clinical course. *Hepatology* **36**, 1285-1291 (2002).

171. Liaw, Y.F. *et al.* Impact of acute hepatitis C virus superinfection in patients with chronic hepatitis B virus infection. *Gastroenterology* **126**, 1024-1029 (2004).

172. Guo, F. *et al.* STING agonists induce an innate antiviral immune response against hepatitis B virus. *Antimicrob Agents Chemother* **59**, 1273-1281 (2015).

173. Lanford, R.E. *et al.* GS-9620, an oral agonist of Toll-like receptor-7, induces prolonged suppression of hepatitis B virus in chronically infected chimpanzees. *Gastroenterology* **144**, 1508-1517, 1517 e1501-1510 (2013).

174. Menne, S. *et al.* Sustained efficacy and seroconversion with the Toll-like receptor 7 agonist GS-9620 in the Woodchuck model of chronic hepatitis B. *J Hepatol* **62**, 1237-1245 (2015).

175. Gane, E.J. *et al.* The oral toll-like receptor-7 agonist GS-9620 in patients with chronic hepatitis B virus infection. *J Hepatol* **63**, 320-328 (2015).

176. Jo, J. *et al.* Toll-like receptor 8 agonist and bacteria trigger potent activation of innate immune cells in human liver. *PLoS Pathog* **10**, e1004210 (2014).

177. Schurich, A. *et al.* The third signal cytokine IL-12 rescues the anti-viral function of exhausted HBV-specific CD8 T cells. *PLoS Pathog* **9**, e1003208 (2013).

178. Belloni, L. *et al.* IFN-alpha inhibits HBV transcription and replication in cell culture and in humanized mice by targeting the epigenetic regulation of the nuclear cccDNA minichromosome. *J Clin Invest* **122**, 529-537 (2012).

179. Wieland, S.F., Guidotti, L.G. & Chisari, F.V. Intrahepatic induction of alpha/beta interferon eliminates viral RNA-containing capsids in hepatitis B virus transgenic mice. *J Virol* **74**, 4165-4173 (2000).

180. Uprichard, S.L., Wieland, S.F., Althage, A. & Chisari, F.V. Transcriptional and posttranscriptional control of hepatitis B virus gene expression. *Proc Natl Acad Sci U S A* **100**, 1310-1315 (2003).

181. Xu, C. *et al.* Interferons accelerate decay of replication-competent nucleocapsids of hepatitis B virus. *J Virol* **84**, 9332-9340 (2010).

182. Neumann, A.U. *et al.* Hepatitis C viral dynamics in vivo and the antiviral efficacy of interferon-alpha therapy. *Science* **282**, 103-107 (1998).

183. Micco, L. *et al.* Differential boosting of innate and adaptive antiviral responses during pegylated-interferon-alpha therapy of chronic hepatitis B. *J Hepatol* **58**, 225-233 (2013).

184. Gill, U.S. *et al.* Interferon Alpha Induces Sustained Changes in NK Cell Responsiveness to Hepatitis B Viral Load Suppression In Vivo. *PLoS Pathog* **12**, e1005788 (2016).

185. Fletcher, S.P. *et al.* Correction: Intrahepatic Transcriptional Signature Associated with Response to Interferon-alpha Treatment in the Woodchuck Model of Chronic Hepatitis B. *PLoS Pathog* **12**, e1005541 (2016).

186. Boni, C. *et al.* Restored function of HBV-specific T cells after long-term effective therapy with nucleos(t)ide analogues. *Gastroenterology* **143**, 963-973 e969 (2012).

187. Penna, A. *et al.* Peginterferon-alpha does not improve early peripheral blood HBV-specific T-cell responses in HBeAg-negative chronic hepatitis. *J Hepatol* **56**, 1239-1246 (2012).

188. Rijckborst, V. *et al.* Early on-treatment prediction of response to peginterferon alfa-2a for HBeAg-negative chronic hepatitis B using HBsAg and HBV DNA levels. *Hepatology* **52**, 454-461 (2010).

189. Sonneveld, M.J. *et al.* Response-guided peginterferon therapy in hepatitis B e antigen-positive chronic hepatitis B using serum hepatitis B surface antigen levels. *Hepatology* **58**, 872-880 (2013).

190. Terrault, N.A. *et al.* AASLD guidelines for treatment of chronic hepatitis B. *Hepatology* **63**, 261-283 (2016).

191. Matsumoto, M., Kikkawa, S., Kohase, M., Miyake, K. & Seya, T. Establishment of a monoclonal antibody against human Toll-like receptor 3 that blocks double-stranded RNA-mediated signaling. *Biochem Biophys Res Commun* **293**, 1364-1369 (2002).

192. Alexopoulou, L., Holt, A.C., Medzhitov, R. & Flavell, R.A. Recognition of double-stranded RNA and activation of NF-kappaB by Toll-like receptor 3. *Nature* **413**, 732-738 (2001).

193. McCartney, S. *et al.* Distinct and complementary functions of MDA5 and TLR3 in poly(I:C)-mediated activation of mouse NK cells. *J Exp Med* **206**, 2967-2976 (2009).

194. Kawai, T. *et al.* IPS-1, an adaptor triggering RIG-I- and Mda5-mediated type I interferon induction. *Nat Immunol* **6**, 981-988 (2005).

195. Palchetti, S. *et al.* Transfected poly(I:C) activates different dsRNA receptors, leading to apoptosis or immunoadjuvant response in androgen-independent prostate cancer cells. *J Biol Chem* **290**, 5470-5483 (2015).

196. Yang, K. *et al.* Functional RIG-I-like receptors control the survival of mesenchymal stem cells. *Cell Death Dis* **4**, e967 (2013).

197. Kawai, T. & Akira, S. Toll-like receptor and RIG-I-like receptor signaling. *Ann N Y Acad Sci* **1143**, 1-20 (2008).

198. Salem, M.L., Kadima, A.N., Cole, D.J. & Gillanders, W.E. Defining the antigen-specific T-cell response to vaccination and poly(I:C)/TLR3 signaling: evidence of enhanced primary and memory CD8 T-cell responses and antitumor immunity. *J Immunother* **28**, 220-228 (2005).

199. Hoebe, K. *et al.* Upregulation of costimulatory molecules induced by lipopolysaccharide and double-stranded RNA occurs by Trif-dependent and Trif-independent pathways. *Nat Immunol* **4**, 1223-1229 (2003).

200. de Jong, E.C. *et al.* Microbial compounds selectively induce Th1 cell-promoting or Th2 cell-promoting dendritic cells in vitro with diverse th cell-polarizing signals. *J Immunol* **168**, 1704-1709 (2002).

201. Schwarz, K. *et al.* Role of Toll-like receptors in costimulating cytotoxic T cell responses. *Eur J Immunol* **33**, 1465-1470 (2003).

202. Salem, M.L., El-Naggar, S.A., Kadima, A., Gillanders, W.E. & Cole, D.J. The adjuvant effects of the toll-like receptor 3 ligand polyinosinic-cytidylic acid poly (I:C) on antigen-specific CD8+ T cell responses are partially dependent on NK cells with the induction of a beneficial cytokine milieu. *Vaccine* **24**, 5119-5132 (2006).

203. Sivori, S. *et al.* CpG and double-stranded RNA trigger human NK cells by Toll-like receptors: induction of cytokine release and cytotoxicity against tumors and dendritic cells. *Proc Natl Acad Sci U S A* **101**, 10116-10121 (2004).

204. Salem, M.L. *et al.* The TLR3 agonist poly(I:C) targets CD8+ T cells and augments their antigen-specific responses upon their adoptive transfer into naive recipient mice. *Vaccine* **27**, 549-557 (2009).

205. Isogawa, M., Robek, M.D., Furuichi, Y. & Chisari, F.V. Toll-like receptor signaling inhibits hepatitis B virus replication in vivo. *J Virol* **79**, 7269-7272 (2005).

206. Wu, J. *et al.* Toll-like receptor-mediated control of HBV replication by nonparenchymal liver cells in mice. *Hepatology* **46**, 1769-1778 (2007).

207. Wu, J. *et al.* Poly(I:C) treatment leads to interferon-dependent clearance of hepatitis B virus in a hydrodynamic injection mouse model. *J Virol* **88**, 10421-10431 (2014).

208. Fisicaro, P. *et al.* Antiviral intrahepatic T-cell responses can be restored by blocking programmed death-1 pathway in chronic hepatitis B. *Gastroenterology* **138**, 682-693, 693 e681-684 (2010).

209. Bengsch, B., Martin, B. & Thimme, R. Restoration of HBV-specific CD8+ T cell function by PD-1 blockade in inactive carrier patients is linked to T cell differentiation. *J Hepatol* **61**, 1212-1219 (2014).

210. El-Khoueiry, A.B. *et al.* Nivolumab in patients with advanced hepatocellular carcinoma (CheckMate 040): an open-label, non-comparative, phase 1/2 dose escalation and expansion trial. *Lancet* **389**, 2492-2502 (2017).

211. Gane, E. *et al.* Anti-PD-1 blockade with nivolumab with and without therapeutic vaccination for virally suppressed chronic hepatitis B: A pilot study. *J Hepatol* **71**, 900-907 (2019).

212. Kosinska, A.D., Bauer, T. & Protzer, U. Therapeutic vaccination for chronic hepatitis B. *Curr Opin Virol* **23**, 75-81 (2017).

213. Fontaine, H. *et al.* Anti-HBV DNA vaccination does not prevent relapse after discontinuation of analogues in the treatment of chronic hepatitis B: a randomised trial--ANRS HB02 VAC-ADN. *Gut* **64**, 139-147 (2015).

214. Mancini-Bourgine, M. *et al.* Induction or expansion of T-cell responses by a hepatitis B DNA vaccine administered to chronic HBV carriers. *Hepatology* **40**, 874-882 (2004).

215. Pol, S. *et al.* Efficacy and limitations of a specific immunotherapy in chronic hepatitis B. *J Hepatol* **34**, 917-921 (2001).

216. Godon, O. *et al.* Immunological and antiviral responses after therapeutic DNA immunization in chronic hepatitis B patients efficiently treated by analogues. *Mol Ther* **22**, 675-684 (2014).

217. Vandepapeliere, P. *et al.* Therapeutic vaccination of chronic hepatitis B patients with virus suppression by antiviral therapy: a randomized, controlled study of co-administration of HBsAg/AS02 candidate vaccine and lamivudine. *Vaccine* **25**, 8585-8597 (2007).

218. Lok, A.S. *et al.* Randomized phase II study of GS-4774 as a therapeutic vaccine in virally suppressed patients with chronic hepatitis B. *J Hepatol* **65**, 509-516 (2016).

219. Pancholi, P. *et al.* DNA prime/canarypox boost-based immunotherapy of chronic hepatitis B virus infection in a chimpanzee. *Hepatology* **33**, 448-454 (2001).

220. Cavenaugh, J.S. *et al.* Partially randomized, non-blinded trial of DNA and MVA therapeutic vaccines based on hepatitis B virus surface protein for chronic HBV infection. *PLoS One* **6**, e14626 (2011).

221. Backes, S. *et al.* Protein-prime/modified vaccinia virus Ankara vector-boost vaccination overcomes tolerance in high-antigenemic HBV-transgenic mice. *Vaccine* **34**, 923-932 (2016).

222. Michler, T. *et al.* Knockdown of Virus Antigen Expression Increases Therapeutic Vaccine Efficacy in High-titer HBV Carrier Mice. *Gastroenterology* (2020).

223. Krebs, K. *et al.* T cells expressing a chimeric antigen receptor that binds hepatitis B virus envelope proteins control virus replication in mice. *Gastroenterology* **145**, 456-465 (2013).

224. Qasim, W. *et al.* Immunotherapy of HCC metastases with autologous T cell receptor redirected T cells, targeting HBsAg in a liver transplant patient. *J Hepatol* **62**, 486-491 (2015).

225. Sprinzl, M.F., Oberwinkler, H., Schaller, H. & Protzer, U. Transfer of hepatitis B virus genome by adenovirus vectors into cultured cells and mice: crossing the species barrier. *J Virol* **75**, 5108-5118 (2001).

226. Khan, O. *et al.* TOX transcriptionally and epigenetically programs CD8(+) T cell exhaustion. *Nature* **571**, 211-218 (2019).

227. Joshi, N.S. *et al.* Inflammation directs memory precursor and short-lived effector CD8(+) T cell fates via the graded expression of T-bet transcription factor. *Immunity* **27**, 281-295 (2007).

228. Xin, A. *et al.* A molecular threshold for effector CD8(+) T cell differentiation controlled by transcription factors Blimp-1 and T-bet. *Nat Immunol* **17**, 422-432 (2016).

229. Manske, K. *et al.* Outcome of Antiviral Immunity in the Liver Is Shaped by the Level of Antigen Expressed in Infected Hepatocytes. *Hepatology* **68**, 2089-2105 (2018).

230. McCaffrey, A.P. *et al.* Inhibition of hepatitis B virus in mice by RNA interference. *Nat Biotechnol* **21**, 639-644 (2003).

231. Keck, K. *et al.* Rational design leads to more potent RNA interference against hepatitis B virus: factors effecting silencing efficiency. *Mol Ther* **17**, 538-547 (2009).

232. Michler, T. *et al.* Blocking sense-strand activity improves potency, safety and specificity of anti-hepatitis B virus short hairpin RNA. *EMBO Mol Med* **8**, 1082-1098 (2016).

233. Kahan, S.M., Wherry, E.J. & Zajac, A.J. T cell exhaustion during persistent viral infections. *Virology* **479-480**, 180-193 (2015).

234. Shiow, L.R. *et al.* CD69 acts downstream of interferon-alpha/beta to inhibit S1P1 and lymphocyte egress from lymphoid organs. *Nature* **440**, 540-544 (2006).

235. Urban, S.L., Berg, L.J. & Welsh, R.M. Type 1 interferon licenses naive CD8 T cells to mediate anti-viral cytotoxicity. *Virology* **493**, 52-59 (2016).

236. Urban, S.L. & Welsh, R.M. Out-of-sequence signal 3 as a mechanism for virus-induced immune suppression of CD8 T cell responses. *PLoS Pathog* **10**, e1004357 (2014).

237. Battegay, M. *et al.* Enhanced establishment of a virus carrier state in adult CD4+ T-cell-deficient mice. *J Virol* **68**, 4700-4704 (1994).

238. Matloubian, M., Concepcion, R.J. & Ahmed, R. CD4+ T cells are required to sustain CD8+ cytotoxic T-cell responses during chronic viral infection. *J Virol* **68**, 8056-8063 (1994).

239. Thimme, R. & Dandri, M. Dissecting the divergent effects of interferon-alpha on immune cells: time to rethink combination therapy in chronic hepatitis B? *J Hepatol* **58**, 205-209 (2013).

240. Sadler, A.J. & Williams, B.R. Interferon-inducible antiviral effectors. *Nat Rev Immunol* **8**, 559-568 (2008).

241. Klenerman, P. & Hill, A. T cells and viral persistence: lessons from diverse infections. *Nat Immunol* **6**, 873-879 (2005).

242. Park, J.J. *et al.* Hepatitis B Virus--Specific and Global T-Cell Dysfunction in Chronic Hepatitis B. *Gastroenterology* **150**, 684-695 e685 (2016).

243. Dusseaux, M. *et al.* Viral Load Affects the Immune Response to HBV in Mice With Humanized Immune System and Liver. *Gastroenterology* **153**, 1647-1661 e1649 (2017).

244. Tay, S.S. *et al.* Antigen expression level threshold tunes the fate of CD8 T cells during primary hepatic immune responses. *Proc Natl Acad Sci U S A* **111**, E2540-2549 (2014).

245. Maini, M.K. *et al.* The role of virus-specific CD8(+) cells in liver damage and viral control during persistent hepatitis B virus infection. *J Exp Med* **191**, 1269-1280 (2000).

246. Liu, X. *et al.* PD-1(+) TIGIT(+) CD8(+) T cells are associated with pathogenesis and progression of patients with hepatitis B virus-related hepatocellular carcinoma. *Cancer Immunol Immunother* **68**, 2041-2054 (2019).

247. Alfei, F. *et al.* TOX reinforces the phenotype and longevity of exhausted T cells in chronic viral infection. *Nature* **571**, 265-269 (2019).

248. Blank, C.U. *et al.* Defining 'T cell exhaustion'. *Nat Rev Immunol* **19**, 665-674 (2019).

249. Schietinger, A. & Greenberg, P.D. Tolerance and exhaustion: defining mechanisms of T cell dysfunction. *Trends Immunol* **35**, 51-60 (2014).

250. Gish, R.G. *et al.* Chronic hepatitis B: Virology, natural history, current management and a glimpse at future opportunities. *Antiviral Res* **121**, 47-58 (2015).

251. Rosenberg, E.S. *et al.* Vigorous HIV-1-specific CD4+ T cell responses associated with control of viremia. *Science* **278**, 1447-1450 (1997).

252. Rosenberg, E.S. *et al.* Immune control of HIV-1 after early treatment of acute infection. *Nature* **407**, 523-526 (2000).

253. Boni, C. *et al.* Lamivudine treatment can restore T cell responsiveness in chronic hepatitis B. *J Clin Invest* **102**, 968-975 (1998).

254. Kamal, S.M. *et al.* Pegylated interferon alpha therapy in acute hepatitis C: relation to hepatitis C virus-specific T cell response kinetics. *Hepatology* **39**, 1721-1731 (2004).

255. Altfeld, M. *et al.* Cellular immune responses and viral diversity in individuals treated during acute and early HIV-1 infection. *J Exp Med* **193**, 169-180 (2001).

256. Oxenius, A. *et al.* Early highly active antiretroviral therapy for acute HIV-1 infection preserves immune function of CD8+ and CD4+ T lymphocytes. *Proc Natl Acad Sci U S A* **97**, 3382-3387 (2000).

257. Lauer, G.M. *et al.* Full-breadth analysis of CD8+ T-cell responses in acute hepatitis C virus infection and early therapy. *J Virol* **79**, 12979-12988 (2005).

258. Grossi, G., Vigano, M., Loglio, A. & Lampertico, P. Hepatitis B virus long-term impact of antiviral therapy nucleot(s)ide analogues (NUCs). *Liver Int* **37 Suppl 1**, 45-51 (2017).

259. Levrero, M., Subic, M., Villeret, F. & Zoulim, F. Perspectives and limitations for nucleo(t)side analogs in future HBV therapies. *Curr Opin Virol* **30**, 80-89 (2018).

260. Boni, C. *et al.* HBV Immune-Therapy: From Molecular Mechanisms to Clinical Applications. *Int J Mol Sci* **20** (2019).

261. Dagenais-Lussier, X. *et al.* Sustained IFN-I Expression during Established Persistent Viral Infection: A "Bad Seed" for Protective Immunity. *Viruses* **10** (2017).

262. Cheng, L. *et al.* Blocking type I interferon signaling enhances T cell recovery and reduces HIV-1 reservoirs. *J Clin Invest* **127**, 269-279 (2017).

263. Cheng, L. *et al.* Type I interferons suppress viral replication but contribute to T cell depletion and dysfunction during chronic HIV-1 infection. *JCI Insight* **2** (2017).

264. Zvonova, E.A. *et al.* PASylation technology improves recombinant interferon-beta1b solubility, stability, and biological activity. *Appl Microbiol Biotechnol* **101**, 1975-1987 (2017).

265. Curtsinger, J.M., Valenzuela, J.O., Agarwal, P., Lins, D. & Mescher, M.F. Type I IFNs provide a third signal to CD8 T cells to stimulate clonal expansion and differentiation. *J Immunol* **174**, 4465-4469 (2005).

266. Le Bon, A. *et al.* Direct stimulation of T cells by type I IFN enhances the CD8+ T cell response during cross-priming. *J Immunol* **176**, 4682-4689 (2006).

ABBREVIATIONS

AAV	Adenovirus-associated vector
Ad	Adenovirus
AdV	Adenoviral vector
AIDS	Aquired immunodeficiency syndrome
ALT	Alanine aminotransferase
APOBEC3	apolipoprotein B mRNA-editing catalytic polypeptide-like 3
CAR	chimeric antigen receptor
CBG	Click beetle green
cccDNA	covalently closed circular DNA
CHB	Chronic hepatitis B virus infection
CTLA-4	Cytotoxic T cell associated protein 4
CXCR3	C-X-C Motif Chemokine Receptor 3
DHBV	duck hepatitis virus
EBV	Epstein-Barr virus
EOMES	Eomesdermin
HBc	Hepatitis B virus core protein
HBeAg	Hepatitis B virus envelope antigen
HBs	Hepatitis B virus surface protein
HBx	Hepatitis B virus x protein
HBsAg	Hepatitis B virus surface antigen
HBV	Hepatitis B Virus
HCC	hepatocellular carcinoma
HCV	Hepatitis C virus
HDV	Hepatitis delta virus
HIV	Human immunodeficiency virus
ICI	Immune checkpoint inhibition
IFN	Interferone
IFNAR	type I interferon receptor
IFNy	Interferon gamma
IL-10	Interleukin-10
IL-12	Interleukin 12
IL-18	Interleukin 18
IL-2	Interleukin 2
IL-7	Interleukin 7
IRF1	interferon regulatory factor 1

IU	International unit
KLRG-1	Killer cell lectin-like receptor gene 1
Lag3	Lymphocyte activation gene-3
LCMV	lymphocytic choriomeningitis mammarenavirus
LSEC	Liver sinusoidal endothelial cell
MDA-5	Melanoma differentiation associated protein 5
MPEC	memory precursor effector cell pool
MVA	modified vaccinia virus Ankara
NAs	nucleos(t)ide analogues
NAs	Nucleos(t)ide analogues
NK cell	Natural killer cell
NK T cell	Natural killer T cell
nM	nanometer
NTCP	Sodium taurocholate cotransporting polypeptide
ORF	Open reading frame
PBMC	peripheral blood mononuclear cell
PD1	Programmed cell death protein 1
pDC	plasmacytoid dendritic cells
PDL1	Programmed cell death protein 1 ligand
PEG-IFNα	Pegylated IFNα
pgRNA	Pregenomic RNA
PKR	Protein kinase R
PRR	Pattern recognition receptor
rcDNA	Relaxed circular DNA
RIG-I	Retinoic acid inducible gene I
sALT	serum alanine aminotransferase
shRNA	Short hairpin RNA
siRNA	Small interfering RNA
SIV	Simian immunodeficiency virus
SVP	subviral particle
Tbet	T-box binding transcription factor expressed in T cells
TCF1	T cell factor 1
TCR	T cell receptor
Teff	Effector T cells
Tex	Exhausted T cells
TGFβ	Transforming growth factor beta
TIGIT	T cell immunoglobulin and ITIM domain

TIL	Tumor infiltrating lymphocyte
TIM3	T cell immunoglobulin mucin-3
TLR	Toll like receptor
Tmem	Memory T cells
TNF	Tumor necrosis factor
Treg	Regulatory T cell
WHO	world health organization
WHV	Woodchuck hepatitis virus

PUBLICATIONS

Publications

Schneider A*, Kurz S*, Manske K, Janas M, Heikenwälder M, Misgeld T, Aichler M, Weissmann SF, Zischka H, Knolle P, Wohlleber D.: Single organelle analysis to characterize mitochondrial function and crosstalk during viral infection. *Sci Rep 9, 8492 (2019), doi: 10.1038/s41598-019-44922-9*

Manske K, Kallin N, König V, **Schneider A**, Kurz S, Bosch M, Welz M, Cheng RL, Bengsch B, Steiger K, Protzer U, Thimme R, Knolle PA, Wohlleber D.: Outcome of Antiviral Immunity in the Liver Is Shaped by the Level of Antigen Expressed in Infected Hepatocytes. *Hepatology 68, 2089-2105 (2018), doi: 10.1002/hep.30080*

Lampl S, Janas MK, Donakonda S, Brugger M, Lohr K, **Schneider A**, Manske K, Sperl LE, Wettmarshausen J, Müller C, Laschinger M, Hartmann D, Hüser N, Perrochi F, Schmitt-Kopplin P, Hagn F, Zender L, Hornung V, Borner C, Pichlmair A, Kashkar H, Klingenspor M, Prinz M, Schreiner S, Conrad M, Jost PJ, Zischka H, Steiger K, Krönke M, Zehn D, Protzer U, Heikenwälder M, Knolle PA, Wohlleber D.: Reduced mitochondrial resilience enables non-canonical induction of apoptosis after TNF receptor signaling in virus-infected hepatocytes. *J Hepatol (2020),doi: 10.1016/j.jhep.2020.06.026*

Laschinger M, Wang Y, Holzmann G, Wang B, Stöß C, Lu M, Brugger M, **Schneider A**, Knolle P, Wohlleber D, Schulze S, Steiger K, Tsujikawa K, Altmayr F, Friess H, Hartmann D, Hüser N, Holzmann B.:The CGRP receptor component RAMP1 links sensory innervation with YAP activity in the regenerating liver. *FASEB J (2020), doi: 10.1096/fj.201903200R.*

** Authors contributed equally to this work*

Oral presentations at scienctific conferences

Schneider A., Kurz S., Manske K., Knolle P.A., Wolleber D.: „Viral infection sensitizes hepatocytes towards CD8 T cell mediated antiviral immunity"
Annual Meeting of the German Association for the Study of the Liver (GASL), 2018, Hamburg, Germany

Schneider A., Kurz S., Manske K., Knolle P.A., Wolleber D.: "A decisive role of target cells during antiviral immunity in the liver"
Global Hepatitis Summit, 2018, Toronto, Canada

Schneider A., Manske K., Mutz P., Laschinger M., Bartenschlager R., Heikenwälder M., Knolle P.A., Wolleber D.: "The pivotal role of target cells in modulating efficacy of antiviral CD8 T cell immunity in the liver"
Annual Meeting of the German Association for the Study of the Liver (GASL), 2019, Heidelberg, Germany

Schneider A., Manske K., Anton M., Schmelas C., Grimm D., Ko C., Kurz S., Protzer U., Knolle P.A., Wolleber D.: “Re-activation of anti-viral immune cells and antigen reduction enables clearance of chronic HBV in mice”
Joint Meeting of the German Society for Immunology (DGfI) and the Italian Society of Immunology, Clinical Immunology and Allergology, 2019, Munich, Germany

Schneider A., Manske K., Anton M., Schmelas C., Grimm D., Ko C., Kurz S., Protzer U., Knolle P.A., Wolleber D.: “Re-activation of anti-viral immune cells and antigen reduction enables clearance of chronic HBV in mice”
International HBV Meeting, 2019, Melbourne, Australia

ACKNOWLEDGEMENTS

Ich möchte mich an dieser Stelle bei den Menschen bedanken, die mich die letzten vier Jahre unterstützt und begleitet haben und ohne die diese Promotionsarbeit nicht möglich gewesen wäre.

Zuerst möchte ich meinem Doktorvater Prof. Percy Knolle danken. Danke für für die Freiheiten, den Rückhalt und das entgegengebrachte Vertrauen.

Ich danke Prof. Bernhard Küster für freundliche Unterstützung bei der Zwischenevaluierung meines Promotionsprojektes und für die Bereitschaft diese Arbeit zu begutachten.

Einen ganz besonderen Dank möchte ich Dr. Dirk Wohlleber aussprechen. Danke Dirk, dass du mich durchgehend betreut, unterstützt, motiviert und gefördert hast. Ich schätze deine Flexibilität, deinen Humor, deine Geduld und deine Kreativität. Es macht Spaß mit dir zu arbeiten. Danke.

Von ganzem Herzen danke ich auch allen meinen wundervollen Kollegen für Beiträge unterschiedlichster Art. Ganz besonders möchte ich Katrin, Verena und Sandra danken: Ich habe es genossen, mit euch das Büro zu teilen. Außerdem möchte ich Silke und Sava dafür danken, dass sie so wundervoll hilfsbereit sind und immer wieder einspringen und aushelfen.

Ebenfalls möchte ich Prof. Ulrike Protzer und dem gesamten Institut für Virologie für die Unterstützung danken. Ich danke Dr. Katja Steiger und ihrem Team vom Institut für Pathologie und Prof. Matthias Heikenwälder und seinem Team für die Anfertigung der Immunhistochemischen Färbungen. Ich danke Dr. Martina Anton und Katja Dummler für die Generierung der AAVs und die nette Zusammenarbeit. Außerdem bedanken ich mich bei allen Mitgliedern und dem Organisationsteam SFP TRR179 und meinen externen Kollaborationspartnern für die konstruktive Zusammenarbeit.